Astrophysics after almost three years of the Imaging X-ray Polarimetry Explorer (IXPE)

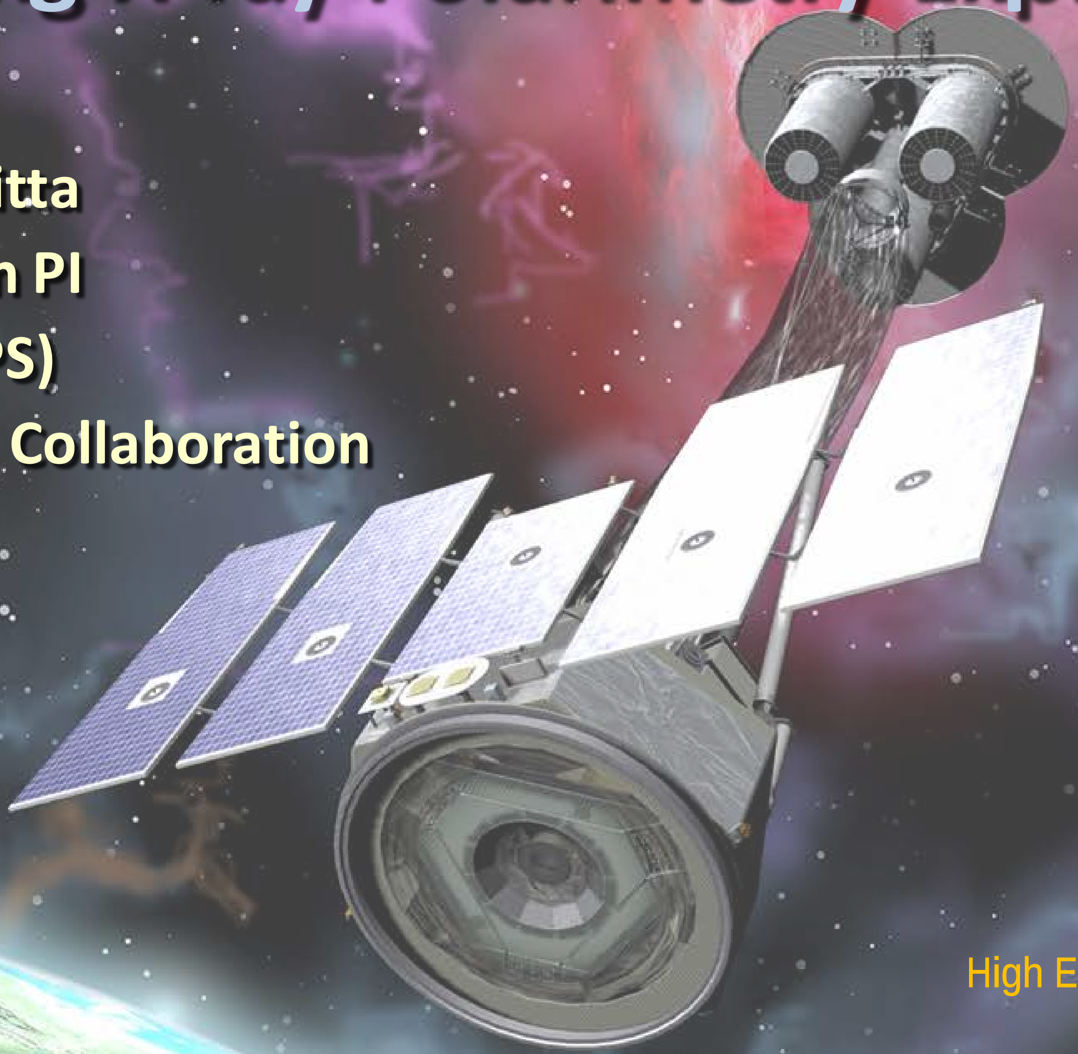

Paolo Soffitta
IXPE Italian PI
(INAF-IAPS)
On behalf of the IXPE Collaboration

High Energy Astrophysics and Cosmology
In the Era of all-sky surveys.
HEACOSS Yerevan (Armenia) 7-11 October 2024

WHY X-RAY ASTROPHYSICAL POLARIMETRY ?

Polarization from celestial sources may derive from:

- **Emission processes themselves: cyclotron, synchrotron, non-thermal bremsstrahlung**

(Westfold, 1959; Gnedin & Sunyaev, 1974; Rees, 1975)

- **Scattering on aspherical accreting plasmas: disks, blobs, columns.**

(1975; Sunyaev & Titarchuk, 1985; Mészáros, P. et al. 1988)

- **Vacuum polarization and birefringence through extreme magnetic fields**

(Gnedin et al., 1978; Ventura, 1979; Mészáros & Ventura, 1979)

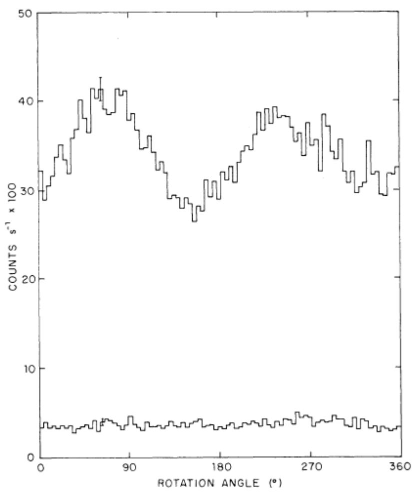

Notwithstanding the theoretical previsions the polarization of only one source was detected by OSO-8 back in the ’70 until IXPE:

Positive measurement: of X-ray polarization of the Crab Nebula without pulsar contamination
(by lunar occultation, Weisskopf et al., 1978).

P = (19.2 ± 1.0) %; θ = 156°.4 ± 1°.4 (2.6 keV)

P = (19.5 ± 2.8) % ; θ = 152°.6 ± 4°.0 (5.2 keV)

The technique was the limit !

The modern X-ray polarimetry technique started in the late ‘80ies

The Stellar X-ray Polarimeter

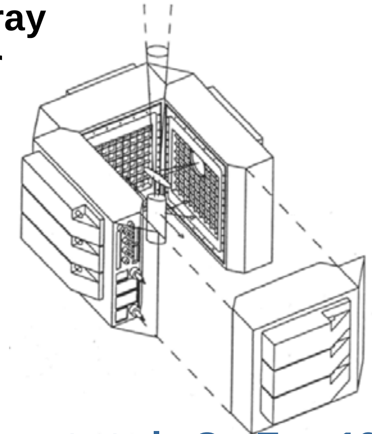

Kaaret et al., OptEng 1990, Weisskopf et al. SPIE 1991, Tomsick et al., SPIE 1997, Soffitta et al., NIM A, 1998

R. Novick & R. Sunyaev
(picture taken by Enrico Costa)

SXRP at the calibration facility at LLNL.

SXRP was built, tested and calibrated but never flown!

The large lithium stage was too much limited by background. The Bragg (imaging) one, better for dim sources, was very limited in area and energy band

It was clear that Imaging polarimetry by using the photoelectric effect in gas was the way to go.

Modern techniques: photoelectric effect at 2-10 keV

Costa, Nature, 2001

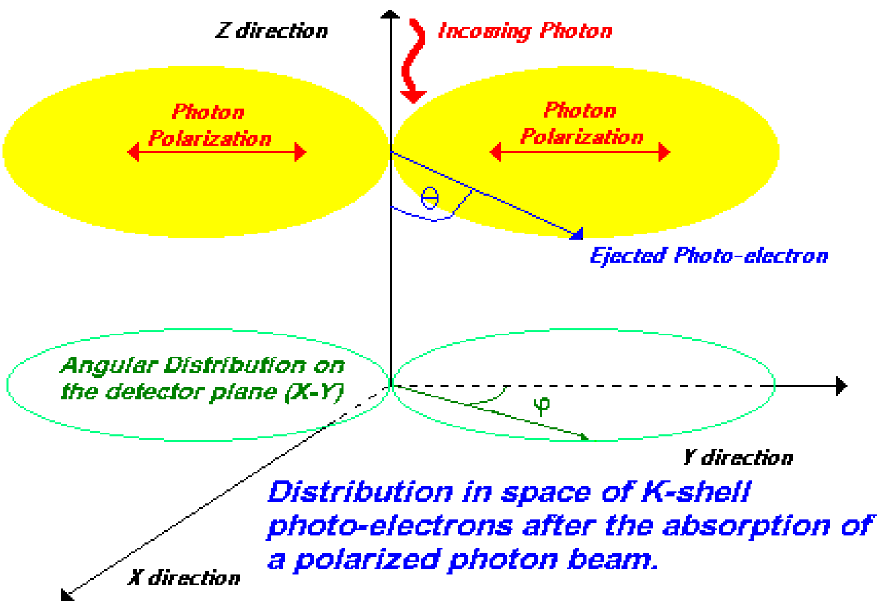

Costa et al., Nature, 2001

Heitler W.,The Quantum Theory of Radiation $\beta = v/c$

$$\frac{\partial \sigma}{\partial \Omega} = r_o^2 \frac{Z^5}{137^4} \left(\frac{mc^2}{h\nu} \right)^{7/2} \frac{4\sqrt{2}\sin^2(\theta)\cos^2(\varphi)}{\left(1-\beta\cos(\theta)\right)^4}$$

One-stage polarimeter

The analyzer and the detector are the same device.

Border-effect polarimeter

Polarimeter sensitive to a ‘borderline’ crossed by the carrier of the polarization information. The polarimetric response is sensitive to the interaction point (CCD, AC polarimeter) leading to large systematic effects.

Subdivided Polarimeter

The detection pixel is smaller than the path of the carrier of the polarization information (rise-time =>*dispersive* , photoimager, charge-imager => *non dispersive*) The polarimetric response is much less sensitive to the interaction point (smaller systematic effects) .

Focal-Plane Non Dispersive Imaging One-Stage Subdivided Wide-Band Photoelectric effect

By measuring the angular distribution of the ejected photoelectrons (the modulation curve) it is possible to derive the X-ray polarization.

WHY POLARIMETRY IN THE CLASSICAL X-RAY ENERGY BAND

Scientific goal	Sources	< 1 keV	1-10	> 10 keV
Acceleration phenomena	PWN	yes (but absorption)	yes	yes
	SNR	no	yes	yes
	Jet (Microquasars)	yes (but absorption)	yes	yes
	Jet (Blazars)	yes	yes	yes
Emission in strong magnetic fields	WD	yes (but absorption)	yes	difficult
	AMS	no	yes	yes
	X-ray pulsator	difficult	yes (no cyclotron ?)	yes
	Magnetar	yes (better)	yes	no
Scattering in aspherical geometries	Corona in XRB & AGNs	difficult	yes	yes (difficult)
	X-ray reflection nebulae	no	yes (long exposure)	yes
Fundamental Physics	QED (magnetar)	yes (better)	yes	no
	GR (BH)	no	yes	no
	QG (Blazars)	difficult	yes	yes
	Axions (Blazars, Clusters)	yes ?	yes	difficult

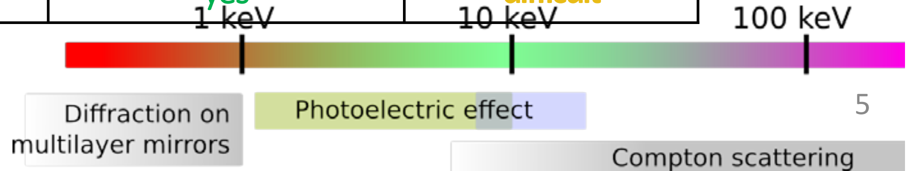

X-RAY POLARIMETRY WITH A GAS PIXEL DETECTOR

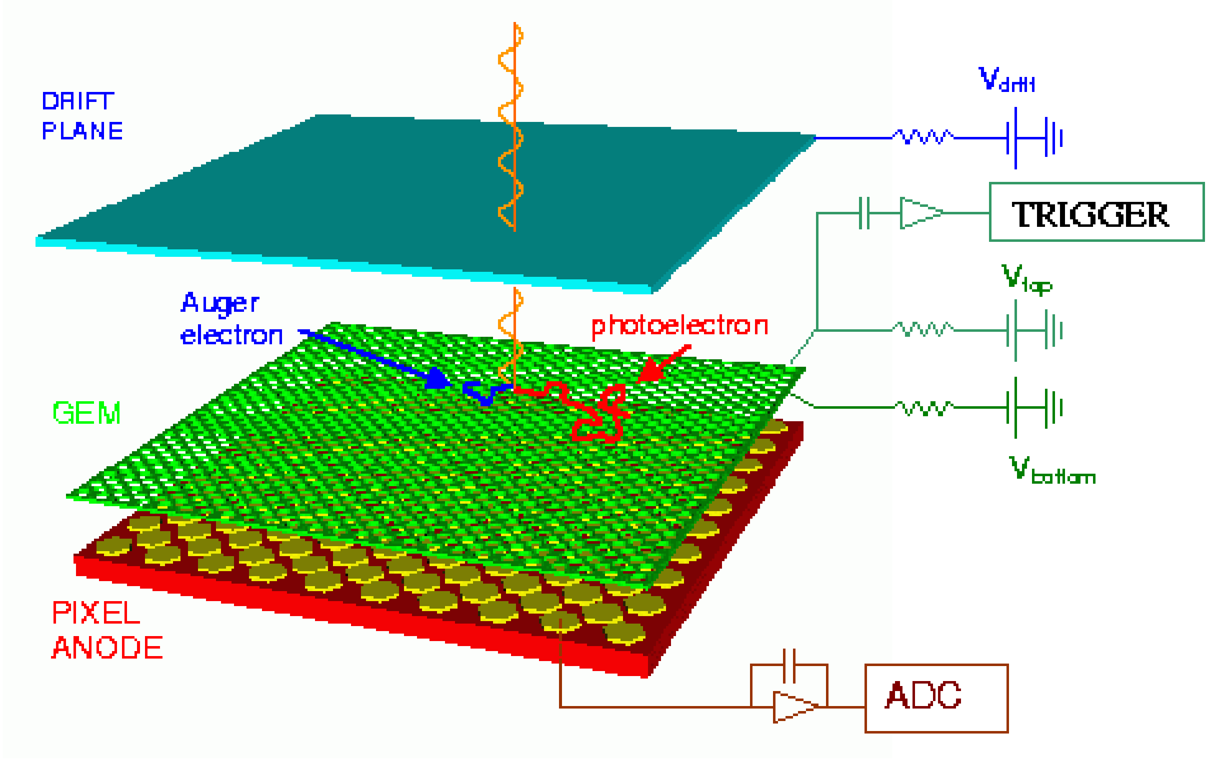

Costa et al., 2001, Bellazzini et al. 2006, 2007

- A Beryllium window
- A gas cell for photon conversion
- An electric field to drift the track
- A multiplication plane to get more charge
- An ASIC CMOS chip to make the image of the track

GEM electric field

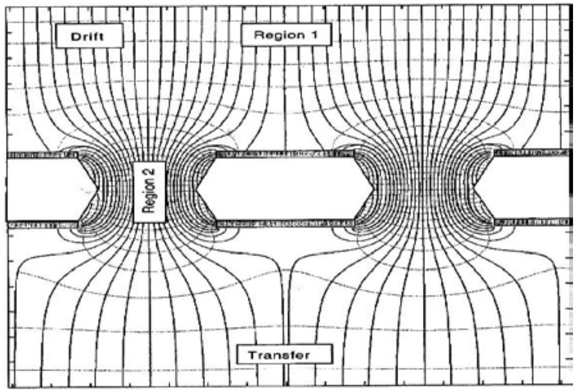

The Gas Pixel Detector makes the charge image of the photoelectron track. .

IXPE
Imaging
X-Ray
Polarimetry
Explorer

Photoelectric effect to measure polarization of X-rays

Proposed missions to date

Mission	Date	PI
XMM	Late 80’	G.W. Fraser (UK)
SXRP /SRG	Late 80’ Early 00’	R.Novick (USA)
XEUS/IXO	2007-2012	R. Bellazzini (IT)
POLARIX	2007-2008	E. Costa (IT)
IXPE (OLD)	2007	M. Weisskopf (USA)
HXMT	2007-2009	E. Costa (IT)
NHXM	2011	G. Tagliaferri (IT)
LAMP	2013	H. Feng (China)
XIPE (Small)	2014	E. Costa (IT)
ADAELI+	2014	F. Berrilli (IT)
SEEPE (ESA-CAS)	2014	S.Liu-P. Soffitta
XIPE M4	2014-2017	P. Soffitta (IT)
IXPE	**2017+**	**M. Weisskopf (USA)**

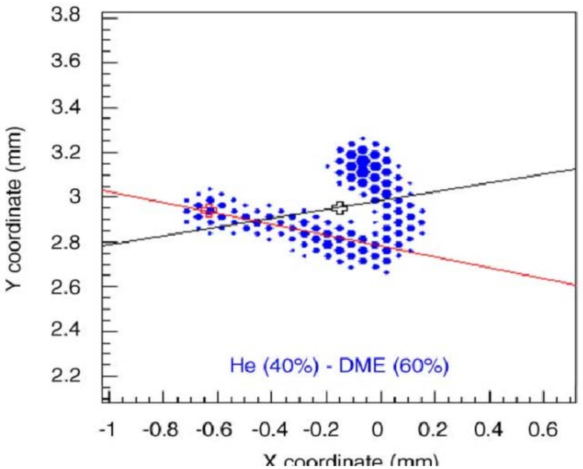

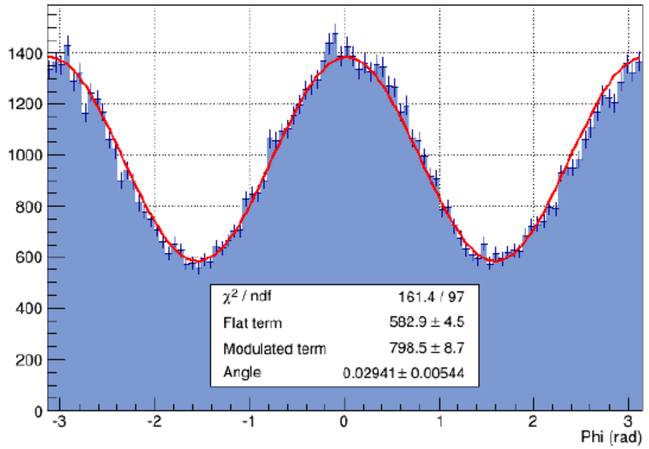

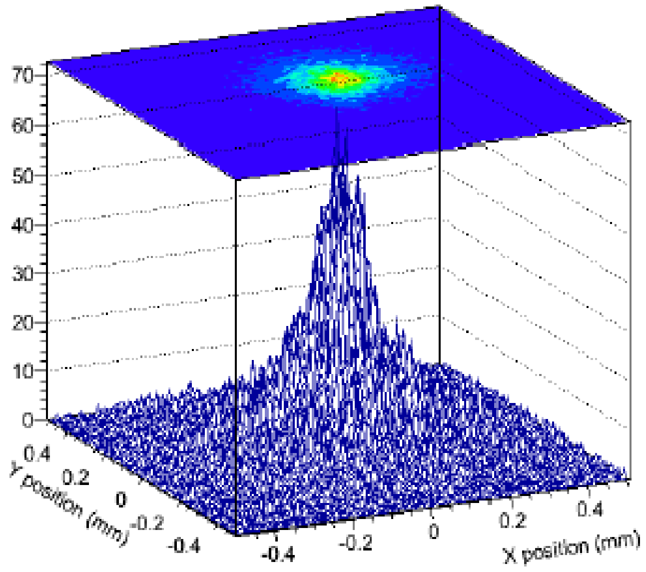

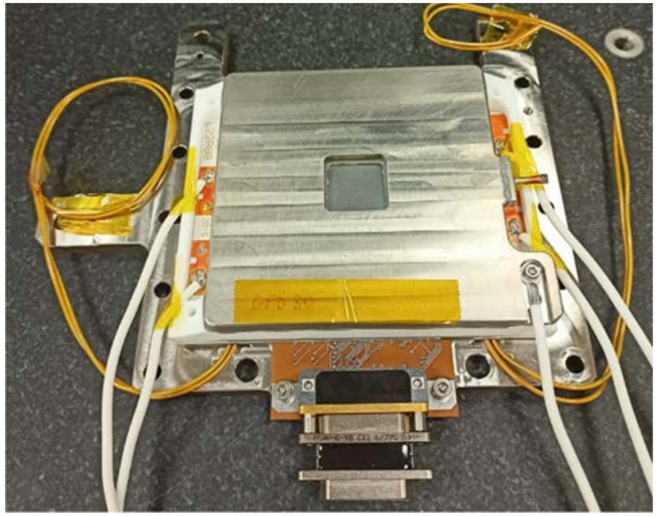

Costa et al., 2001, Bellazzini et al, 2005,2006, Baldini et al., 2021, Soffitta et al. 2022

The IXPE Observatory

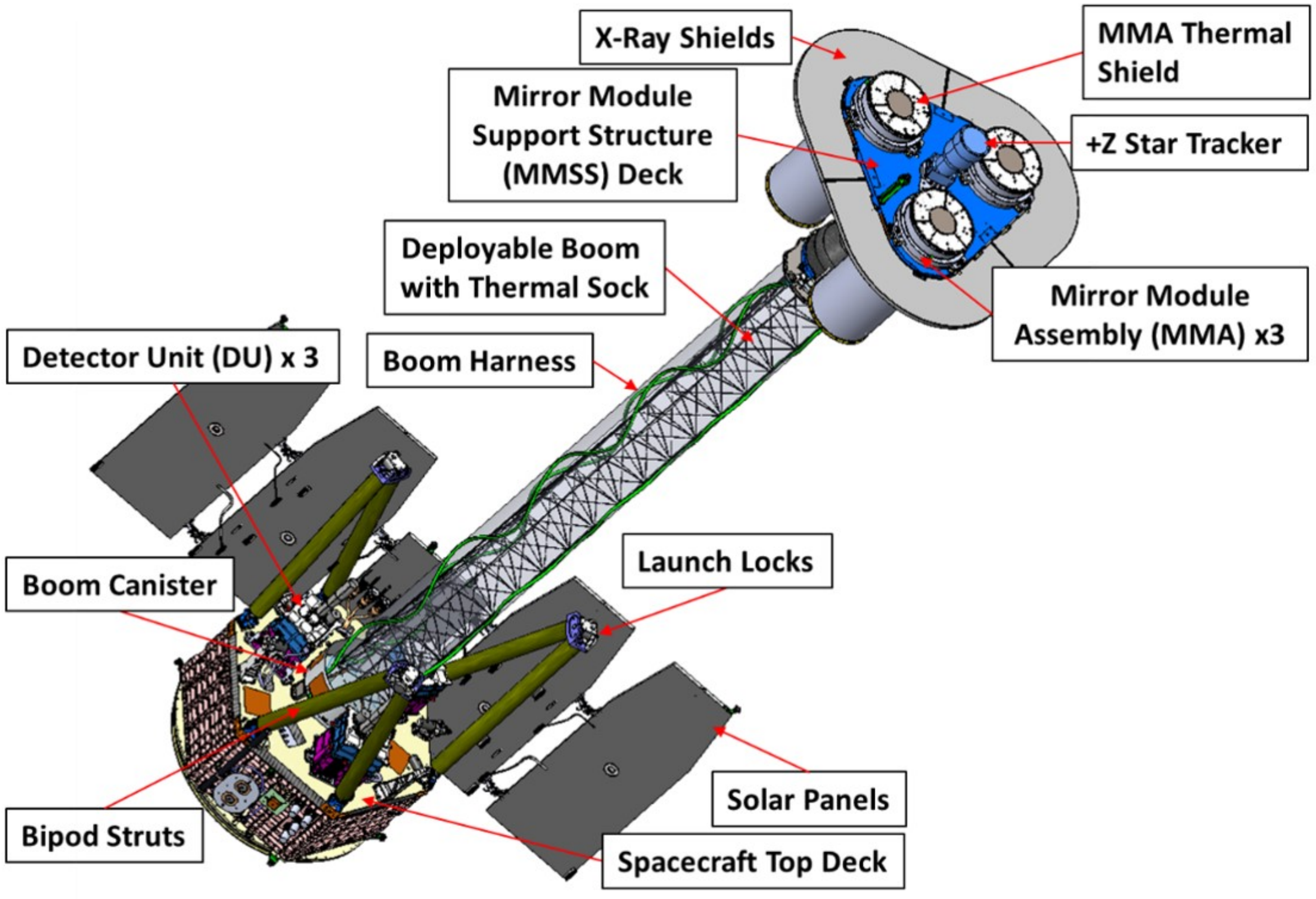

IXPE
Imaging X-Ray Polarimetry Explorer

IXPE Institutions and Industries

NASA Marshall Space Flight Center: PI team, project management, SE and S&MA oversight, mirror module fabrication, X-ray calibration, science operations, and data analysis and archiving	IAPS, INAF (Istituto Nazionale di Astrofisica / National Institute for Astrophysics), INFN, OAC, OHB Italia: Polarization-sensitive imaging detector systems
	CU LASP: Mission operations
ASI (agenzia spaziale italiana): Detector system funding, ground station	Roma Tre (Università degli Studi), Stanford University: Scientific theory
	Nagoya University: Thermal shields
Ball: Spacecraft, payload structure, payload, observatory I&T	Massachusetts Institute of Technology: Co-Investigator

Science Advisory Team

PI Philip E. Kaaret (formerly Martin Weisskopf [Emeritus])

FALCON 9 LAUNCHER VS PEGASUS XL LAUNCHER

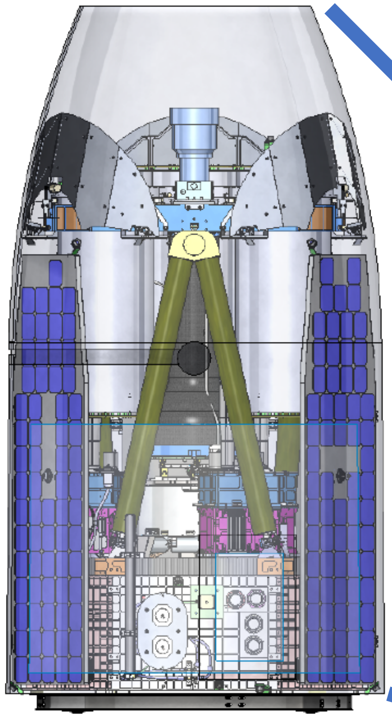

IXPE in the Pegasus XL fairing.

Required in proposal and phase A and phase B

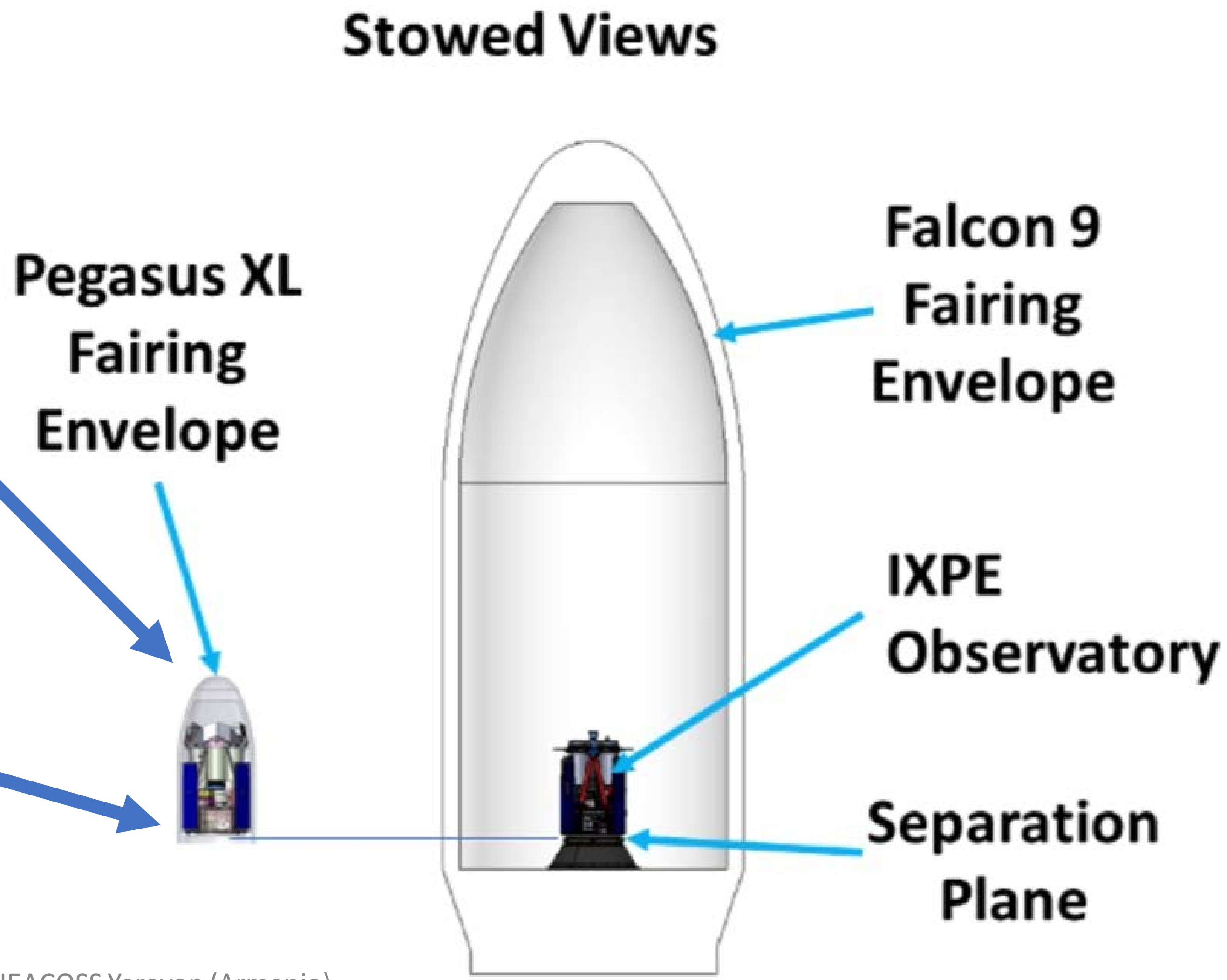

On July 8, 2019, NASA announced that Space-X of Hawthorne, California will provide launch services for IXPE.

Before Pandemic!

INFN-TEAM ASSEMBLY & TEST OF THE DUs

- DU mechanical housing design and procurement.
- DU thermal design and parts procurement
- Stray-light collimator design & procurement
- DU alignment system (collab. with MSFC & Ball &INAF)
- BEE electronics design and procurement
- BEE DAQ firmware, BEE software
- BEE Test

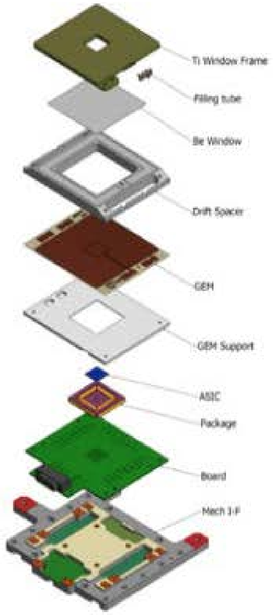

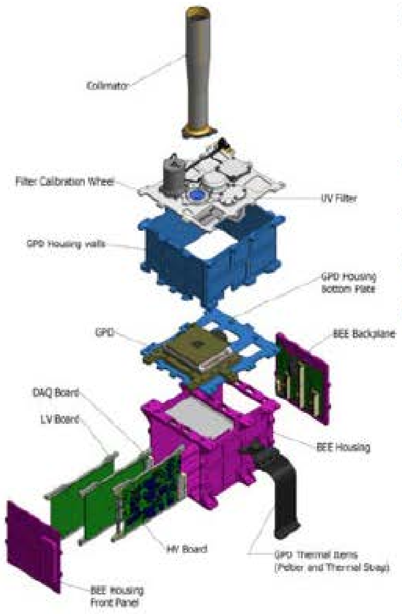

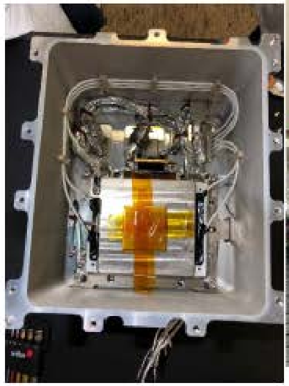

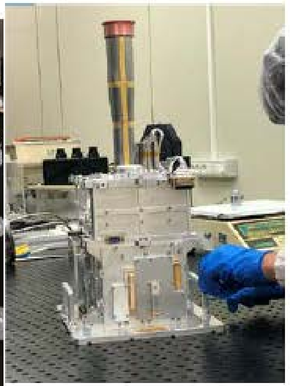

INAF: Flight Polarized & Unpolarized sources: design, Construction & test

Calibration of 3 flight DUs + 1 DU Spare, Instrument AIV&T

DURING PANDEMIC!

- Calibration of DU have been carried out in Italy at INAF-IAPS, before Instrument integration and delivery to USA
- 40 days for each DU (3 flight + 1 spare units)
  - Up to 24/7 data acquisition
- First unit started calibration on 26th July, DU-FM2 started on 6th Sep 2019, DU3 on 23 Oct. 2019, DU 4 on 16 Dec. 2019
- 60% of time dedicated to characterization of the response to unpolarized radiation at 6 energies
- 17.5% of time dedicated to measurements of modulation factor at 7 energies
- Remaining time to calibrate other parameters of interest
- Energy calibration and dead-time are by-product of previous measurements

Ferrazzoli R. et al., JATIS 2021

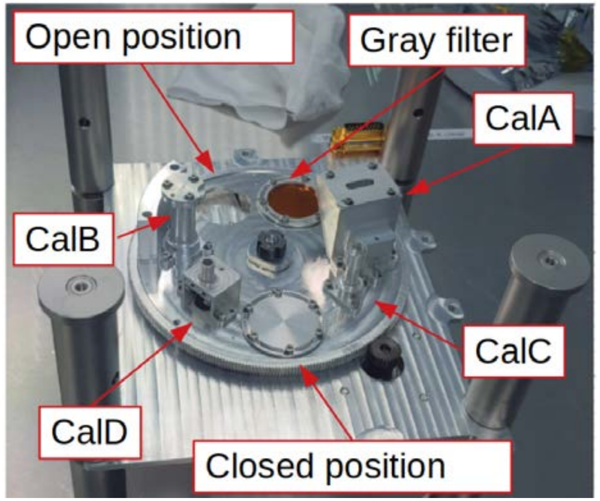

Delivery of DU 2 & EGSE

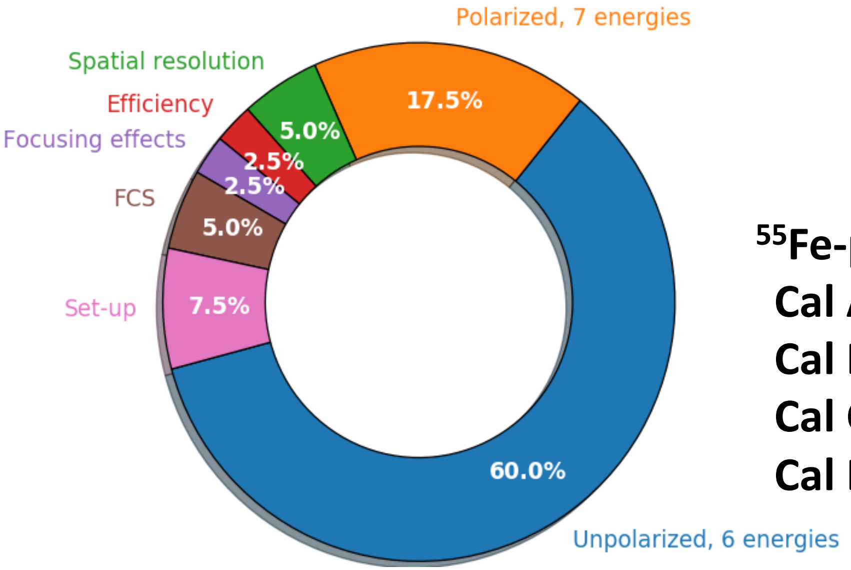

Muleri F. et al., Astr. Phys, 2022

^{55}Fe**-powered calibration sources:**

Cal A – polarized 2.98-keV and 5.89-keV
Cal B – unpolarized 5.89-keV spot
Cal C – unpolarized 5.89-keV flood
Cal D – unpolarized 1.74-keV

FILTER Calibration Wheel Assembly (In-flight calibration)

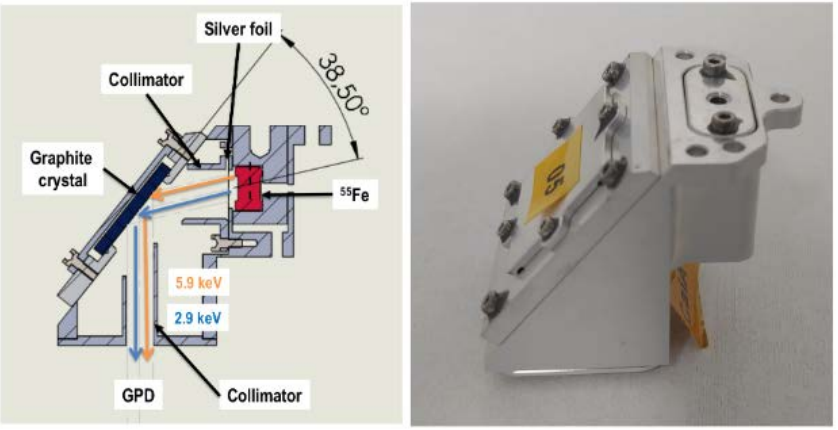

Flight Polarized X-ray sources

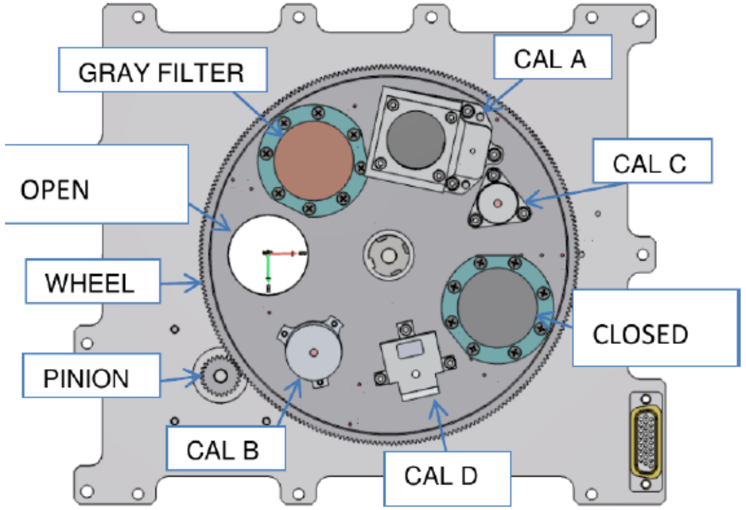

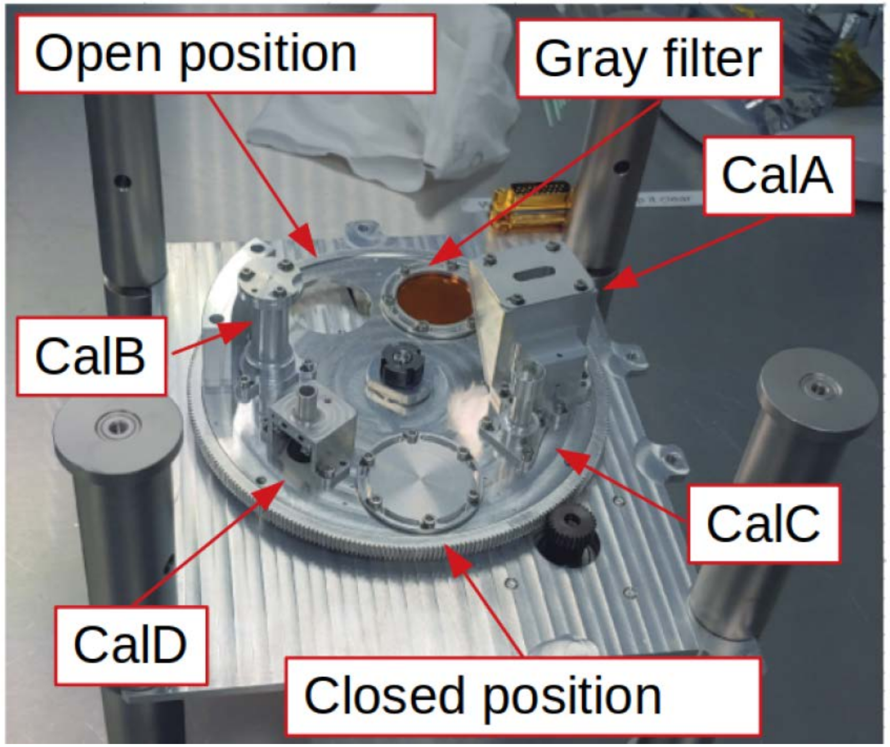

Ferrazzoli et al., 2020

^{55}Fe-powered calibration sources:

Cal A – Bragg-reflected polarized 2.98-keV (Ag-Lα fluorescence) and 5.89-keV (Mn-Kα)
Cal B – unpolarized 5.89-keV spot
Cal C – unpolarized 5.89-keV flood
Cal D – unpolarized 1.74-keV (Si-Kα fluorescence) flood

IXPE Imaging X-Ray Polarimetry Explorer

WE FIRSTLY APPLIED THE CALIBRATION TO CAS-A SPECTRUM

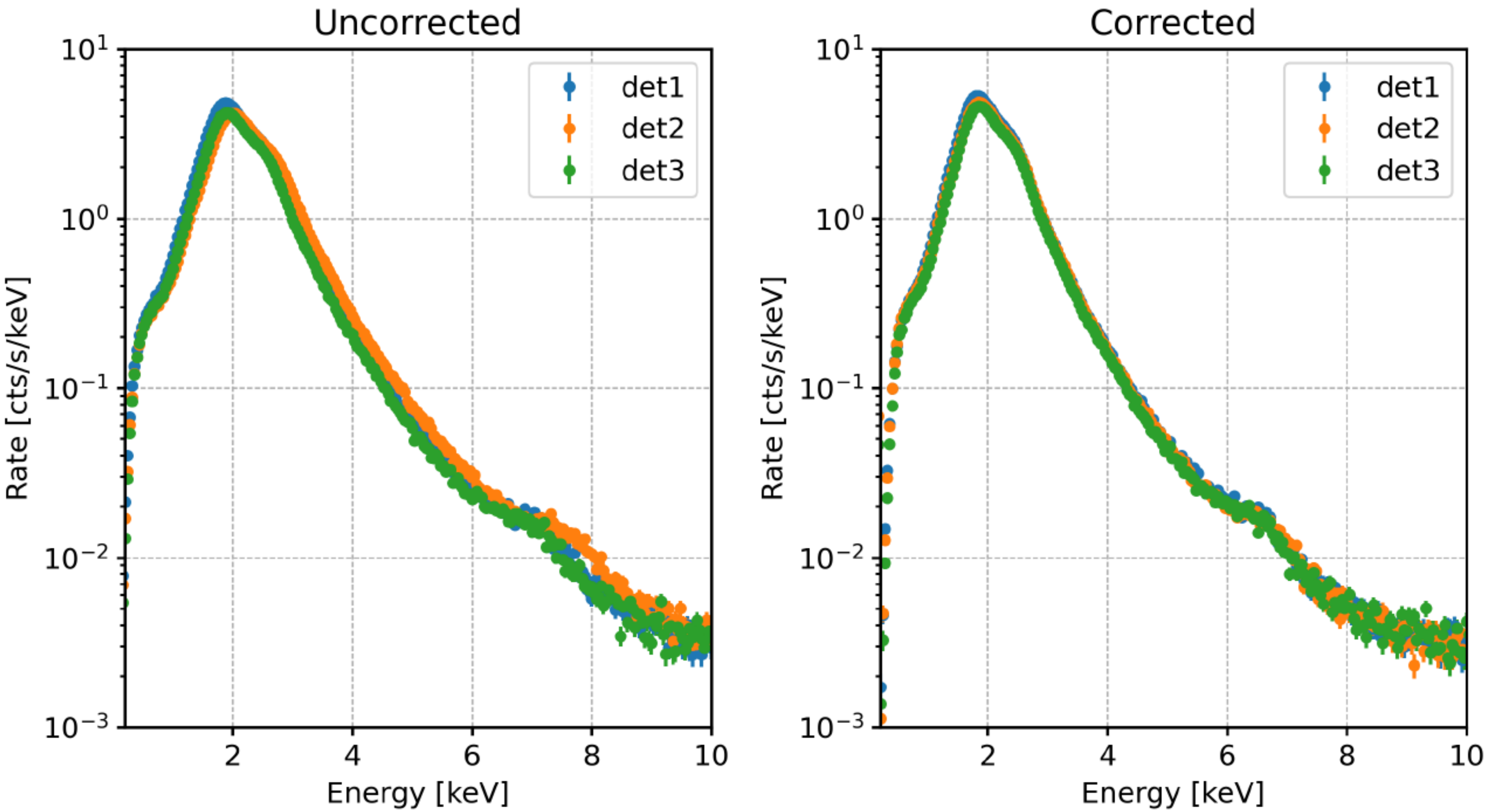

DETECTOR PROPERTIES

Parameter	Value
Sensitive area	15 mm x 15 mm (13 x 13 arcmin)
Fill gas and composition	DME @ 0.8 bar
Detector window	50-um thick beryllium
Absorption and drift region depth	10 mm
GEM (gas electron multiplier)	copper-plated 50-pm liquid-crystal polymer
GEM hole pitch	50 um triangular lattice
Number ASIC readout pixels	300 x 352
ASIC pixelated anode	Hexagonal @ 50-pm pitch
Spatial resolution (FWHM)	< 120 um (6.4 arcsec) @ 2 keV
Energy resolution (FWHM)	1.0 keV @ 6.4 keV (scaling as sqrt(E))
Useful energy range	2 - 8 keV

Mirror Module assembly properties

Property	Value
Number of modules	3
Mirror shells per module	24
Inner, outer shell diameter	162, 272 mm
Total shell length	600 mm
Inner, outer shell thickness	180, 250 um
Shell material	Nickel cobalt alloy
Effective area per module	163 cm^2 (2.3 keV) ~ 192 cm^2 (3-6 keV)
Angular resolution	< 30 arcsec HPD
Detector limited FOV	12.9 arcmin
Focal length	4 m
Mass (3 assemblies)	93.12 kg

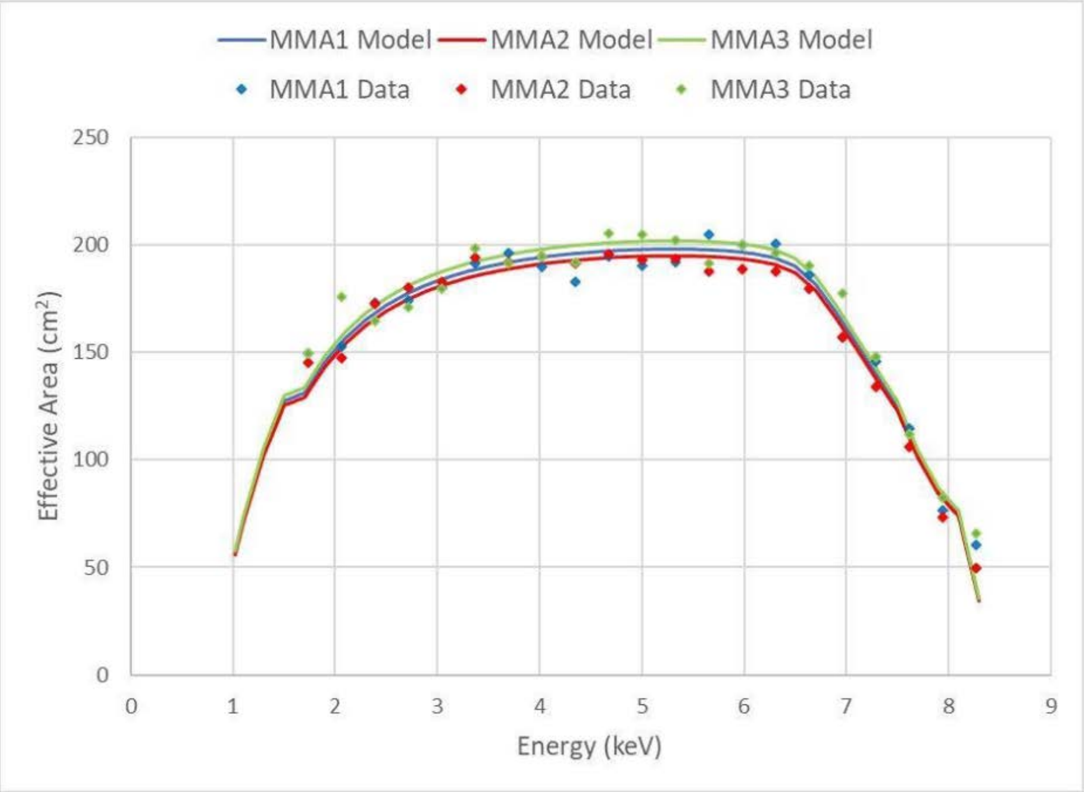

ANGULAR RESOLUTION

MMA	#1	#2	#3
6.4 keV	18.9"	24.8"	24.2"
4.5 keV	18.9"	25.0"	26.9"
2.3 keV	18.7"	24.5"	26.7"

Values in the table are half-power diameters (HPDs) for the individual MMAs alone.

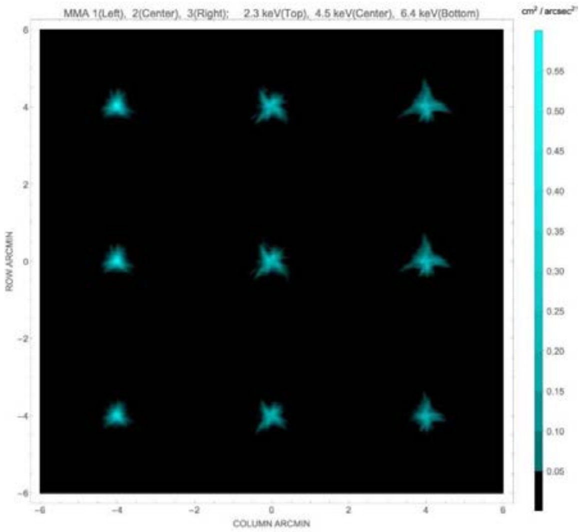

Point Spread Function (Mirror+Detector)

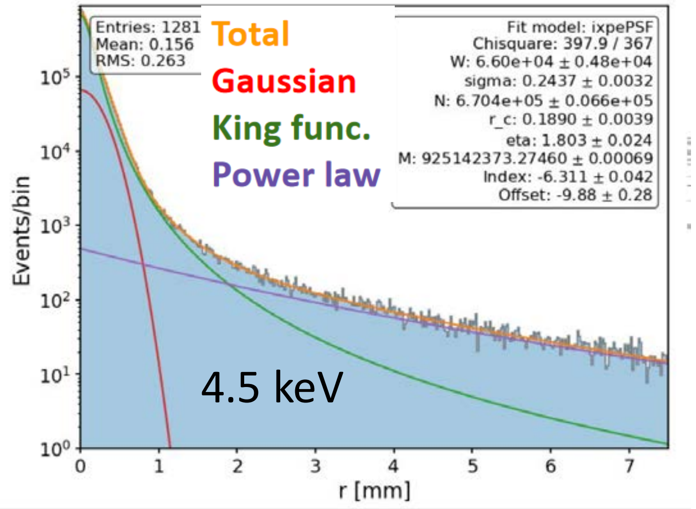

Based upon X-ray calibration, analysis, and on-orbit performance the telescope performance is = 30" HPD (25'' HPD for Telescope 1)

The presence of a power-law component in the Point Spread Function requires background subtraction be done only for dim sources not to subtract source photons

(see Di Marco, A. et al., ApJ 2023)

TOPICAL WORKING GROUPS ACTING IN THE FIRST TWO YEARS

Science Advisory Team (chaired by Giorgio Matt and Roger Romani)

Coordinates science activities required for planning, analyzing, interpreting, and reporting IXPE observations

Organized into seven Topical Working Groups

- *TWG1 **Pulsar Wind Nebulae**, led by Niccolò Bucciantini (INAF-Arcetri)*

Obtain polarimetric imaging to constrain the magnetic-field geometry of the nebula and the phase-dependent polarization of the pulsar

- *TWG2 **Supernova Remnants**, led by Pat Slane (CfA)*

Obtain spectral polarimetric imaging of Supernova Remnants (SNR) to constrain the magnetic-field structure of the X-ray emitting regions

- *TWG3 **Accreting Black Holes**, led by Michal Dovčiak (CAS-ASU) (Juri Poutanen. Next talk)*

Obtain spectral polarimetry of microquasars to constrain the value of the black-hole spin parameter (if in soft state), or constrain the geometry of the corona (if in hard state)

- *TWG4 **Accreting Neutron Stars**, led by Juri Poutanen (Turku) (Juri Poutanen Next talk)*

Obtain phase-dependent polarimetry of accreting X-ray pulsars (high-magnetic-field binaries) to constrain models and geometries for the pulsing emission. Obtain polarimetry of non pulsating accreting NS to constrain the geometry of the system

- *TWG5 **Magnetars**, led by Roberto Turolla (Uni Padua)*

Obtain phase-dependent polarimetry of magnetars to constrain the effects of vacuum polarization (birefringence in a strong magnetic field)

- *TWG6 **Radio-Quiet AGN & Sgr A**, led by Frédéric Marin (Strasbourg)*

Obtain polarimetry of RQ AGN to constrain the geometry of the emitting regions

- *TWG7 **Blazars & Radio Galaxies**, led by Alan Marscher (Boston U)*

Obtain polarimetry of Blazars and RG to study jet emission

About 75 different sources observed so far

RGB J0710+591 R		Number of objects
TWG -1	5 PWNe and isolated pulsars	Crab PWN, Vela PWN, MSH 15-52, PSR B0540-69, G21.5, 3C 58, PSR B1259-63
TWG-2	7 SNRs (8 pointings)	Cas A, Tycho's, NE SN 1006, RCW 86, RX J1713.7-3946, Vela Jr, RCW 86, SN1006SW
TWG-3	14 Accreting stellar-BH	Cyg X-1, 4U 1630-472, Cyg X-3, LMC X-1, SS433, 4U 1957-115, SS 433 Lobes, LMC X-3, SWIFT J1727.8-1613, 4U 1957+115, Swift J0243.6+6124, Swift J1727.8-1613, GX 339-4, SWIFT J151857.0-572
TWG-4	23 Accreting NS & WD	Cen X-3, Her X-1, GS1826-67, Vela X-1, Cyg X-2, GX 301-2, Xpersei, GX 9-9, 4U 1820, GRO J1008-57, XTE 1701-46, EXO 2030+375, LS V+44 17, GX 5-1, 4U 1624-49, Sco X-1, Cir X1, GX13+1, SMC X-1, SRGA J144459.2-604207, 4U 1538-52, V395 CAR, PSR J1023+00, GX 340+0, GX 3+1, 4U 1728-34
TWG-5	4 Magnetars	4U 0142+61, 1RXS J170849, SGR 1806-20, 1E 2259+586
TWG-6	5 Radio-quiet AGN & 1 Sgr A*	MCG 5-23-16, Circinus Galaxy, NGC 4151, IC 4329 A, Sgr A* Complex, NGC 1068
TWG-7	17 Blazars & radio galaxies	Cen A, S5-0716-714, 1ES 19-59-650, Mrk 421, BL Lac, 3C 454, 3C 273, 3C 279, Mrk 501,1ES 1959-650, BL-Lac, 1ES 0229-200, PG 1553 -113, S4 0954+65, 1E 2259+586, RGB J0710+591, H 1426+428

Some sources have been revisited
Mrk 421, Mrk 501, BL Lac, Vela X1, Her X-1, MCG 5-23-16, Crab, MSH 15-52, Cyg X-1, Sgr A (complex), NGC 4151 even Crab.

About 50 % of the observed celestial sources displayed a polarization with at least 6 σ significance in the Quick Look Analysis (Integrating in time, energy and position) . Resolved analysis showed polarization on a much larger number of sources.

TARGET OF OPPORTUNITIES (TOOS)

IXPE is not a Swift like mission

- Time for a TOO is not earlier than about 3 working days after the proposal
- GRB 221009A was indeed a special case TOO was requested on 10-10-2022 at 16:48 UTC and started on 10-11-2023 at 23:34:28 UTC
- We expect to trigger about one TOO per months.
- After a ToO started, the object that was in the long term planning is somewhat 'lost' and there is some discretion if it will be recovered later in the schedule

TOO (34 requested between new and pre selected 16 sources observed)

- Cyg X-1 (TWG 3)
- 4U 1630-472 (TWG 3)
- XTE 1701-46 (TWG 4)
- GRB 221009A No TWG
- EXO 2030 + 375 (TWG 4)
- Cyg X-3 (TWG 3)
- LS V + 44 17 (TWG 4)
- 4U 1630-47 (TWG 3)
- Swift J0243.6+6124 (TWG 4)
- 1ES 1959+650 (TWG 7)
- Swift J1727.8-1613 x 2 (TWG 3) multiple times
- GX 339-4 (BH, pre assigned)
- SRGA J144459.2-604207 (AMS, pre assigned)
- Swift J151857.0-572147 (BH)
- Cyg X-3 & Cyg X-1 (XL-Calibur simultaneous)
- 1E 1841-045

Mission	Allowed Sun Angle (deg)
HST	60-180 (+/-30 deg)
IXPE	65-115 (+/-25deg)
NICER	45-180
NuSTAR	43-180
SWIFT	47-180
XMM	70-110 (+/-20deg)

From HEASARC tools website

IXPE Allowed Sun Angle now increased up to +/- 34 deg

IXPE
Imaging X-Ray Polarimetry Explorer

Marshall Space Flight Center

agenzia spaziale italiana

THE CRAB NEBULA (BEFORE IXPE)

Radio (VLA)

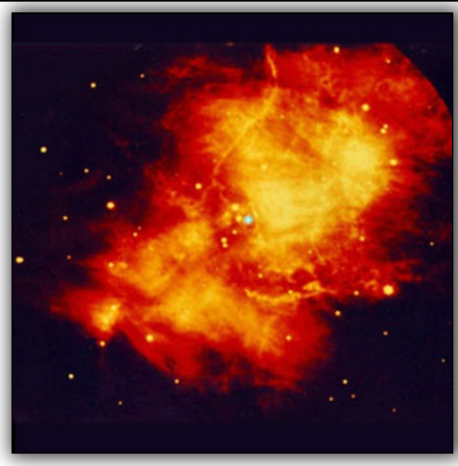

Infrared (Keck)

Optical (Palomar)

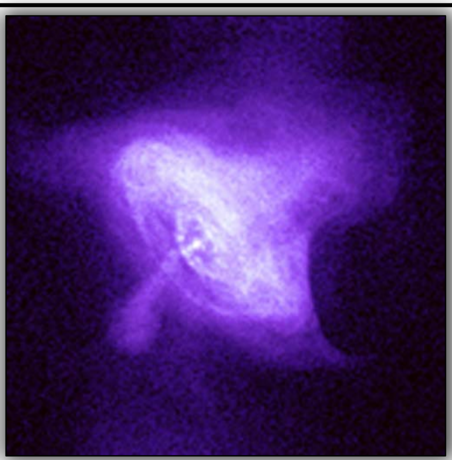

X-rays (Chandra)

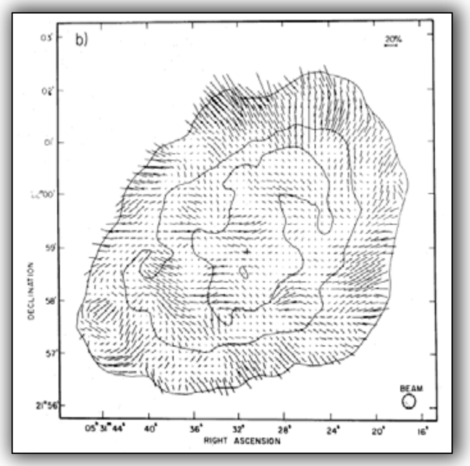

Radio polarisation

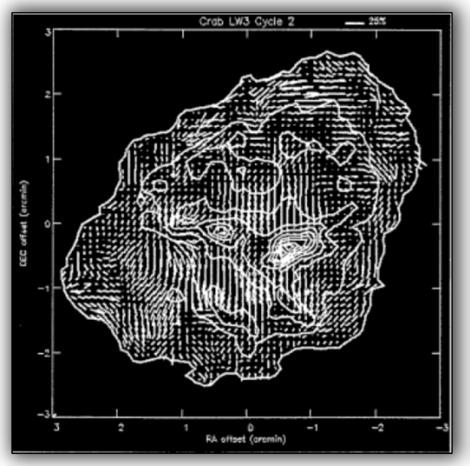

IR polarisation

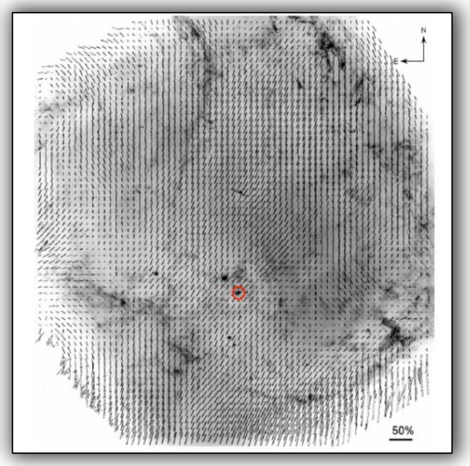

Optical polarisation

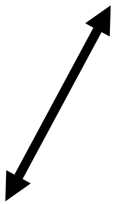

P=19% integrated over the entire nebula (Weisskopf et al. 1978)

X-ray polarisation

X-rays probe freshly accelerated electrons and their acceleration site

PWNe: Vela, Crab and MSH 15-52

Xie, F. et al., Nature, 2022

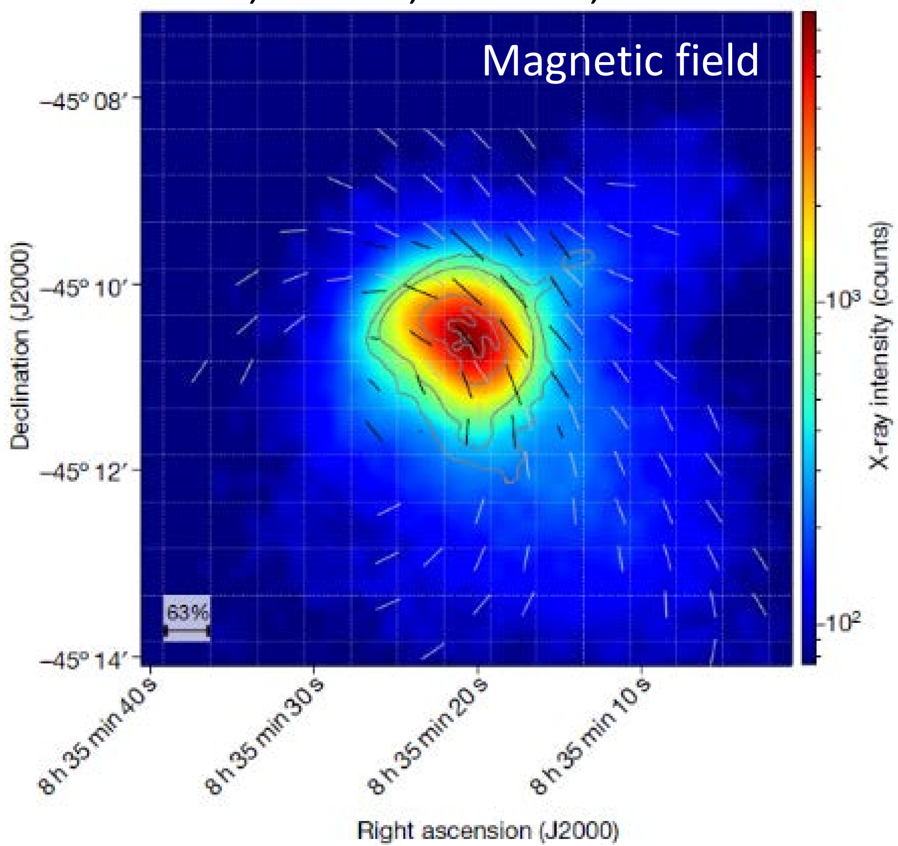

Bucciantini, N. et al., Nature Astronomy, 2023

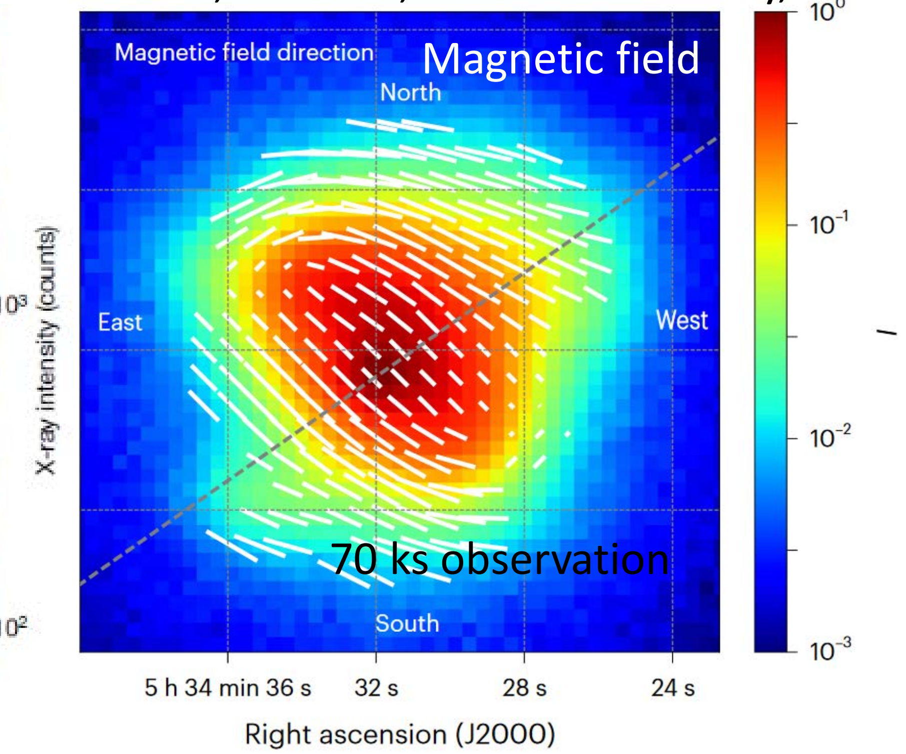

Romani, R. et al., ApJ, 2023

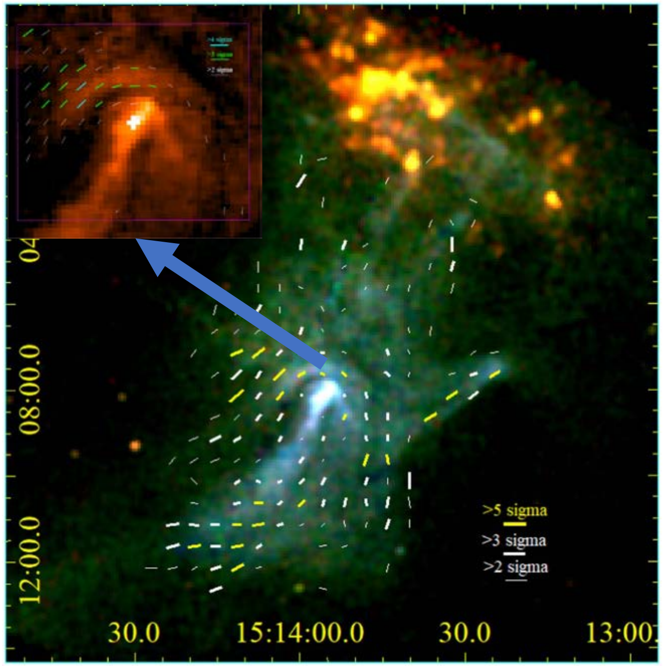

5 PWN observed so far

- High level polarization (Vela up to 63 %, Crab up to 45-50 %, MSH 1552 up to 70 %)->Turbulence less effective than expected.
- Vela polarization structure symmetric with respect to the spin which is parallel to its proper motion.
- Crab IXPE polarization angle is rotated 12° counter-clockwise with respect to OSO-8.
- MSH 15-52 IXPE polarization reaches 70% at the base of the jet, in the arc and in the thumb.

Crab Polarization map

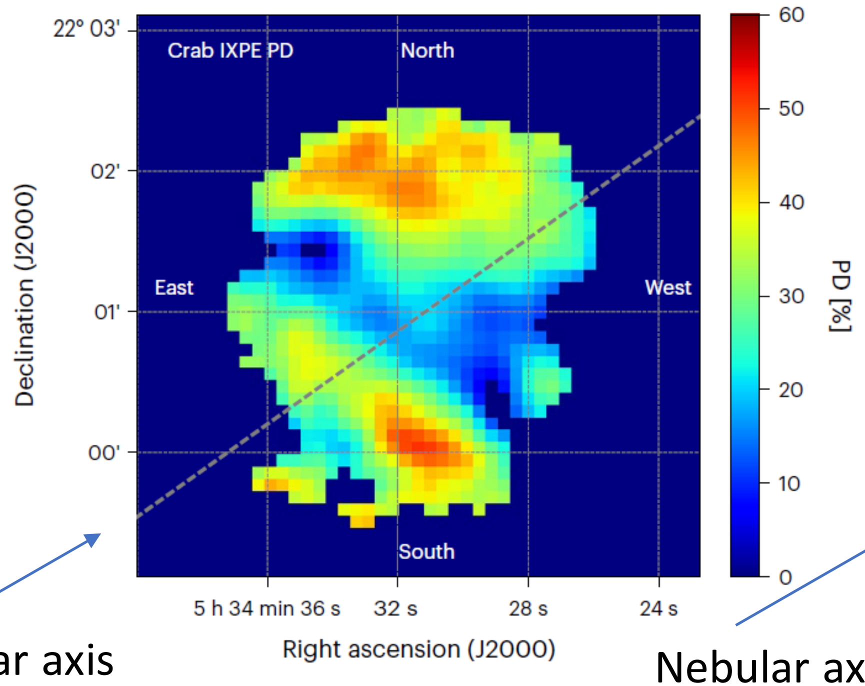

Nebular axis

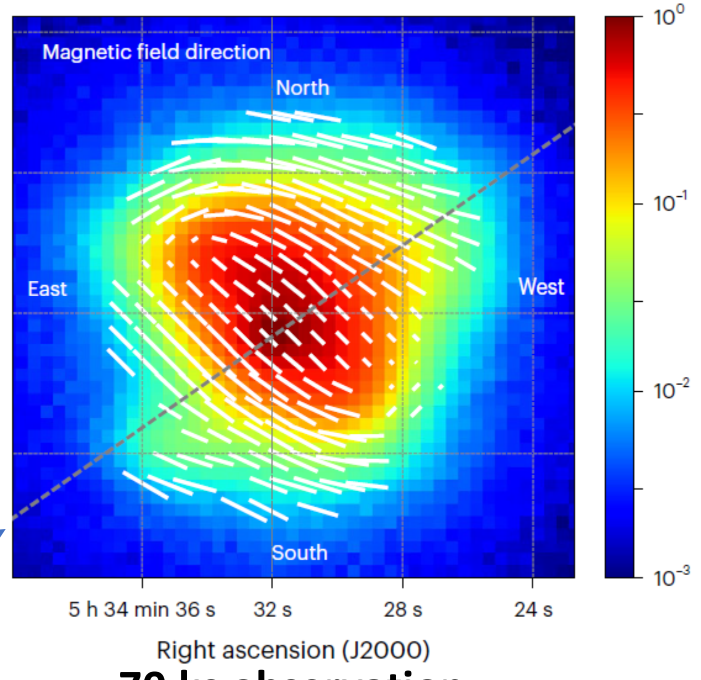

Nebular axis

70 ks observation

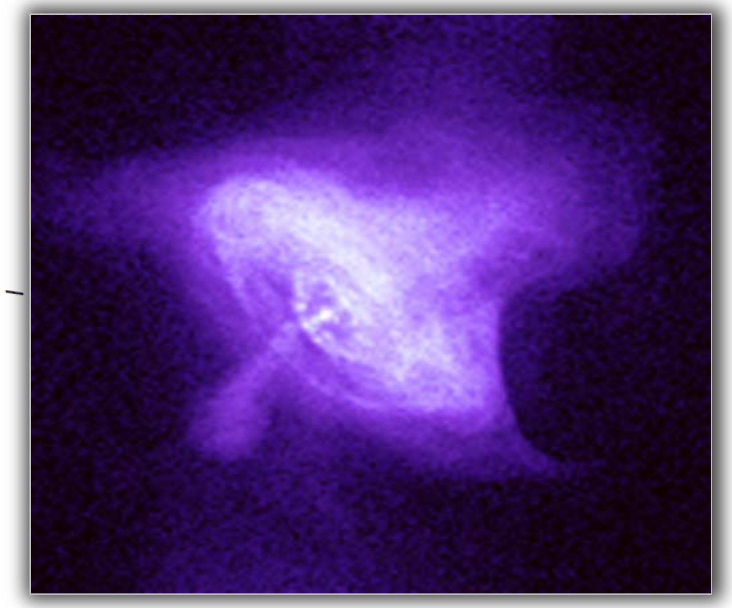

The map of the polarization degree (PD) shows two zones of high polarization and zones with low polarization due to the toroidal magnetic field and changing polarization angle (P.A.) .

The map of polarization degree is not symmetric with respect to the nebular axis. May be instabilities which randomizes the magnetic field are at work in the South-West region.

What about the pulsar ?

- Vela pulsar is too weak in the IXPE energy band

PSR B0531+21 (Crab PSR)

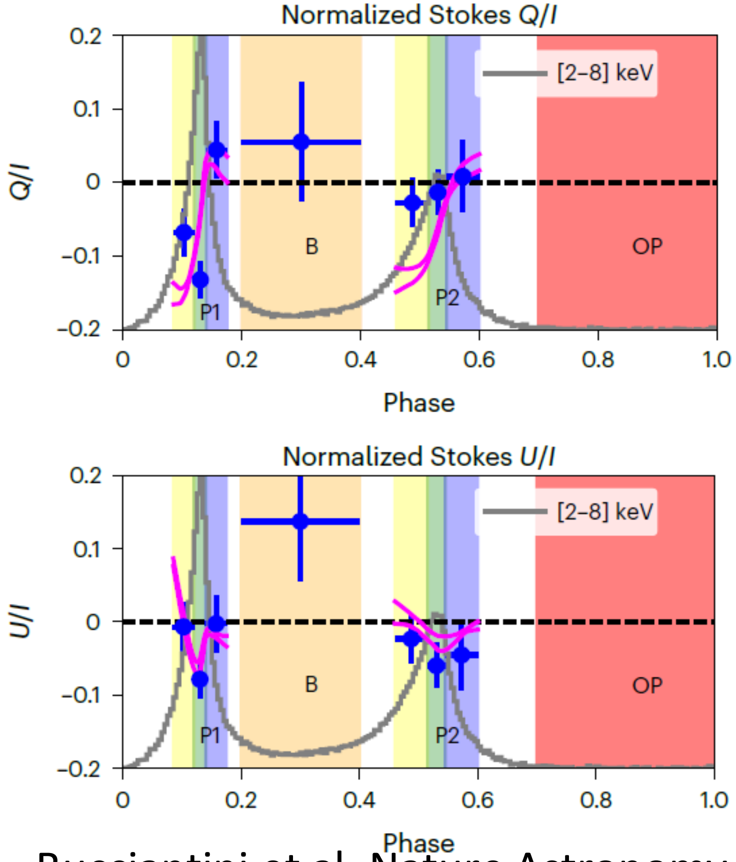

Bucciantini et al. Nature Astronomy 2023

Comparison with optical polarization data

Crab PSR: (70 ks observation)

- **Polarization is > 3-sigma significant in the central bin of P1 (Main Pulse)**
- **Total pulse signal is negligible**
- **Consistency with optical data is marginal. It sweep faster in X-ray than in optical.**

MSH 15-52 PSR:

- **Only the central bin of the peak has been detected with > 3-sigma (17.5 %)**
- **Other bins low PD 10-20 % 2-3-sigma**

PSR B1509-58 (MSH 15-52 PSR)

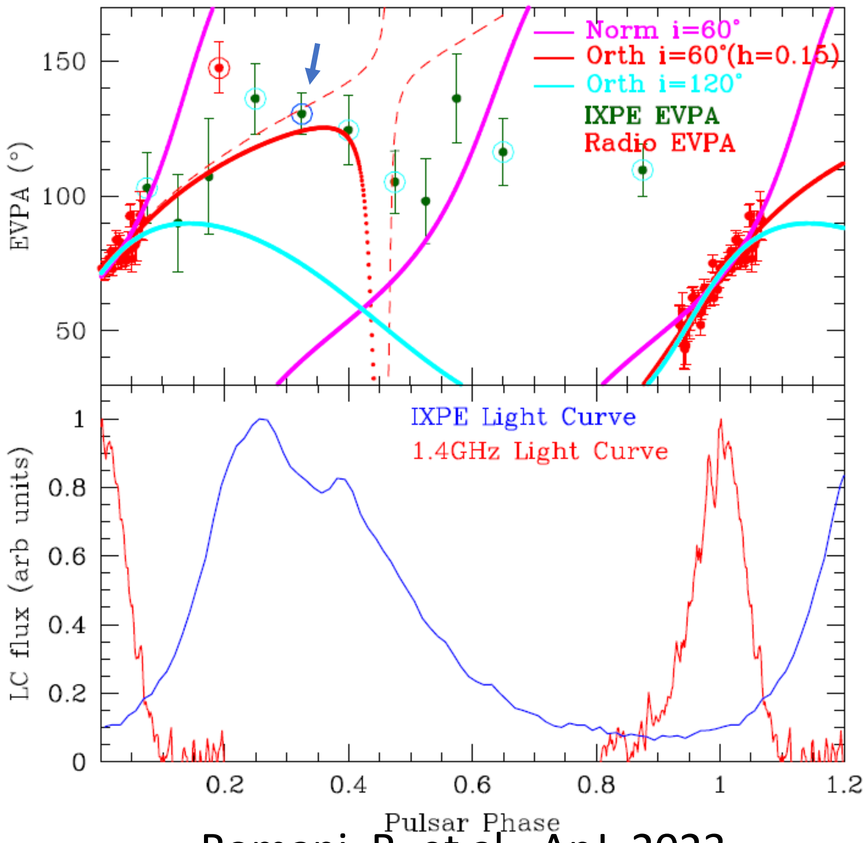

Romani, R. et al., ApJ, 2023

Comparison with radio polarization data

New observations for Crab! Wong, J. et al. 2024.

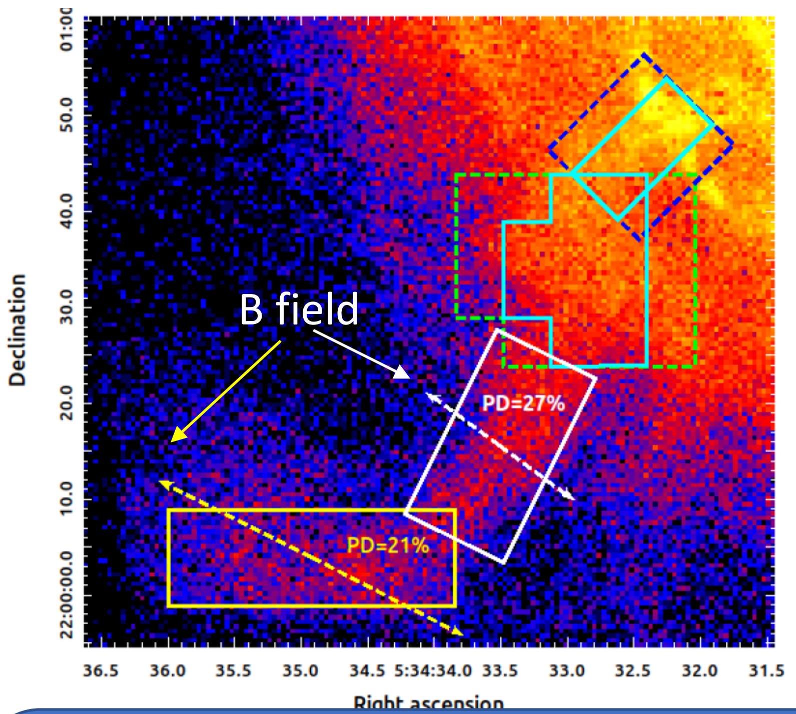

300 ks

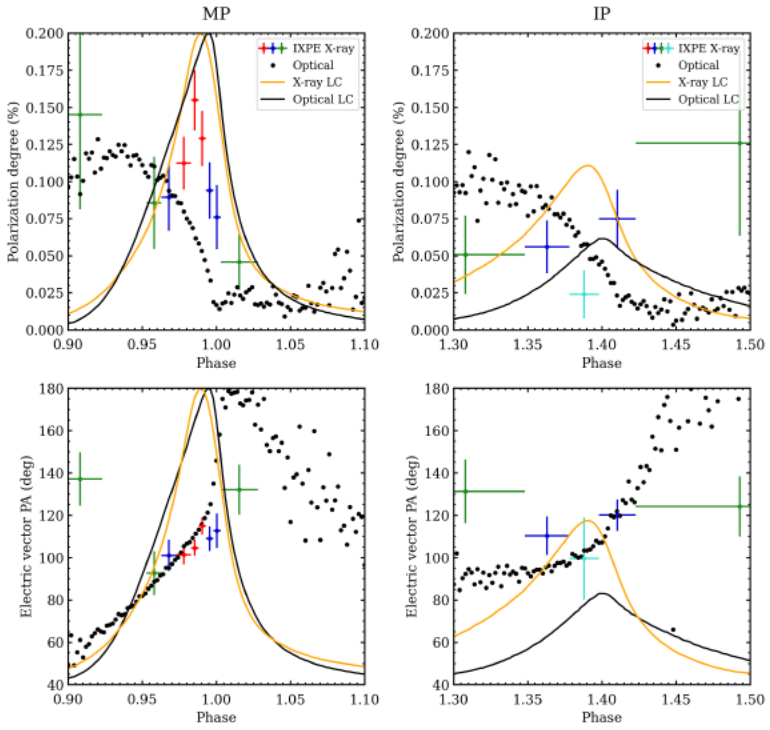

>5σ;
>3 σ
>1.9 σ

The new observation of Crab is confirming polarimetry of the nebula while providing additional points especially for the jet with perpendicular and parallel magnetic field (kink instabilities, or collision with a dense medium).

Additional points for the pulsar polarization especially for the main pulse are compared with the OPTIMA optical data Slowikowska (2009). Deviation in X-rays from the optical polarization degree is evident by the data in the main pulse.

IXPE & Super-Nova Remnants

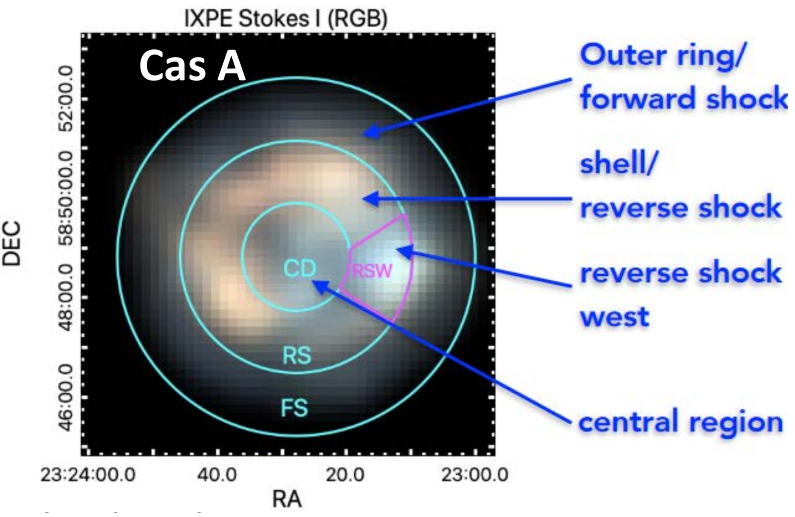

Core collapse, AD 1667?
Vink et al., 2022

- radio polarization 8-10 % outer region (radial B)
- X-ray low PD -> high turbulence close to the shock (**radial B**)

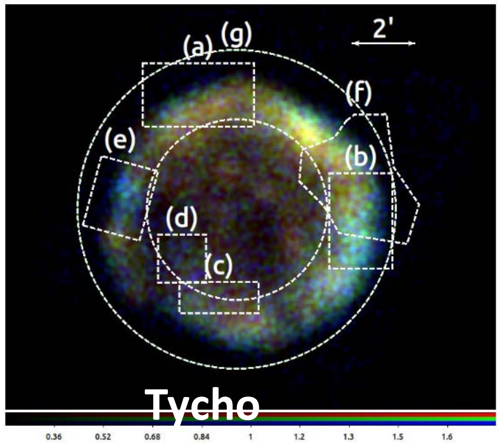

Type Ia, AD 1572
Ferrazzoli et al. ApJ 2023
Radio PD 8 % outer rim (radial B)
X-ray PD-> anisotropic turbulence (**radial B**)

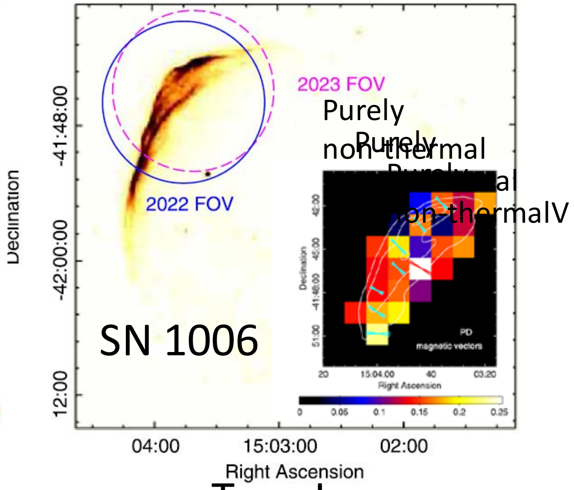

Type Ia
Zhou, P. et al., ApJ 2023
Radio PD 14% large Faraday rotation. X-ray High PD

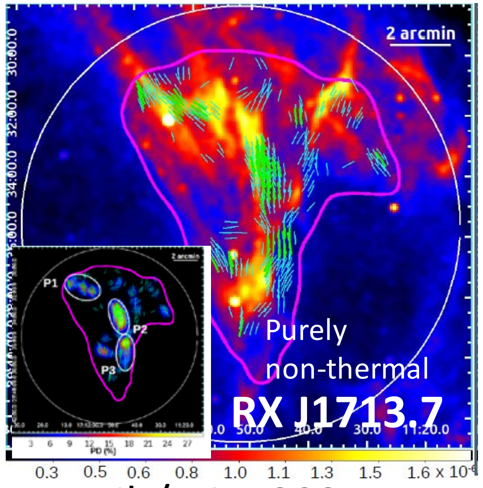

Type Ib/c AD 393
Ferrazzoli, R. et al., ApJ 2024
X-ray -> Shock compressed **tangential B**

	Polarization Degree (%) [a] Rim	SNR	Peak	V_{shock} (km s^{-1})	n_0 (cm^{-3})	Bohm Factor (η)	B_{low}^{b} (μG)
Cas A	4.5 ± 1.0	2.5 ± 0.5	∼15	∼5800	0.9 ± 0.3	∼1–6	25–40
Tycho	12 ± 2	9 ± 2	23 ± 4	∼4600	∼0.1–0.2	∼1–5	30–40
SN 1006 (NE)	22.4 ± 3.5	...	31 ± 8	∼5000	∼ 0.05–0.08	∼6–10	18–26
RX J1713 (W)	13.0 ± 3.5	...	46 ± 10	1400–2900	∼0.01–0.2	∼1.4	∼10

(a) X-ray polarization degree for SNR rim, entire SNR, and peak value within SNR. (b) Lower limit to post-shock magnetic field based on rim width, e.g., [20].

Slane, P. et al. 2024

Shell region	IXPE XSPEC PD (%)	PA (°)	Γ	χ/d.o.f.	Radio PD_{radio} (%)
All	12.0 ± 3.1	93.7 ± 7.4	2.11 ± 0.04	1.10	4.5 ± 1.7
N+S	12.5 ± 3.3	96.7 ± 7.6	2.04 ± 0.04	1.02	4.8 ± 1.4
N	12.3 ± 3.8	114.0 ± 8.9	2.10 ± 0.04	0.99	4.8 ± 1.8
S	19.3 ± 4.7	79.0 ± 7.1	2.21 ± 0.05	0.91	4.8 ± 0.9
W	< 25.6	ND	2.04 ± 0.06	1.22	3.2 ± 1.6
P1	25.2 ± 6.7	135.3 ± 7.6	2.16 ± 0.08	0.93	5.6 ± 1.1
P2	35.6 ± 7.6	103.8 ± 6.1	2.21 ± 0.08	0.90	3.5 ± 1.4
P3	36.9 ± 9.1	76.0 ± 7.0	2.23 ± 0.10	1.03	5.2 ± 0.9

Cas A, Tycho and SN1006: both radio and X-rays point to radial magnetic field → Turbulent magnetic field and realignment close to the shock: They show a relative increase of the polarization: decreasing level of turbulence
The ambient density is decreasing: it might be an environment dependence of the turbulence
RX J1713.7 is the oldest of the sample and it shows magnetic field which is tangential to the shock front.

- **Anomalous X-ray Pulsars and Soft-gamma ray repeaters**
  - $P \approx 2 - 12$ s $\quad \dot{P} \approx 10^{-14} - 10^{-10}$ s s^{-1}
  - $B_{sd} \approx 10^{14} - 10^{15}$ G
  - $L_{X,\mathrm{persist}} \approx 10^{35} - 10^{36}$ erg s^{-1} (typically $> \dot{E}_{\mathrm{rot}} = 10^{33}$ -10^{34})
  - Bursting activity (short bursts – intermediate/giant flares)
  - Enhanced activity in transient sources (outbursts)
  - Two components (two thermal or thermal plus PL) spectra

  - **Powered by their own magnetic energy**

A twisted magnetic field is coupled to flowing charged particles which up-scatters (power law, resonant Compton scattering) the radiation emitted from the neutron star surface (Thermal).

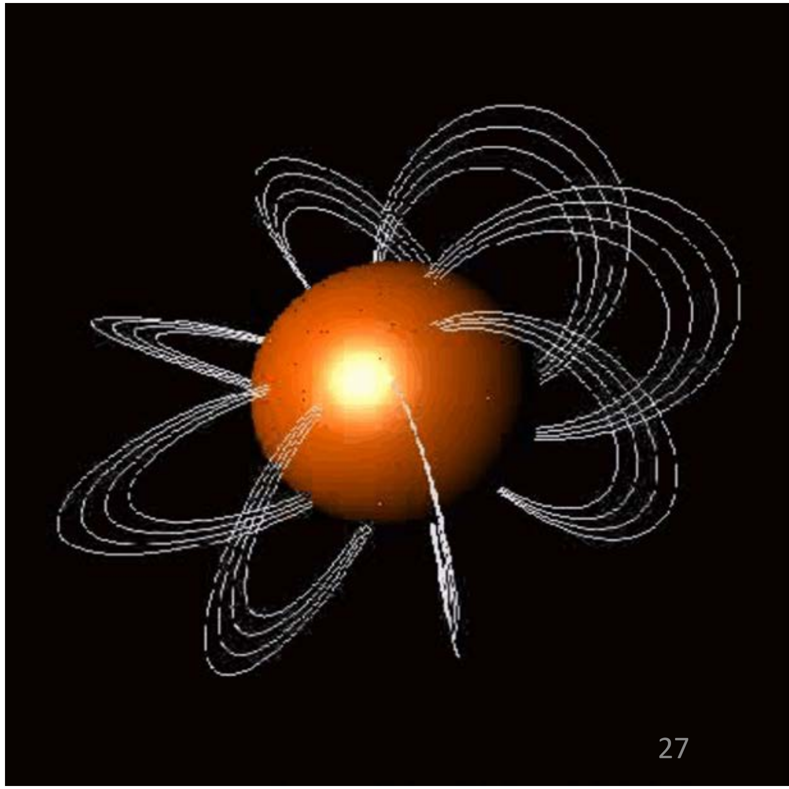

Magnetars

Taverna et al. , Science 2022

4U 0162+61 B=1.5 10^{14} G

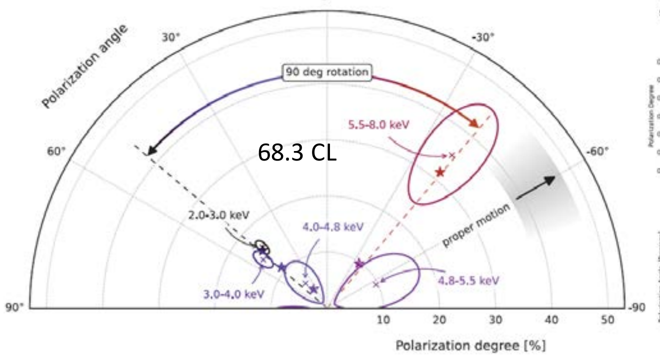

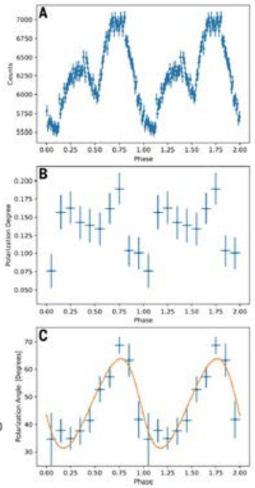

Zane et al. ApJL 2023

1RXS J170849.0-400910

B= 5 10^{14} G

68.3 CL

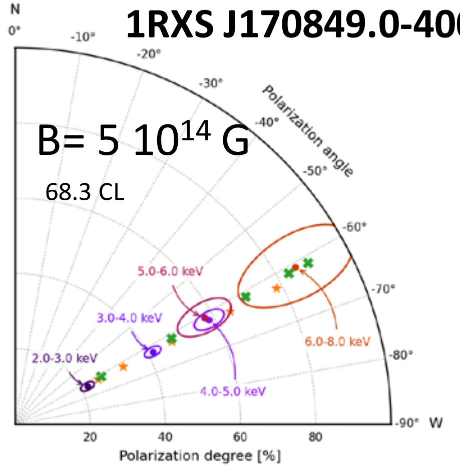

Turolla et al., ApJ 2023

SGR 1806

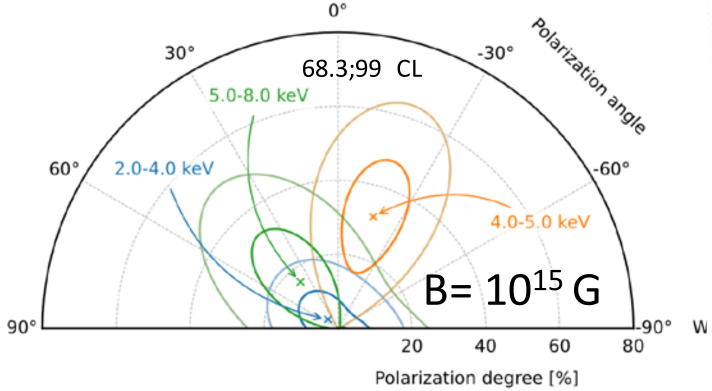

Heyl et al., 2024

1E 2259+586

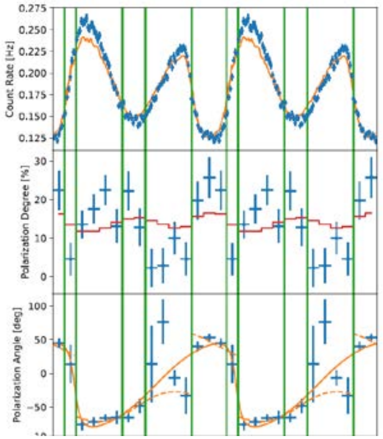

Equatorial belt condensed surface (low energy-O mode). Resonant Compton Scattering at high energy (X-mode)

Black-Body + Power-law

PD = 13.5±0.8%; PA = 48.5°±1.6°

Condensed equatorial belt region (low-P) plus hot polar spot with on-top an atmosphere (high P).

2 Black-Body

PD = 35.1±1.6%; PA = 62.1°±1.3°

Only upper limits (record low-flux). Hint of behavior similar to 4U 0162+61

B= 6 10^{13} G

PD = 5.6±1.4%;

PA =-75.2°±7.4°

Hot condensed spot + plasma loop

The magnetars observed by IXPE have very different polarization dependence with energy may be due to the fact that the atmosphere have different pattern for each one.

The long searched vacuum polarization and birefringence is not definitively proofed because the emitting area is rather small. To eventually prove this QED effect we need small pulsed fraction and high polarization degree detected.

The Radio Quiet AGNs

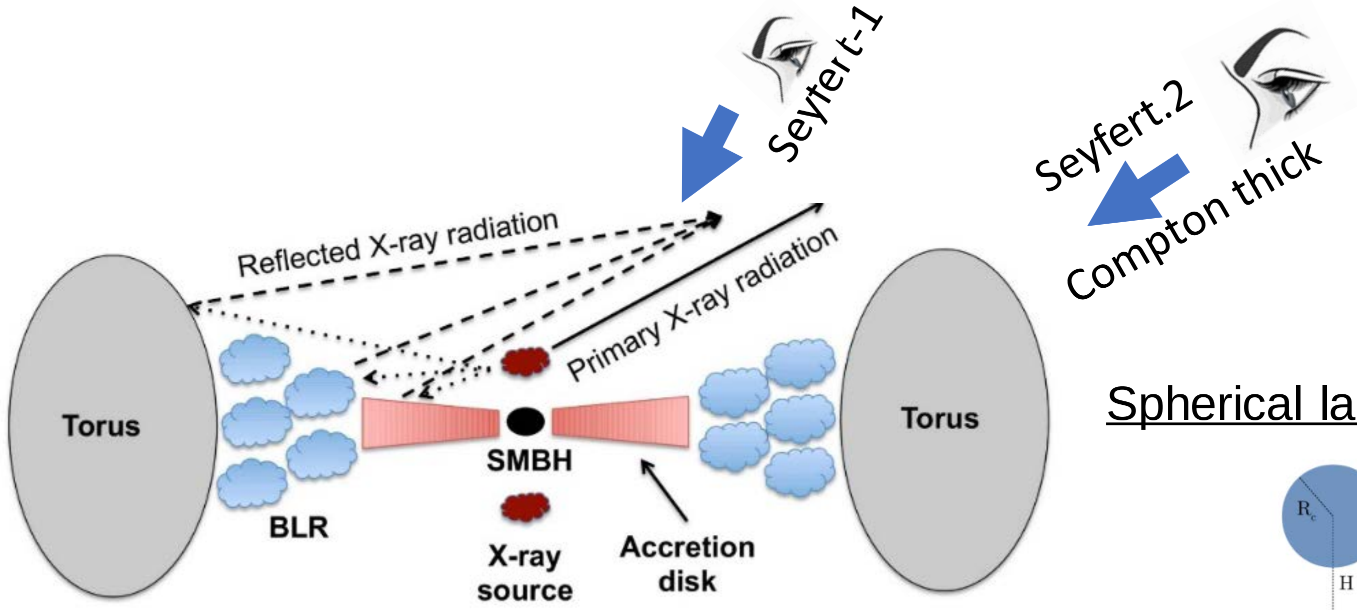

Physical parameters of the AGN's corona are degenerate with respect to geometry. Polarimetry can help to break this degeneration and determine the origin of the corona

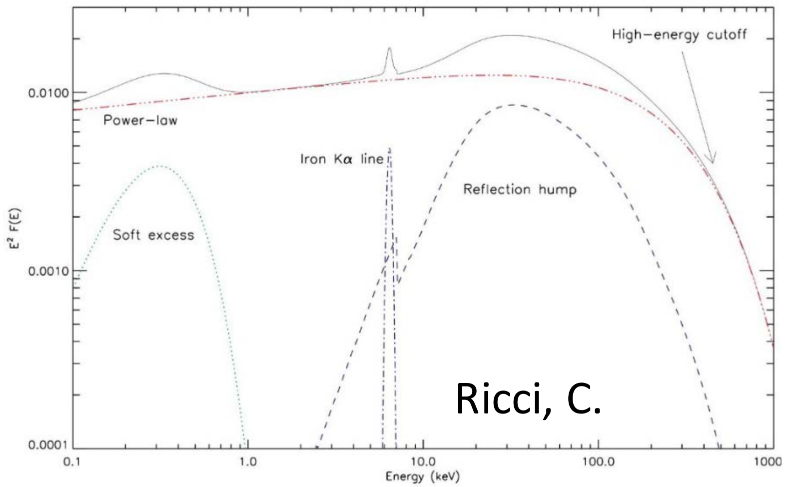

Ricci, C.

Spherical lamppost

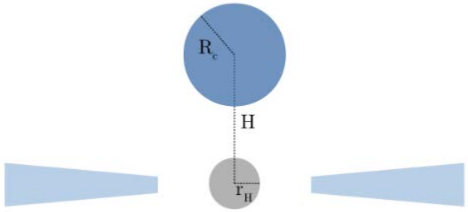

PD: 0-2%
PA: perpendicular to the disc axis;
Phenomenological model

Slab corona

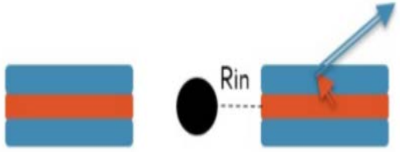

PD: up to 14%;
PA: parallel to the disc axis;
Magnetic loops?

Conical outflow

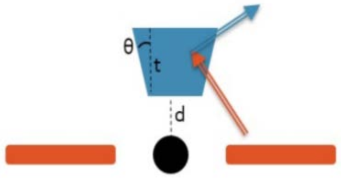

PD: up to 6%;
PA: perpendicular to the disc axis;
Base of a jet?

(Tagliacozzo, D. presentation@ IXPE collaboration)

Radio Quiet AGNs (Seyfert-1)

Physical parameters of the AGN’s corona are degenerate with respect to geometry.
Polarimetry can help to break this degeneration.

MCG-5-23-16 (Sefert-1)

Tagliacozzo, D. et al., MNRAS, 2023

PD < 3.2 % (99 % C.L.)

(68, 90, 99) %

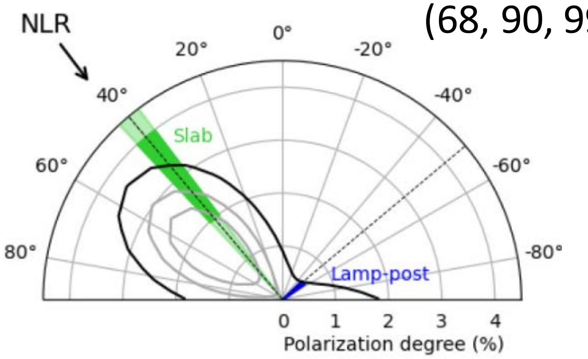

Relativistic ionized reflection + neutral reflection + cutoff power-law (95%)

IC4329A (Sefert-1)
Ingram, A. et al., MNRAS, 2023
3.3+/-1.1 %

Marginal hint of 90°jet

Extended radio emiss.

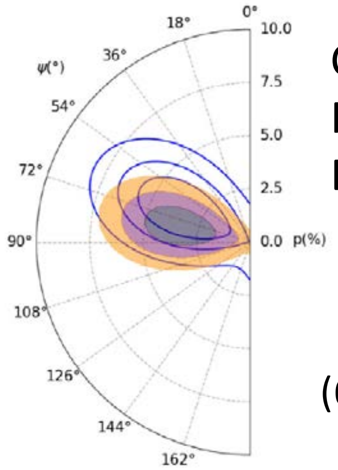

Coronal (66%);
Relat. Refl. (33%)
Distant Refl. (1%)

(68, 90, 99) %

NGC-4151
(Seyfert-1)

Gianolli V, et al MNRAS 2022,
A&A 2004 Submitted.
PD=4.5±0.9%,
(68, 90, 99) %

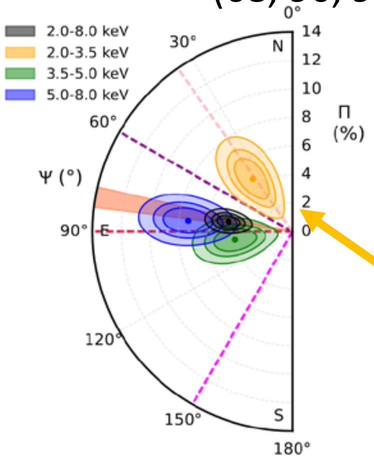

Radio emission
Inner few pc jet
Narrow Line Reg.
Torus axis

Scattering ?

Polarimetry of NGC 4151 showed the corona of the primary emission is not a lamp post but it is parallel to the disk.
MCG-5-23-16 and IC4329A suggest with low significance the same geometry.

IXPE helps to constrain the geometry of the corona.

MCG 05-23-16 (Tagliacozzo et al. 2023)

Simulations with MONK

NCG 4151 (Gianolli et al 2023)

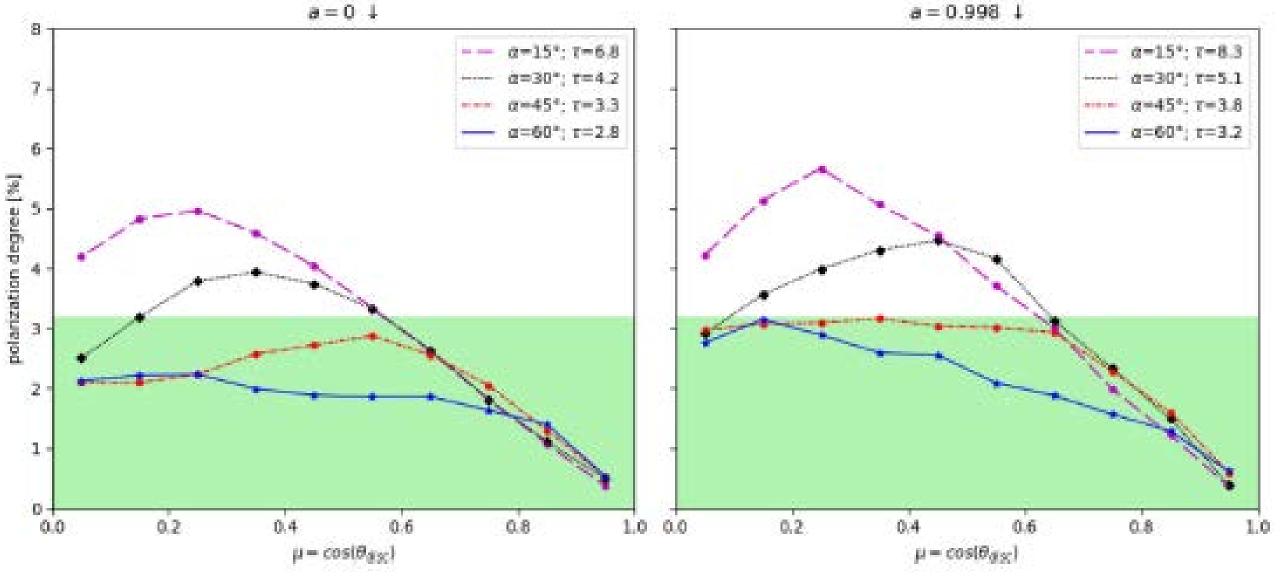

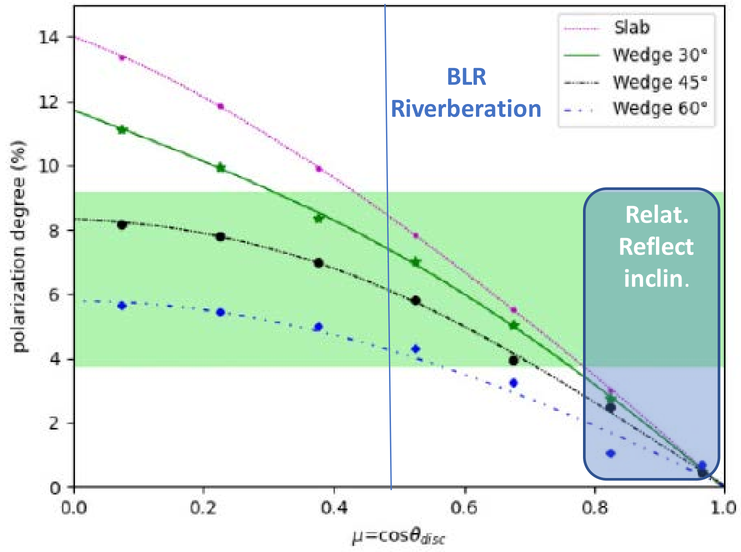

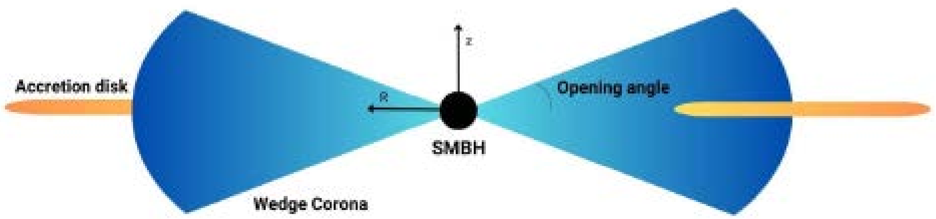

For both MCG 05-23-16 and NGC 4151 Slab o Wedge geometry of he corona are consistent with the IXPE data. NCG4151 favors disk inclinations obtained by reverberation and disfavor inclination obtained by spectra

Radio Quiet AGNs (Seyfert-2)

Circinus galaxy (Compton thick)
Ursini et al., MNRAS 2023

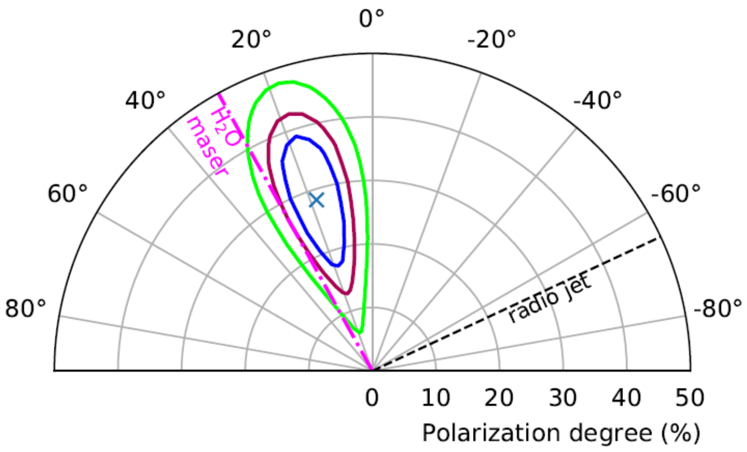

68 %, 90 % 99 %

The cold reflector (torus) IXPE measured a 2-6 keV polarization of:
P = 28 %+/- 7% and Theta = 18° +/-5°

NGC-1068 (Seyfer-2 archetypical)
(Marin et al. 2024)

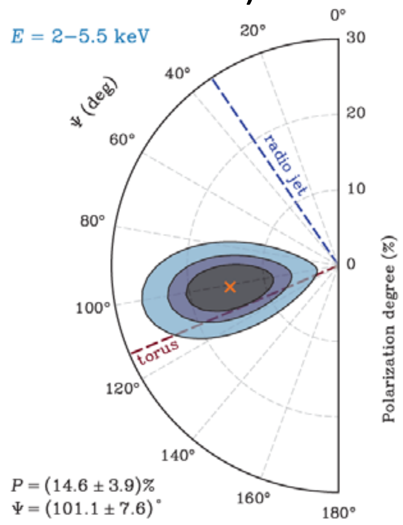

68 %, 90 % 99 %

1.15 Ms observation!
P=12.4%±3.6%
Theta=100.7°±8.3°

Assuming a polarization due to the warm reflector (conical winds) similar to UV
The torus reflection is polarized P = 20%+/-10%
Theta=102°+/-15°

X-ray spectro-polarimetry in Circinus galaxy and NGC-1068 showed that the pc-scale torus axis and the radio jet are aligned. The torus is responsible for the reflected radiation

IXPE HELPS TO CONSTRAIN THE TORUS OPENING ANGLE

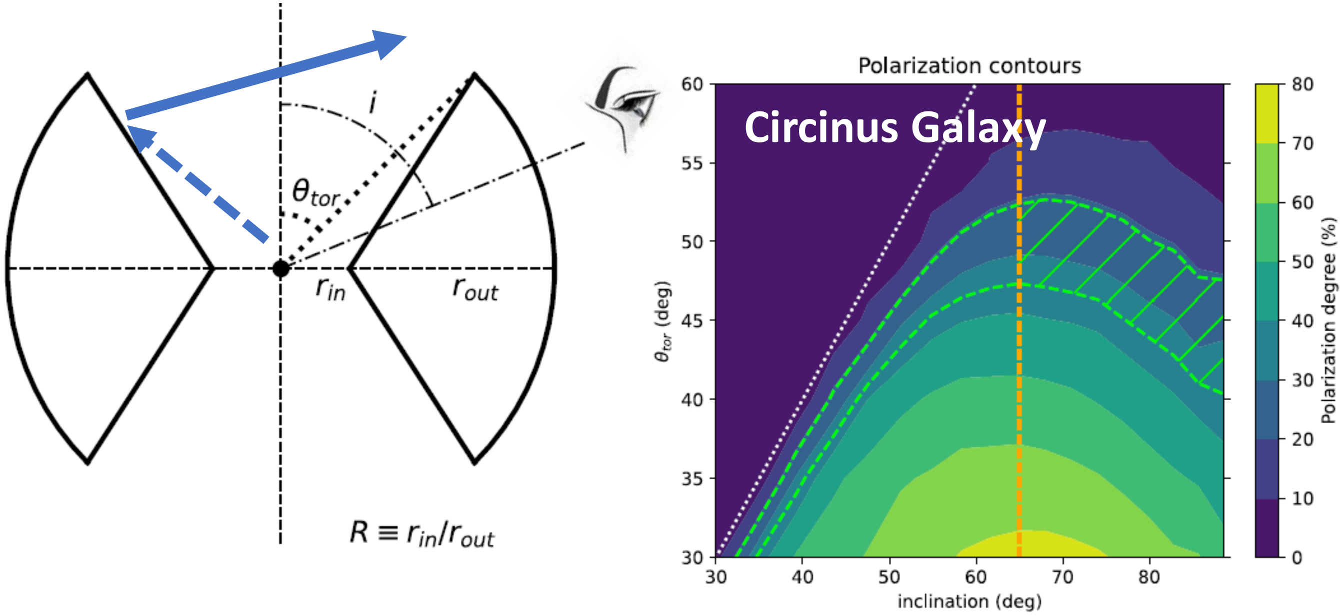

The orange vertical line set the lower limit to the inclination as provided by the inclination of the galaxy. The dashed lines mark the 68% confidence level region consistent with the measured polarization of the cold reflector. The hashed region mark the constraints on inclination and torus aperture.

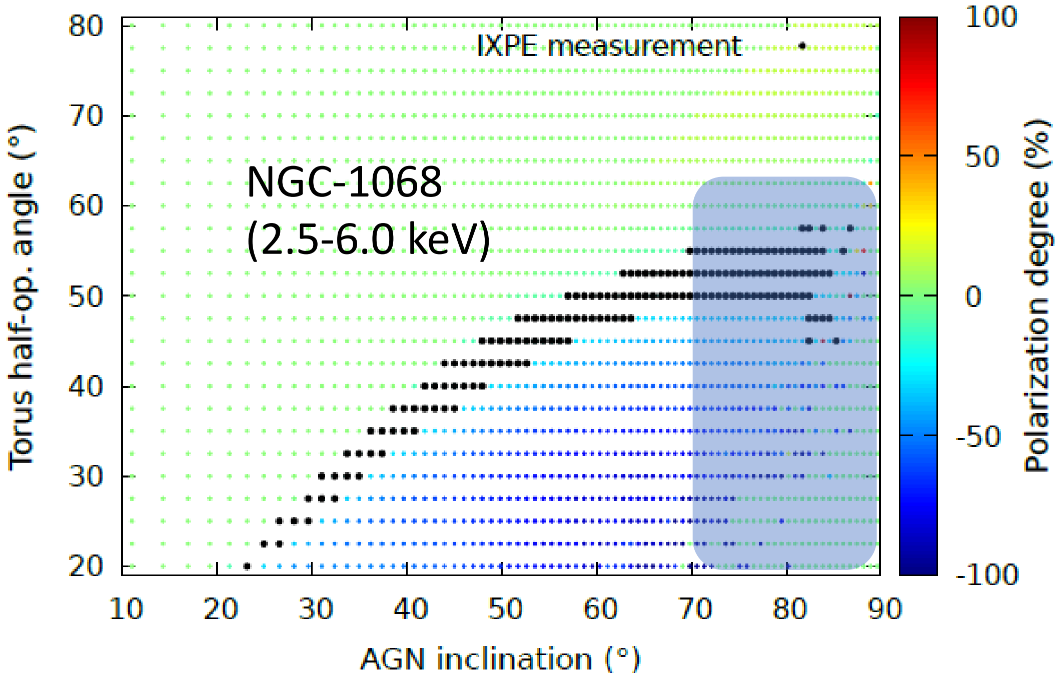

The positive polarization is parallel to the jet, the negative polarization is perpendicular to the jet. Each colored dot represent a simulation. Black dots are consistent with IXPE polarimetry. Shaded region is the constraint from the literature on the torus inclination.

For both Circinus galaxy and NGC-1068 X-ray polarimetry constraints on the torus aperture are similar 50º-55º

900 x 400 LY OF THE GALACTIC CENTER AS SEEN IN X-RAYS BY CHANDRA

117 arcmin; color code : **1-3 keV** ; **3-5 keV**; **5-8 keV**

36 arcmin

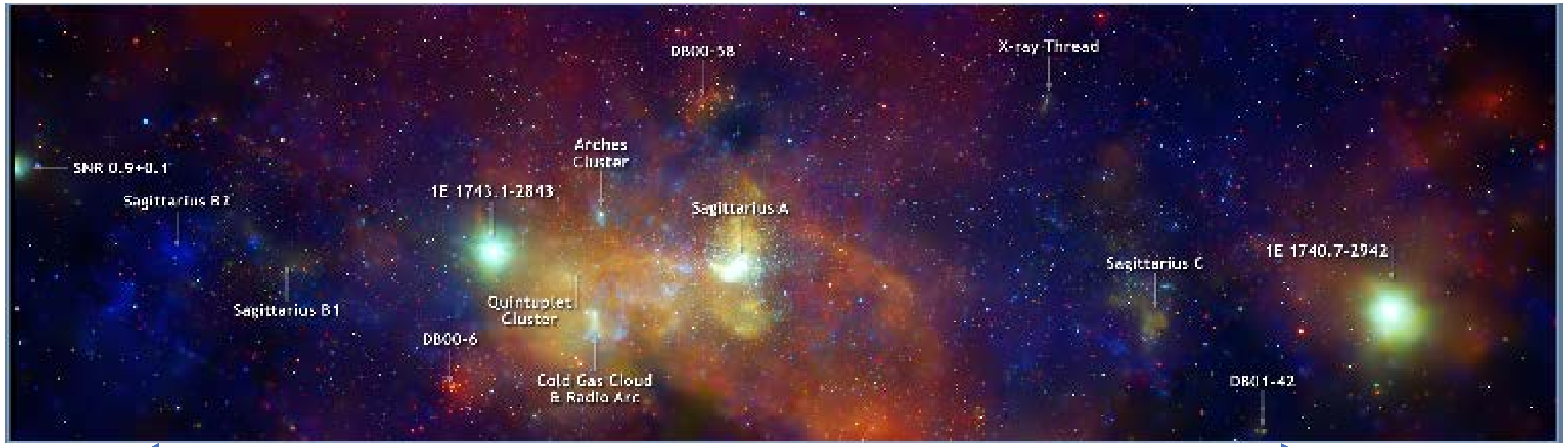

Center Nebular Zone

Sunyaev et al., 1993

Sgr B2

Sgr C

Sgr A Complex

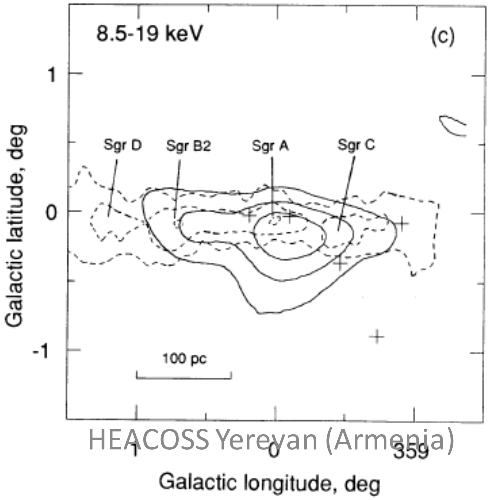

Art-P on GRANAT

Sunyaev et al., suggested that part of the emission in the galactic center region could be due to Thomson scattering by dense molecular clouds of the radiation coming from the galactic center.

CHURAZOV, SUNYAEV & SAZONOV PROPOSED TO USE X-RAY POLARIMETRY !

X-ray polarimetry can definitively proof or reject this hypothesis.

Molecular clouds should be highly polarized with the electric vector perpendicular to the line connecting the two sources.

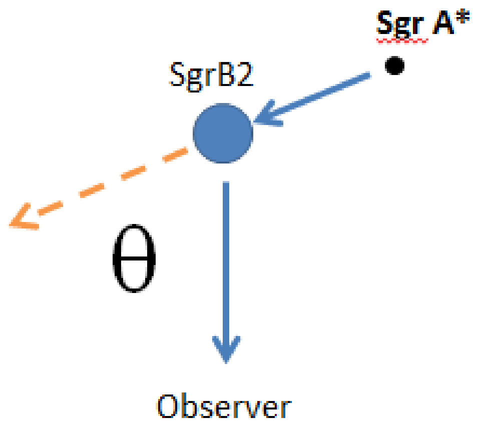

$$P = \frac{1-\mu^2}{1+\mu^2}$$

$$\mu = \cos\theta.$$

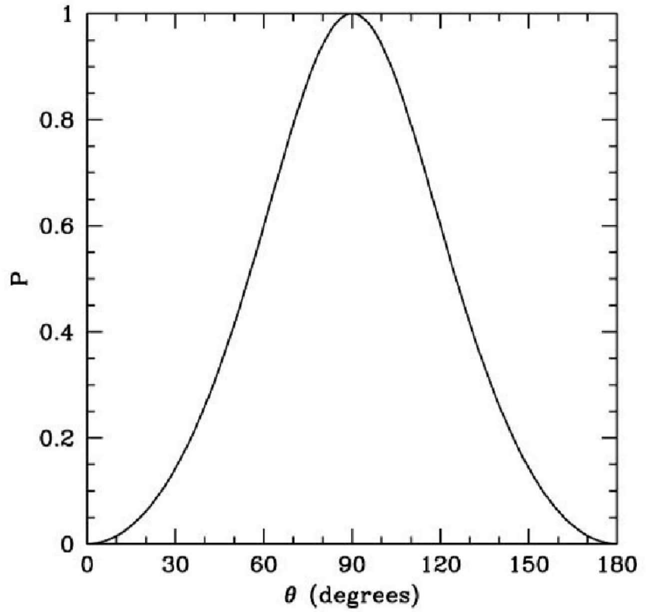

The polarization direction of the scattered radiation is **perpendicular** to the scattering plane.

The degree of polarization would measure the angle and provide a full 3-d representation of the clouds (Churazov, Sunyaev & Sazonov, 2002)

First problem: SgrB2 vanishes !

In Astronomy usually extended sources vary on a time scale longer than the time needed to select and build a satellite. But this was not our case.
The flux varies with a rapidity unusual for extended sources as from an external cause. There is evidence that the reflection components moves as for radiation coming from the side of the center (already in Koyama+ 2001; see e.g. Ponti+ 2010, Clavel+2013, Churazov+2017, Terrier+ 2018)

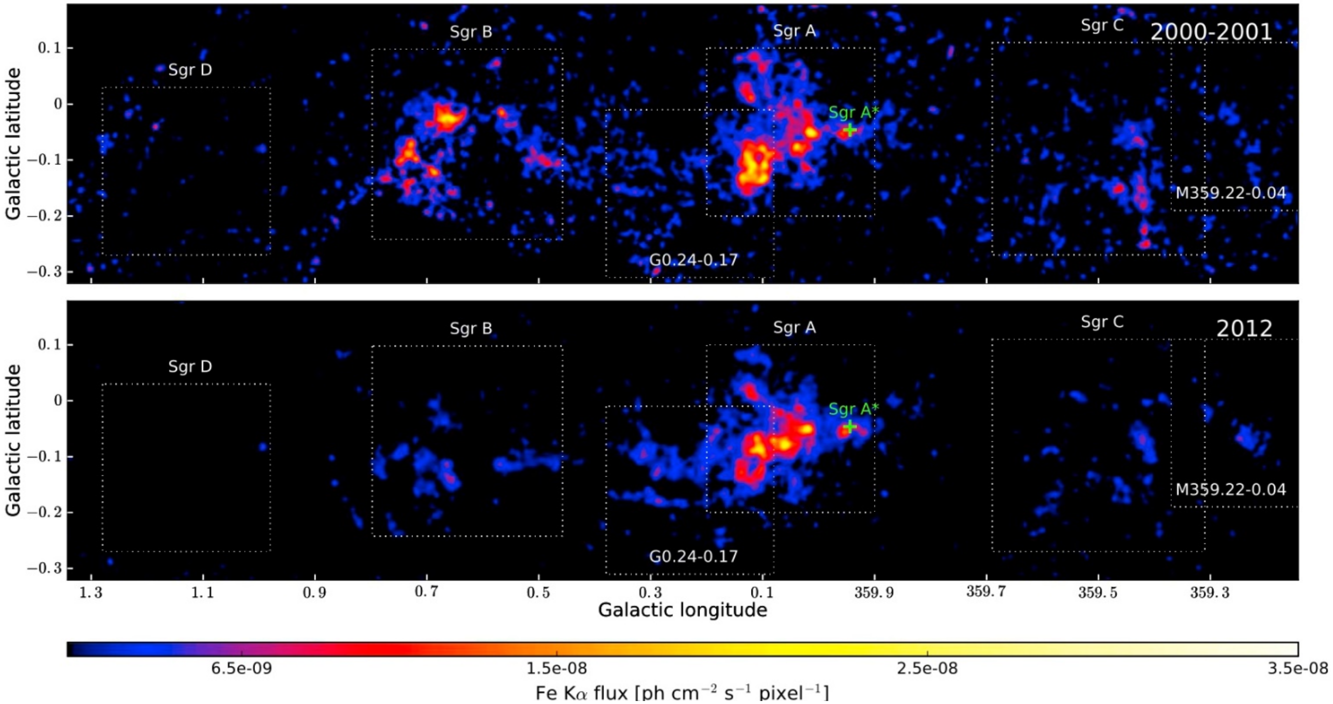

The concept that clouds are reflecting past activity of a source not far from SgrA* is favored. But, waiting for a Polarimetry mission, SgrB2 brightness decreases significantly and makes it no more attractive as a target. Study for alternative targets is performed. It becomes more deep in the proximity of IXPE launch. (Marin 2015, Churazov+ 2017, DiGesu 2019, Ferrazzoli+ 2021).

From talk E. Costa @ MG17

WHAT HAVE WE DONE?
WE SELECTED DIFFERENT CLOUDS BASED ON CHANDRA OBSERVATION

A research lead by Frederic Marin, supported by Eugene Churazov, Laura Di Gesu, Riccardo Ferrazzoli, ………
In the frame of the Radio Quiet AGN TWG.

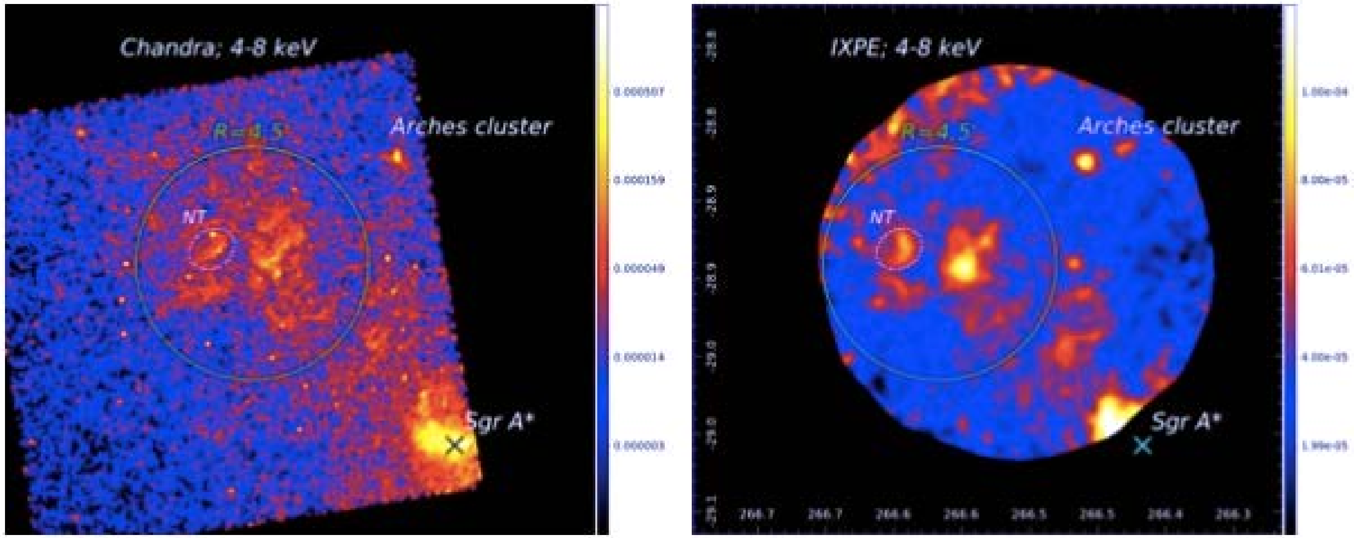

We required an full overlap (the same exposure) for the three Detector Units. Each Unit has a square f.o.v. but they are mounted at 120° each other. Also we avoid regions near the edge of each detector because local conversion background and uncomplete inclusion of tracks can mimic polarization. The result is a circle

From talk E. Costa @ MG17

SECOND PROBLEM: THE PRESENCE OF TWO TEMPERATURE PLASMA CHANDRA SPECTRUM TO DETERMINE THE INGREDIENTS

From Chandra Data we can model a 4-components spectrum

1) A lower temperature plasma (continuum + lines) unpolarized.
2) A higher temperature plasma (continuum + lines) unpolarized
3) Fluorescence lines unpolarized
4) Scattered continuum polarized

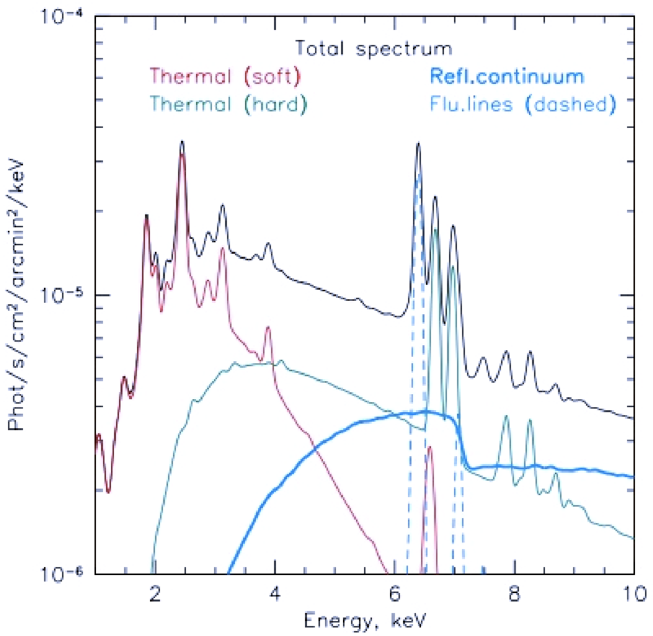

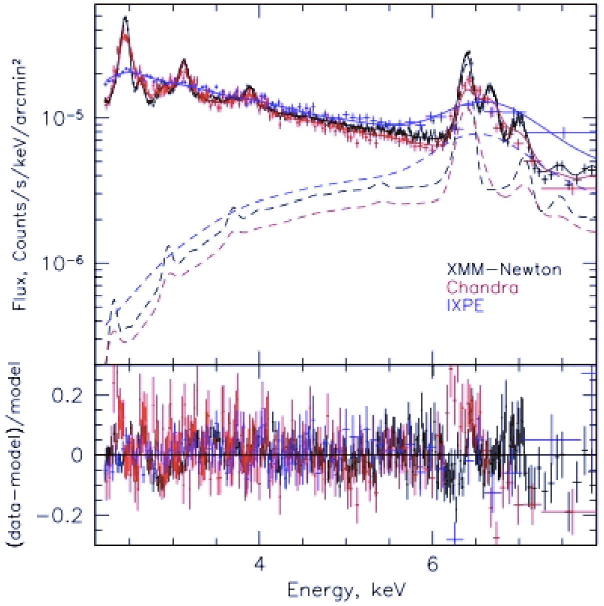

IXPE energy resolution is around 6 times worse than Chandra. Chandra can allow:

- **Select the energy band**
- **Select the best regions**
- **Derive the polarization of the scattered component from the polarization of the whole**

THE GALACTIC CENTER WAS ACTIVE 200 YEARS AGO !

Marin, F., Churazov, E. et al., Nature 2023

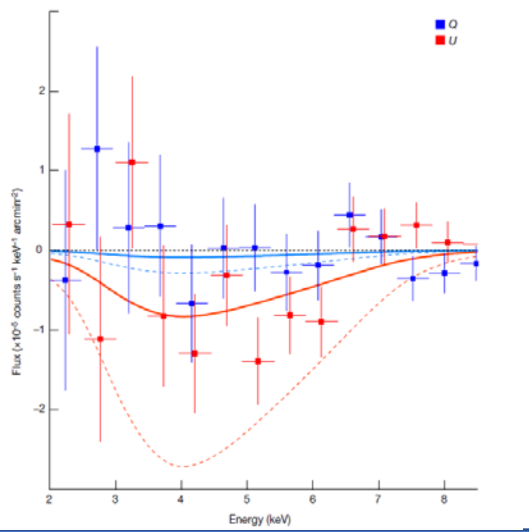

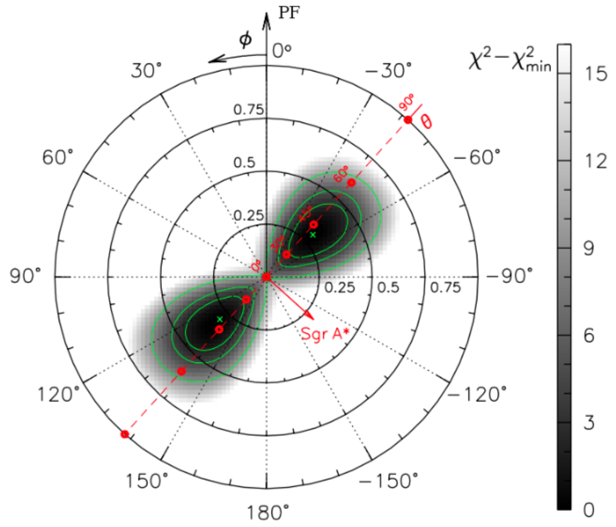

Ponti et al., N&V 2023

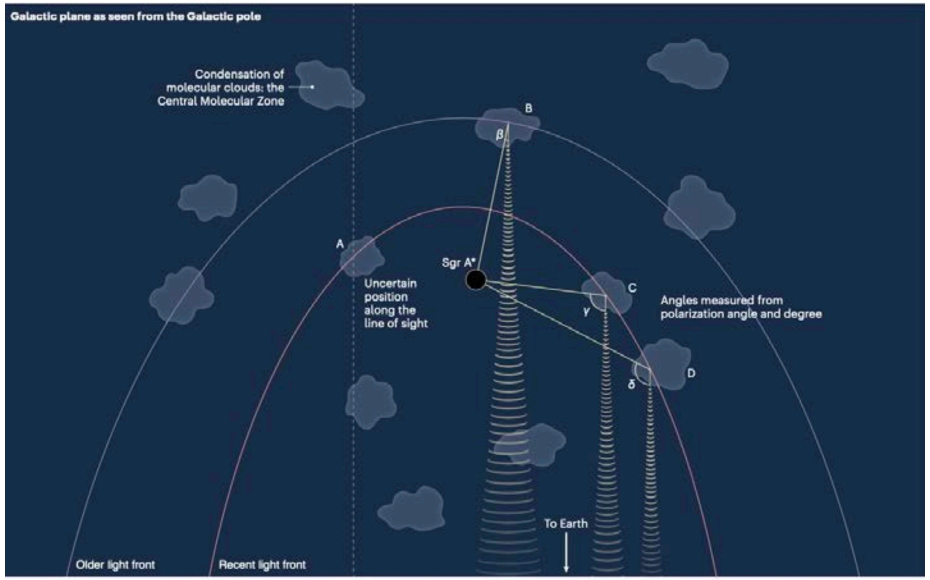

Very difficult measurement!

2.8σ result. P = (31 +/-11)% θ = -48º+/-11º

Polarization angle consistent with Sgr A* as the origin of the illuminating radiation.

From the polarization degree, two solutions for the age of the burst: ~30 or ~200 years ago. Second solution much more probable a flare 30 years old should have been visible by ASCA who detected bright molecular clouds but dim SgrA*

NASA IXPE Imaging X-Ray Polarimetry Explorer

BLAZARS

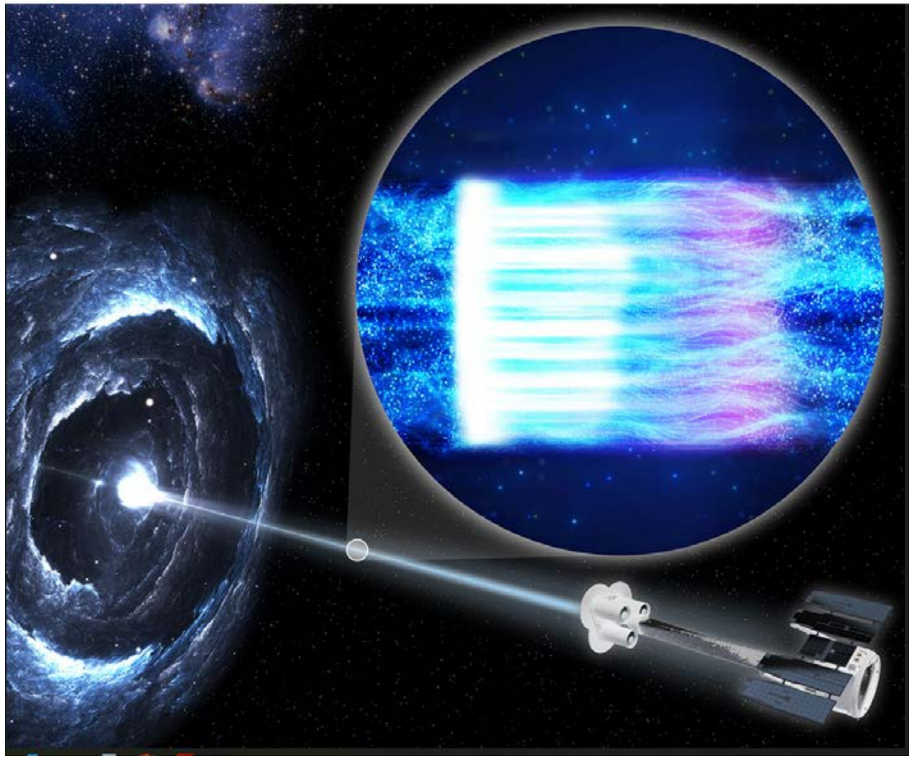

Synchrotron-dominated (with X-ray) Blazars, multi-λ polarimetry probes **the structure** of the jet and of its **magnetic field**

Inverse Compton dominated (with X-ray) Blazars, multi-λ polarimetry observations can determine:

- **the composition of the jet** (hadronic vs. leptonic, Zhang & Bottcher, 2013)
- **the origin of the seed photons** Synchrotron-Self Compton (SSC) or External Compton (EC) (Celotti & Matt, 1994; Poutanen 1994)

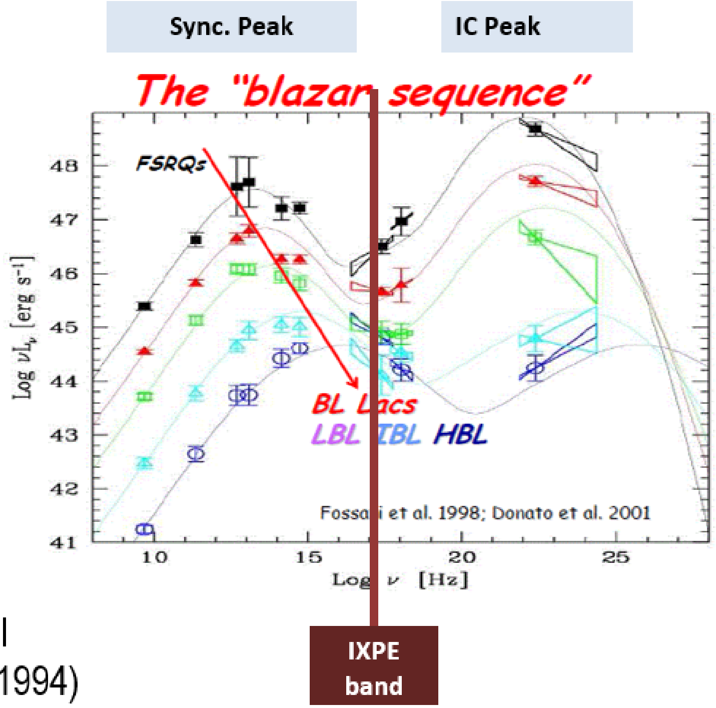

A blazar is an active galactic nucleus (AGN) with a relativistic jet directed closely towards the observer. Relativistic beaming from the jet makes blazars appear much brighter than they would be if the jet were pointed in a direction away from Earth.

MRK-501 & MRK-421

Liodakis et al., Nature 2022

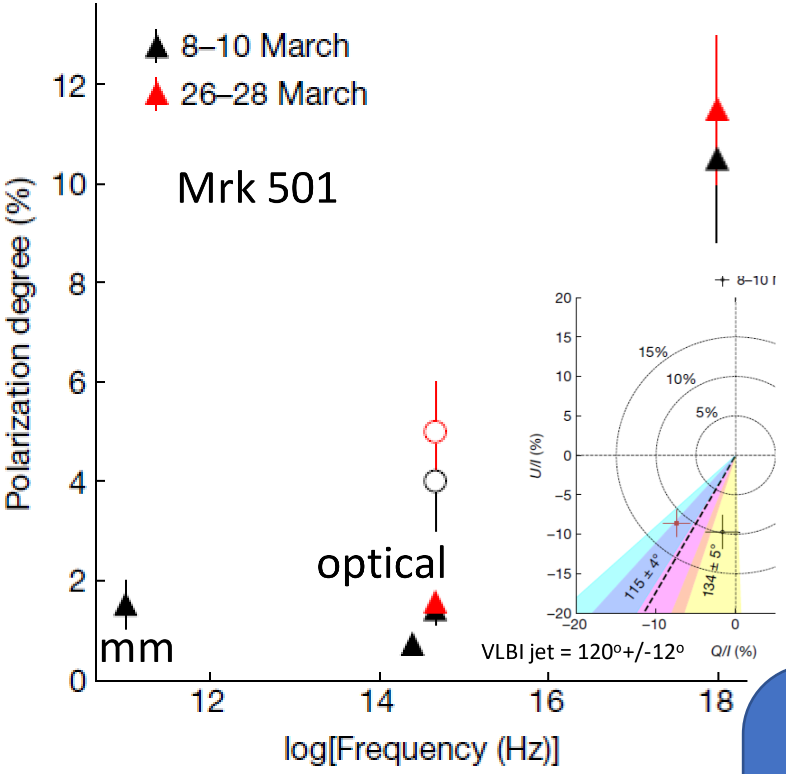

Table 1 | Summary of model properties

Model	Multiwavelength polarization	X-ray polarization variability[a]	X-ray polarization angle
Single zone	Constant[b]	Slow	Any
Multizone	Mildly chromatic	High	Any
Energy stratified (shock)	Strongly chromatic	Slow	Along the jet axis
Magnetic reconnection (kink instability)	Constant	Moderate	Perpendicular to the jet axis
Observed	Strongly chromatic	Slow	Along the jet axis

First, we find an increasing Π towards higher frequencies. Second, we do not find significant variability during the 2–3-day-long IXPE observations, and finally, we find a rough alignment of ψ with the jet axis from radio to X-rays. Therefore, a shock-accelerated, energy-stratified electron population model satisfies all our multiwavelength polarization observations.
[a]Slow variability, a few days to a week; moderate variability, days; high variability, less than 1 day.
[b]There is a slight dependence on the slope of the emission spectrum.

Di Gesu, L. et al. ApJL, 2022

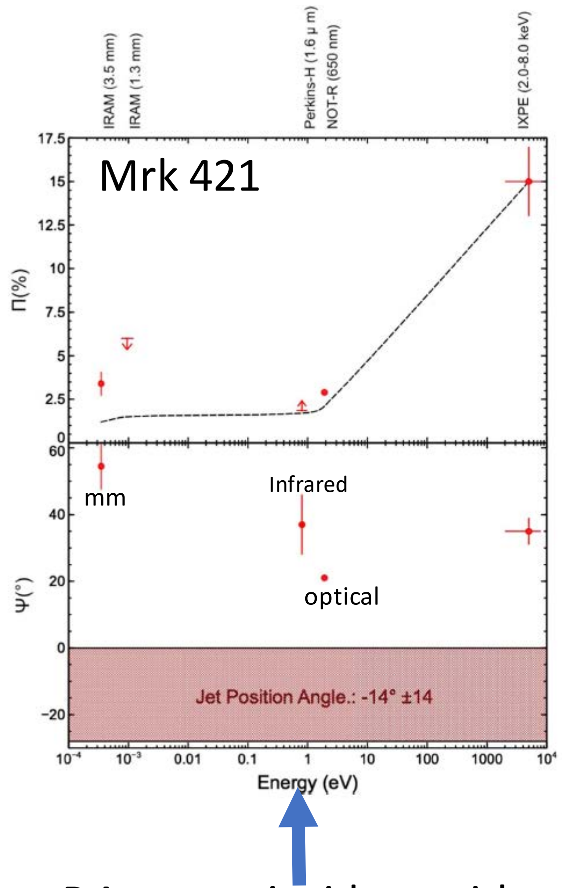

Synchrotron dominated blazars show a polarization in X-rays which is 3-5 times larger than in optical, infrared and mm.

The most probable jet acceleration mechanism is energy stratified shock.

P.A. not coincident with the jet direction

Mrk 421: X-ray polarization angle rotation

- During X-ray rotation millimiter-wave, infrared and optical polarization angle didn't vary substantially.
- Rotation in optical light is few-few tens of degree/day
- PD_X was roughly constant and higher wrt Optical, Infrared and Radio
- At GeV was in a quiescent state

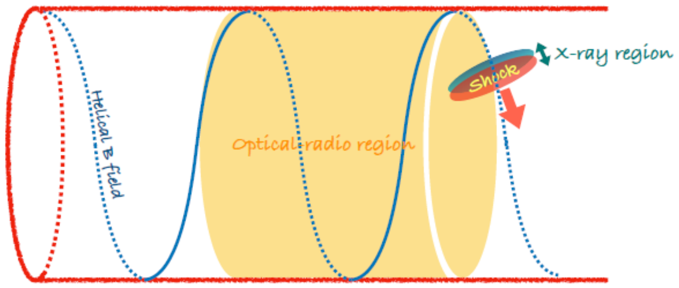

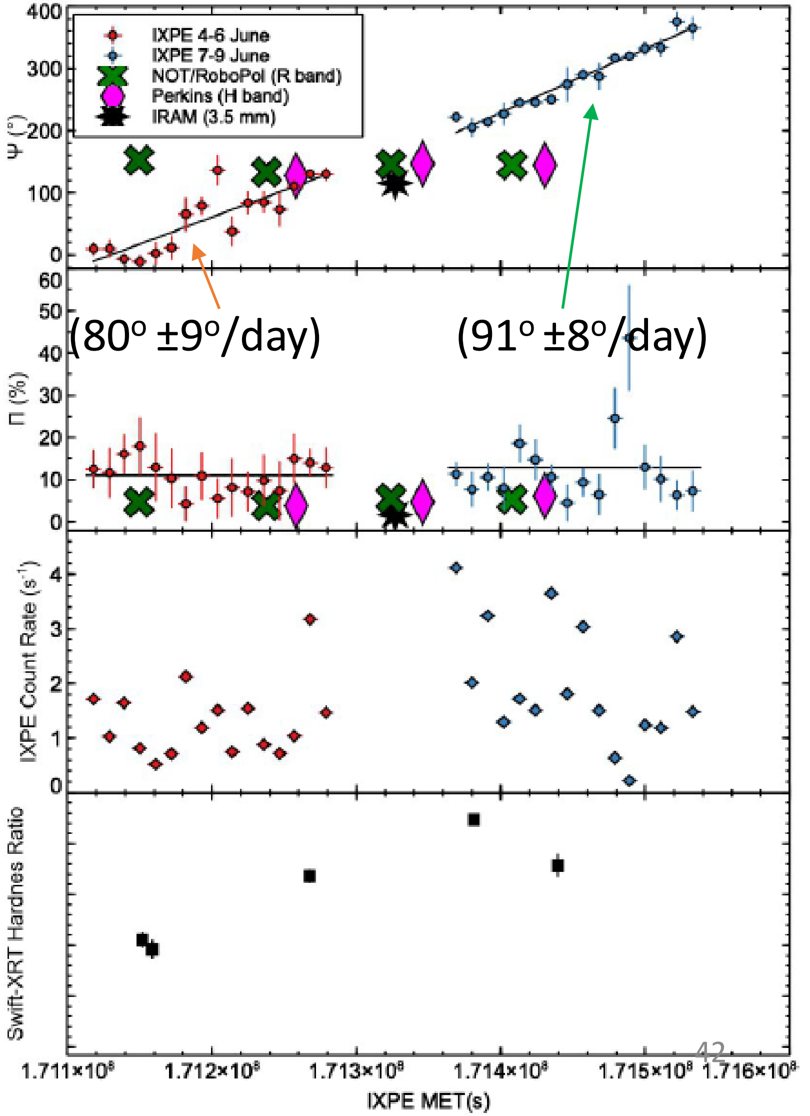

A model may explain the observed rotation is a shock propagating along the helical magnetic field down the jet.

Note: PG1553+113 showed a rotation in optical and infrared but no in X-ray

Di Gesu L. et al., Nature Astronomy 2023

HSP blazars recap:

Marsher, A. et al., 2024

Table 1. Contemporaneous X-ray and optical polarization of HSP blazars.

Object (Date)	X-ray Π_X(%)	X-ray ψ_X(°)	Optical R-Band [a] Π_O(%)	Optical R-Band [a] ψ_O(°)	Jet PA (°) at 43 GHz [b]
1ES0229 + 200 [c] (23 January 2023)	18 ± 3	25 ± 5°	2.4 ± 0.7%	2 ± 8°	163 ± 8
Mrk421 (5 May 2022)	15 ± 2%	35 ± 4	2.9 ± 0.5	32 ± 5	−29 ± 18
Mrk421 (5 June 2022)	10 ± 1	Rotation	4.4 ± 0.4	−40 ± 6	−29 ± 18
Mrk421 (8 June 2022)	10 ± 1	Rotation	5.4 ± 0.4	−35 ± 1	−29 ± 18
Mrk421 (17 December 2022)	14 ± 1	−73 ± 3	4.6 ± 1.3	26 ± 9	−29 ± 18
PG1553 + 113 (2 February 2023)	10 ± 2	86 ± 8	4.2 ± 0.5	Rotation	50 ± 10
Mrk501 (7 March 2022)	9.8 ± 1.7	136 ± 5	6.6 ± 0.4	110 ± 5	120 ± 12
Mrk501 (27 March 2022)	10.3 ± 1.4	115 ± 4	4.7 ± 0.3	120 ± 3	120 ± 12
Mrk501 (9 July 2022)	6.9 ± 1.8	134 ± 8	2.7 ± 0.5	109 ± 5	120 ± 12
Mrk501 (12 February 2023)	9.0 ± 2.4	110 ± 8	6.6 ± 0.9	150 ± 4	120 ± 12
Mrk501 (19 March 2023)	6.0 ± 2.1	107 ± 11	6.1 ± 0.7	125 ± 3	120 ± 12
Mrk501 (16 April 2023)	18.5 ± 2.2	103 ± 3	5.9 ± 1.5	108 ± 6	120 ± 12
1ES1959 + 650 (3 May 2022)	8.0 ± 2.3	123 ± 8	4.5 ± 0.2	159 ± 1	120–150
1ES1959 + 650 (10 June 2022)	< 5.1 [d]	—	4.7 ± 0.6	151 ± 19	120–150
1ES2155−304 (30 October 2023)	31 ± 2	129 ± 2	4.3 ± 0.7	116 ± 8	135 ± 45
1ES2155−304 (4 November 2023)	15 ± 2	125 ± 4	3.8 ± 0.9	116 ± 8	135 ± 45

Dawoon Kim, 2024

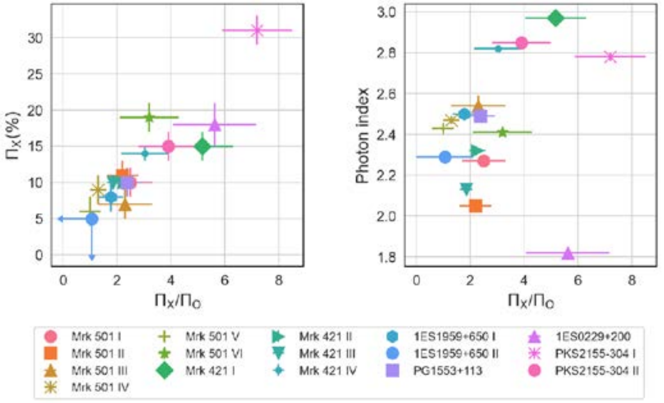

Energy stratified shock acceleration model: If the pre-shock medium is turbulent the PA can fluctuate around the jet direction.

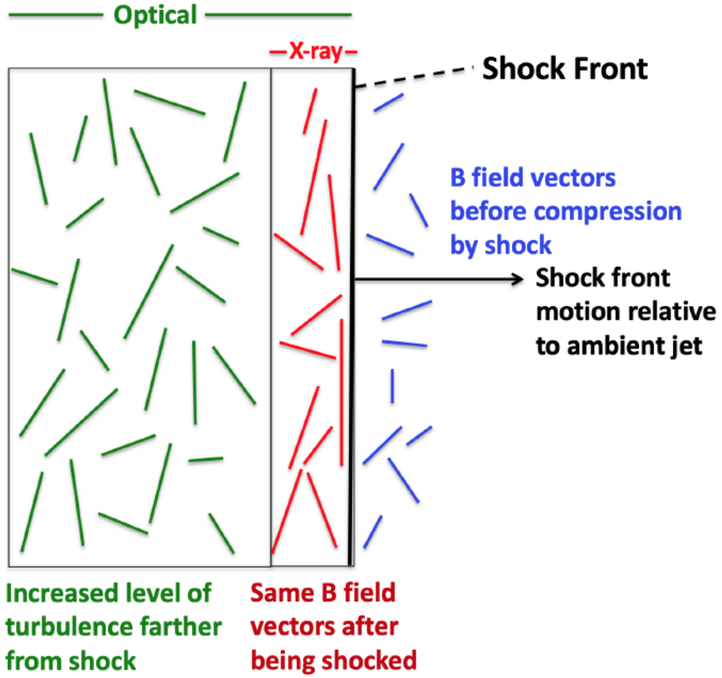

PD & PA shows variability for most of the IXPE observed HSP.

WHAT ABOUT INVERSE COMPTON DOMINATED BLAZARS ?

3C273, 3C 279, 3C 454.3, S6 0716+714 only upper limits 9-38 %

Table 1. Summary of IXPE Observations

Source	Instrument	Observation ID	MJD range	Exposure (ks)[a]	Π_X[b]
3C 273	IXPE	01005901	59732.37 - 59734.45	95.28	< 9.0%
3C 279	IXPE	01005701	59743.02 - 59748.85	264.42	< 12.7%
3C 454.3	IXPE	01005401	59730.19 - 59732.34	98.12	< 28%
S5 0716+714	IXPE	01005301	59669.43 - 59674.80	358.68	< 26%

[a] Average of exposures for the three detector units.

[b] 99% confidence limits using the unbinned, event-based likelihood method (§ 2.1).

Marshall, H. et al. in Astro-ph, 2024 ApJ accepted

An intermediate Blazar BL Lac in outburst showed significant polarization (22 %) but X-rays moved into the synchrotron peak!. Peirson, L. et al., ApJL 2023

The IXPE baseline program ended on February 2024.

NASA on 6 June 2023 approved an extension of IXPE until September 2025.

The next NASA senior review for mission is foreseen in 2025.

GO 1 program is at the present time from February 24 to January 2025

GO 2 (from January 2025 to September 2025) call ends 29 August 2024

Data are public (except special case) one week after the end of the observation
Analysis software (HEASARC-XSPEC and Collaboration software) are public

End of October the panel gathers to select succesfull proposals

Senior Review Decision Spring 2025

eXTP (new ASIC with a dead time 8 times lower than IXPE)

PFA
4 telescopes
Wolter-I, Nickel F = 5.25 m
Gas Pixel Detector (GPD)
PFA
500 cm^2 @ 2 keV 300 cm^2 @ 3 keV
25% @ 6 keV
10 μs
~5 times the area of IXPE, X-ray polar. Pathfinder by NASA; Min. Detectable Polarization ~3% in 2-8 keV energy range

Zhang et al., SPIE 2022

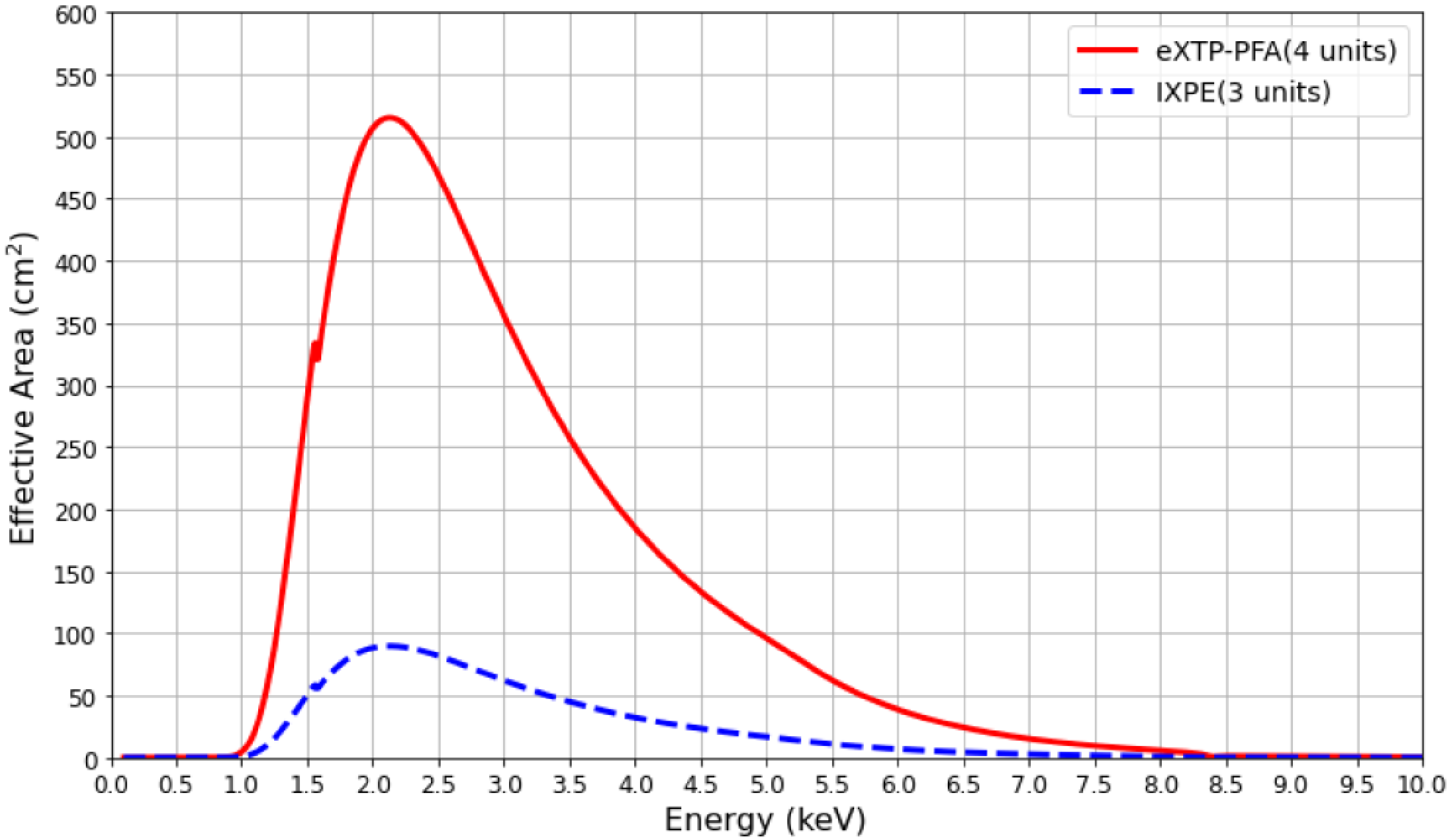

Figure 20. Comparison of the total effective area between PFA and IXPE.

5 times less time to get the same results of IXPE: A factor 5 increase on the number of sources for each class, better study of variability.

From LEP to a Medium Energy Polarimeter (MEP)

Dimethyl-Ether

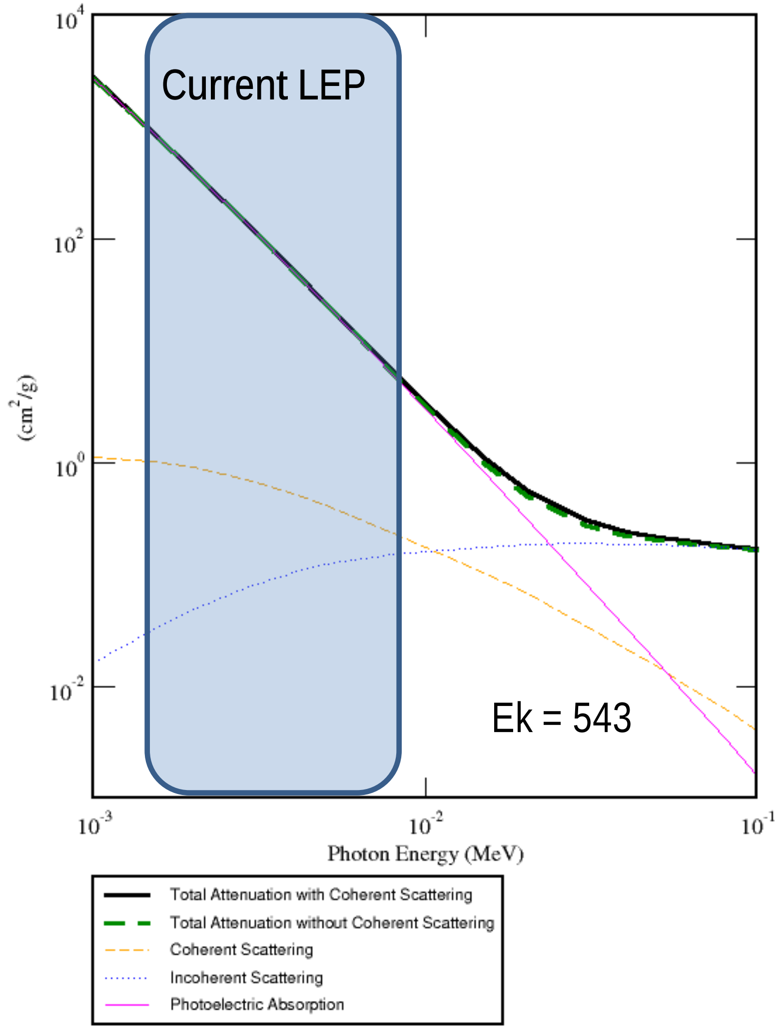

Argon

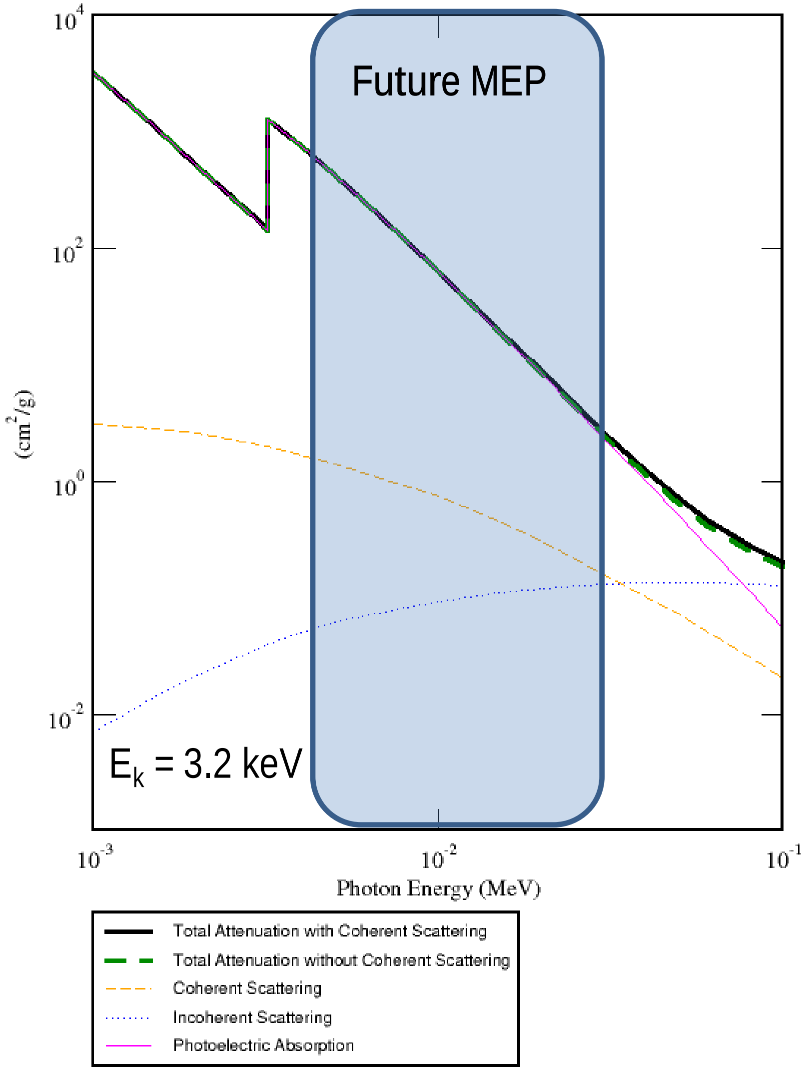

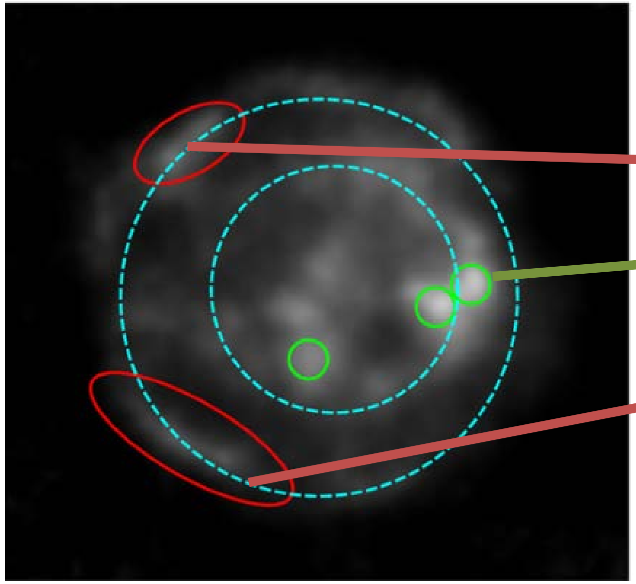

15–20 keV NuSTAR image
of CasA

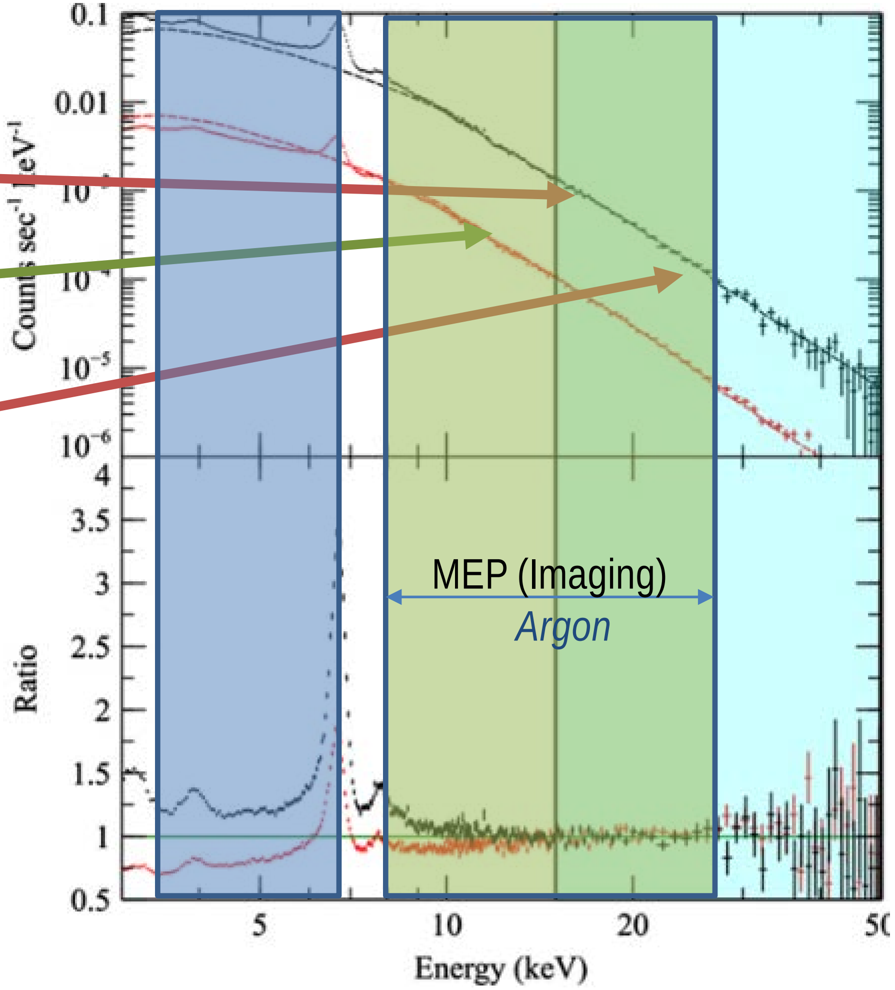

Grefenstette, 2015

The origin of E >15 keV is a mistery.
It is not dominated by forward or reverse shock but by filaments and knots.
Is the bright knots emission synchrotron (10-100 TeV electrons) or non-thermal bremsstrahlung (10-100 keV electrons) ?

IXPE probes the non thermal emission diluted with thermal bremsstrahlung (blue)
Imaging Hard X-ray polarimetry of genuine non thermal emission (Green 9-30 keV)

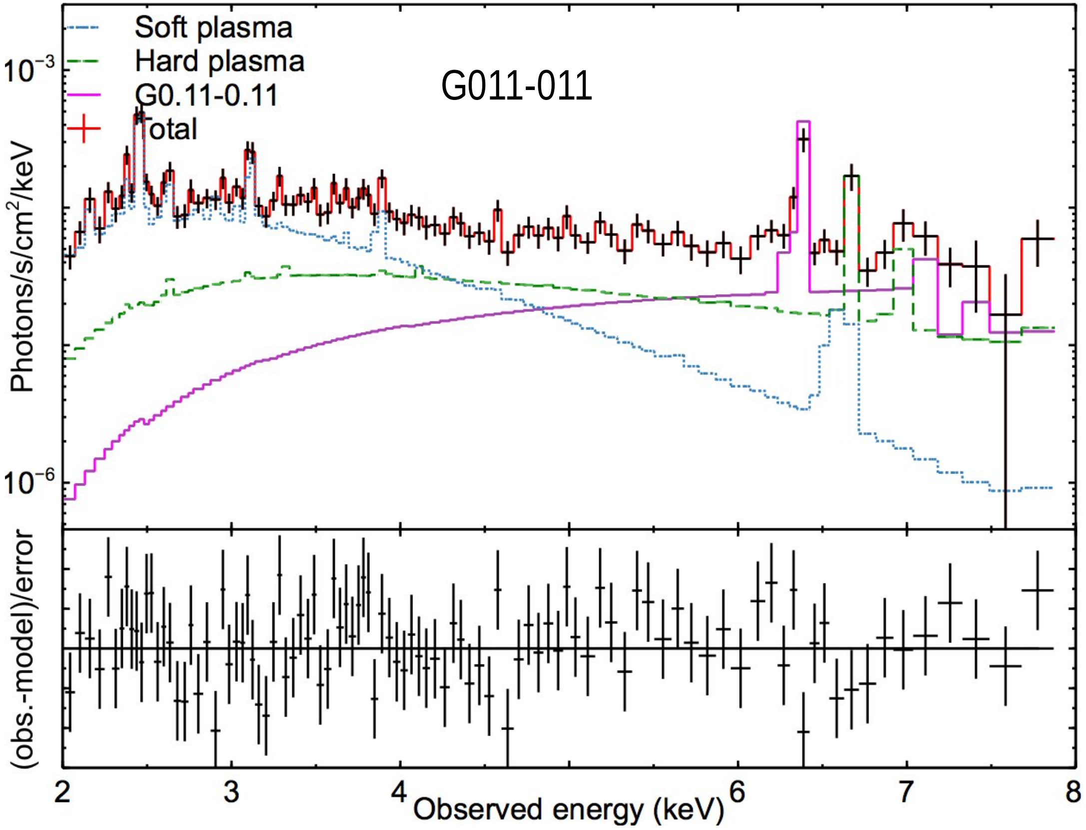

Di Gesu et al 2020

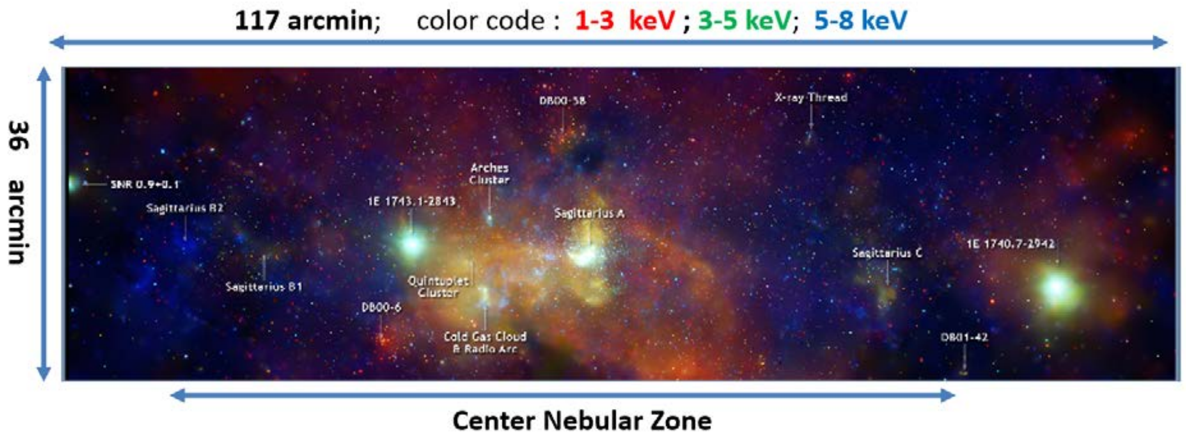

Cold molecular clouds are reflecting X-rays emitted 200 year ago from SgrA* (Marin et al., 2023).

Molecular clouds in the galactic center region are embedded in a two temperatures thermal plasma
The contribution of the thermal plasma can be made negligible above 7 keV

1E 1547.0−5408
Makishima et al., 2021

NuSTAR

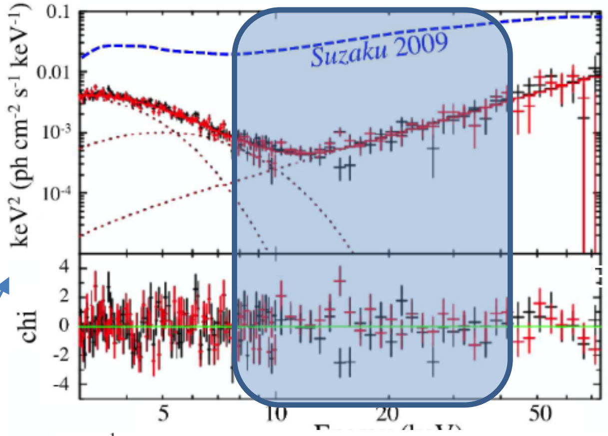

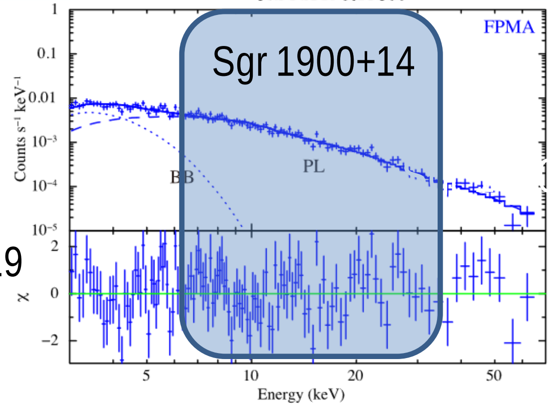

Tamba et al. 2019

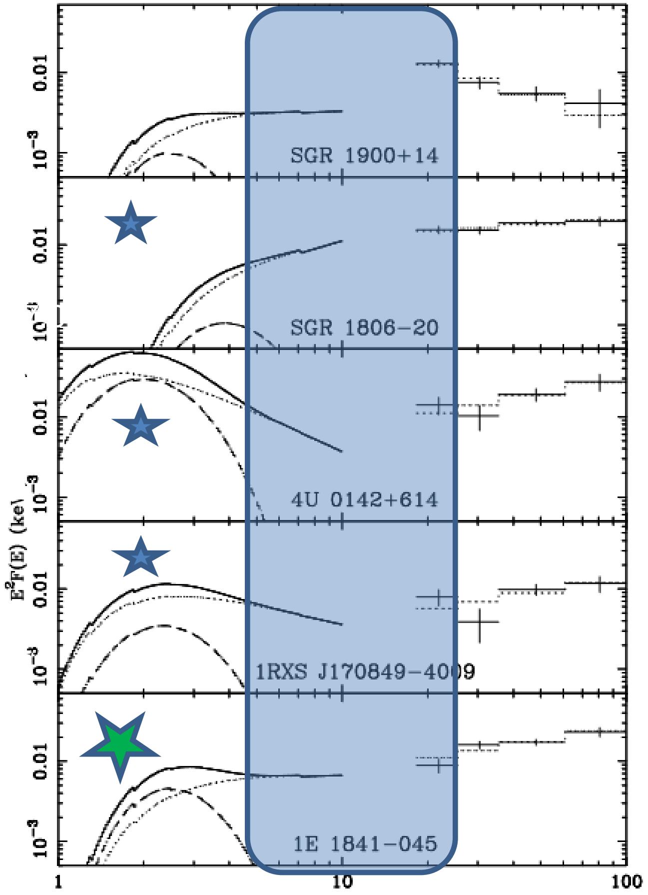

- Hard tails detected by IBIS-Integral and Nustar
- Fluxes in the mCrab range
- Resonant Compton upscattering of soft thermal photons from the neutron star surface

★ Observed by IXPE

★ Next IXPE ToO start 2024/09/23

Götz et al., 2006

With hard X-ray imaging polarimetry we can probe the transition between power-law and hard tail emission

Photoelectric Imaging Polarimetry above 6 keV: reflection phenomena in AGNs

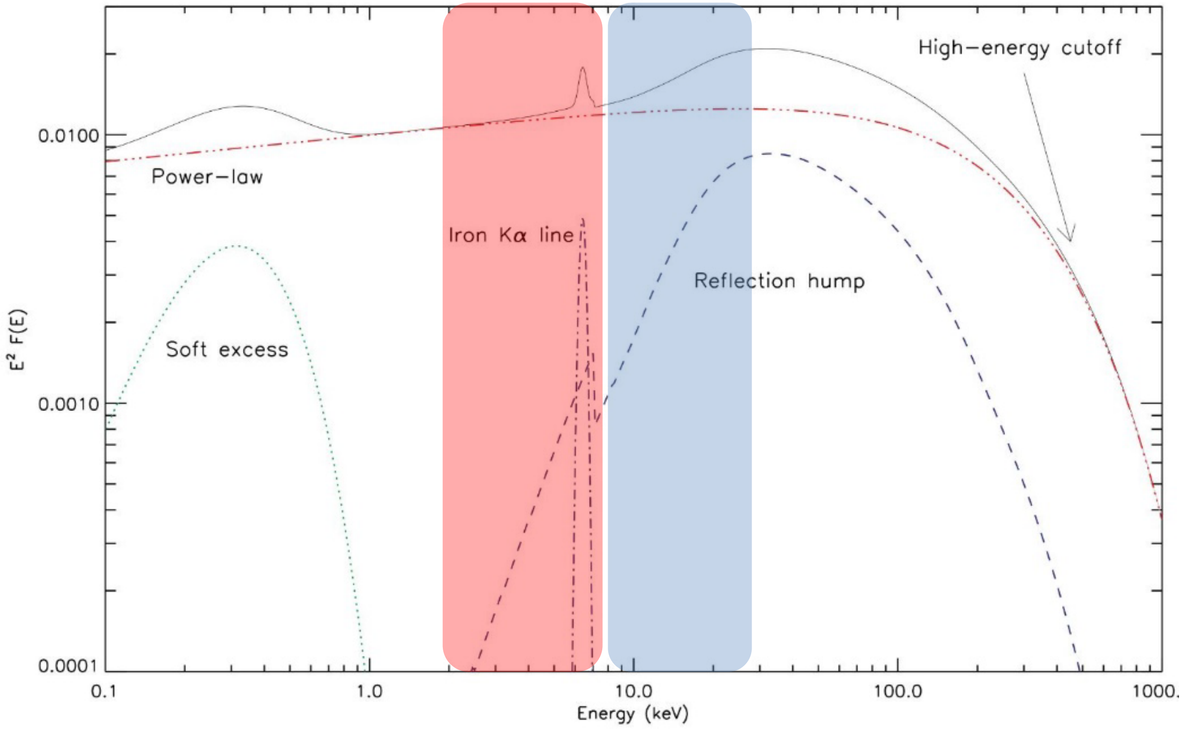

IXPE energy band
Future hard X-ray imaging polarimetry

Wider energy band & imaging for AGNs

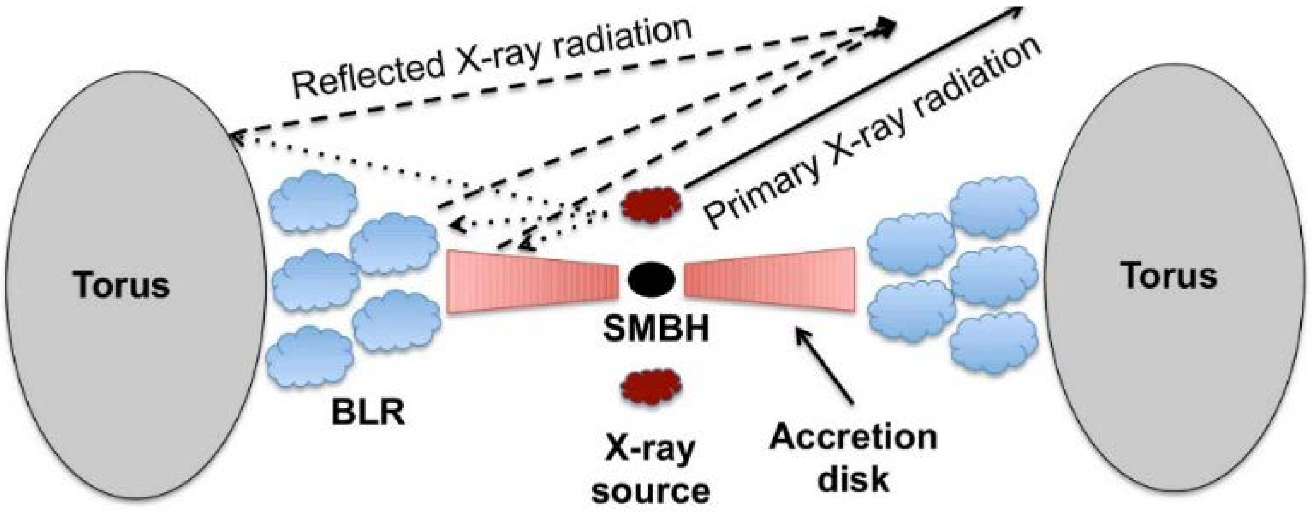

Credit Ricci, C.

IXPE polarimetry to study reflection phenomena suffers of small effective area.
Hard-X ray imaging (low background polarimetry) is highly desirable.

X-ray polarimetry in a wide energy band

Tagliaferri et al., 2010

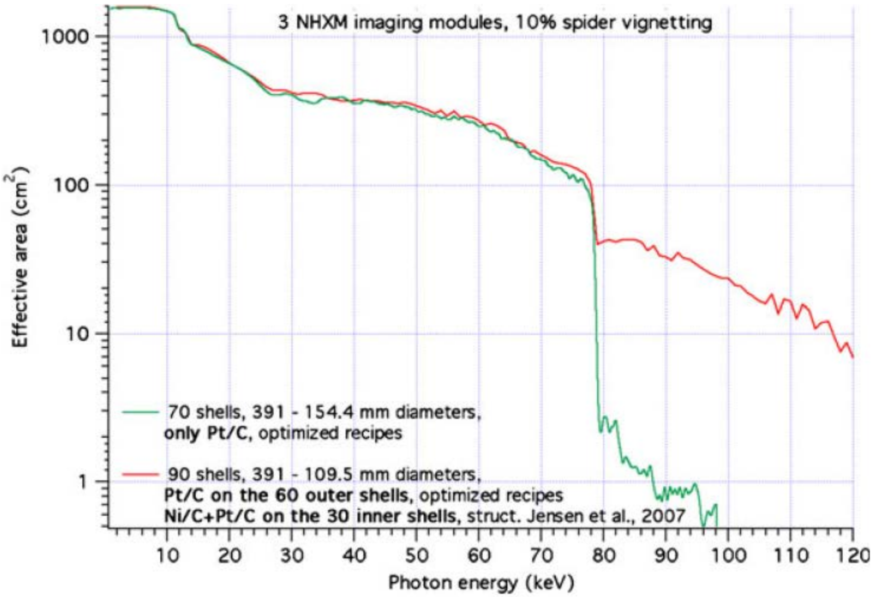

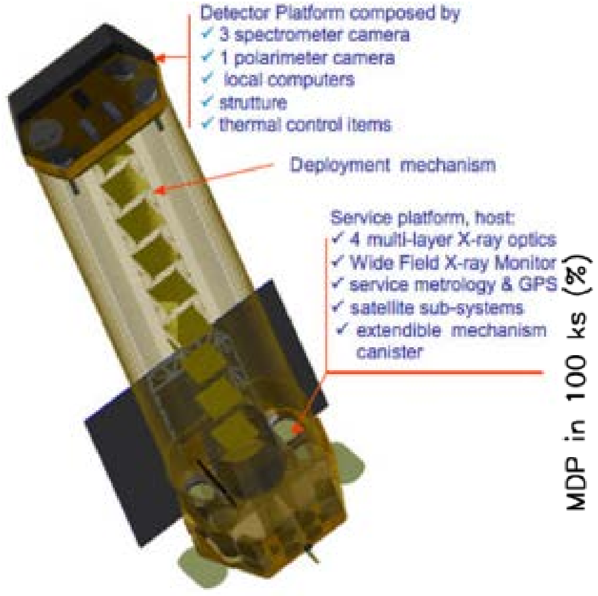

550 cm^2 2-10 keV.
one NHXM optics = whole IXPE.

Tagliaferri et al., 2010

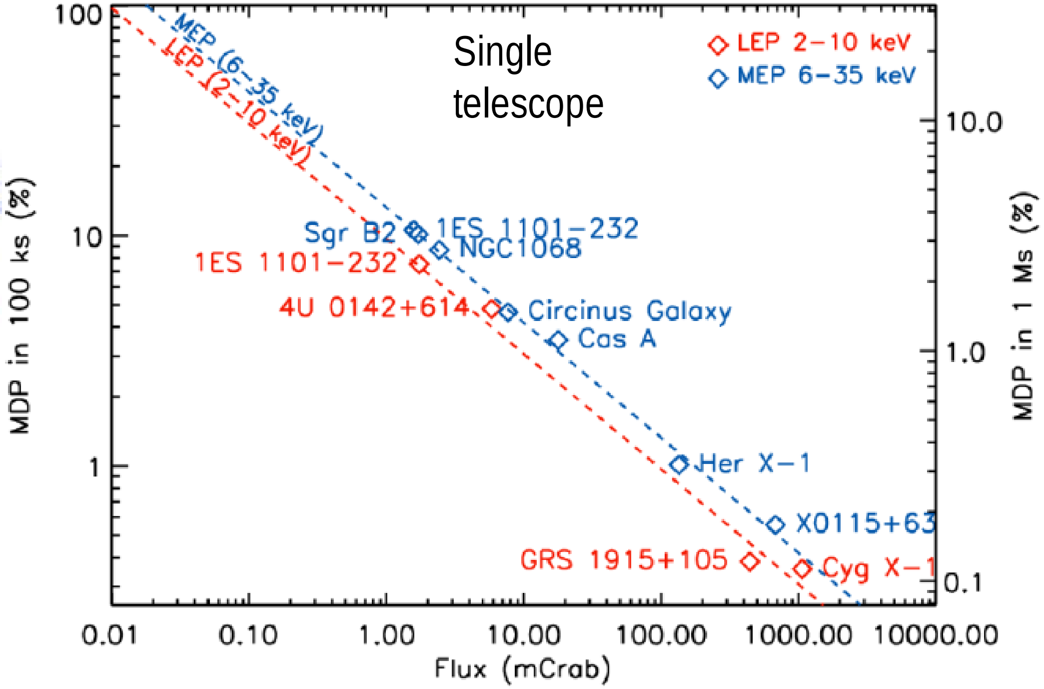

New Hard X-ray Mission (NHXM) was proposed in 2010 as an M-3 ESA mission.
Four multilayer optics 3 optics for spectroscopy/Imaging and 1 optics for polarimetry.

We could revert the NHXM design assigning three optics to polarimetry and one optics to a detector for imaging/spectroscopy. One NHXM mirror is efficient as the three IXPE ones.

END

From a mistake to a true photoelectric X-ray polarimetry

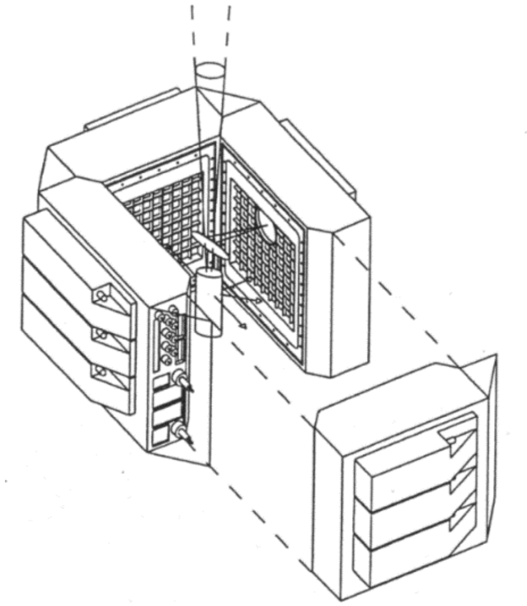

The Stellar X-ray Polarimeter on board Spectrum-X-Gamma SRG (USA, Italy, Russia)

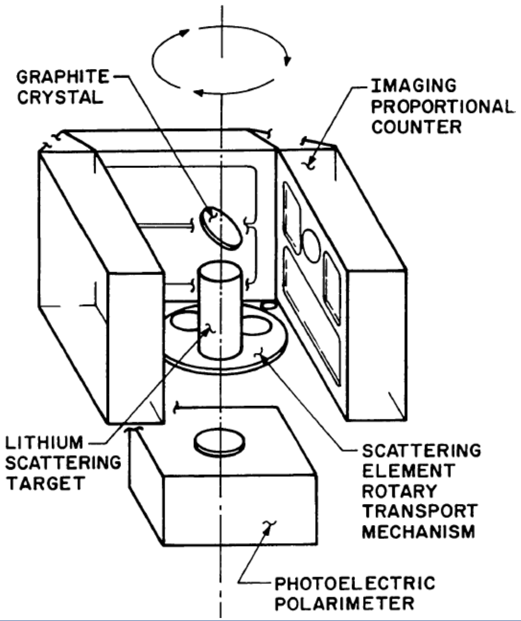

Hanany, S. et al., 1995

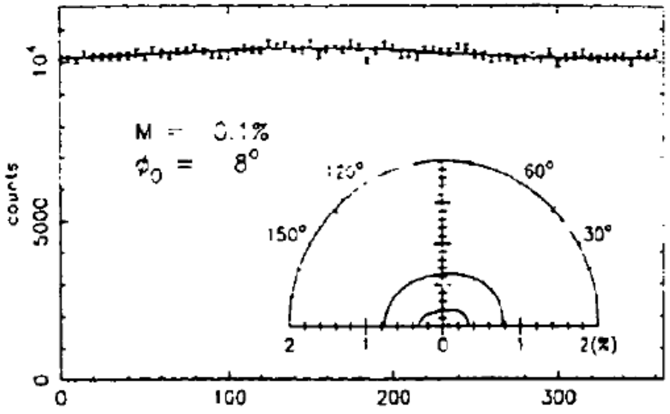

TABLE I. Sample observing plan for the SXRP mission.

Source	Observing Time (10^5sec)	Min. Det. Pol. (%) Graphite	Min. Det. Pol. (%) Lithium	Observing Time (10^5sec)	MDP (%) CsI
Energy (keV)		2.6	5 – 10		0.1 – 5
Radio Pulsars					
Crab Primary Pulse (Avg.)	2	6.0	6.2	1	0.8
Leading Edge	2	8.0	7.6	1	1.1
Trailing Edge	2	9.4	7.6	1	1.2
Supernova Remnants					
Crab Nebula	2	0.5	0.4	1	< 0.1
PSR 1055–52				2	10
Binary Pulsars*					
Her X-1**	7	2.8	1.6	1.5	0.8
4U0900-4	1	2.8	0.9	0.5	0.5
GX1+4	1	4.3	1.2	0.5	0.8
4U1223–62	2	3.8	0.9	1	0.7
4U1626–67	2	3.4	1.8	1	0.6
Cen X-3	1	1.8	0.6	0.2	0.5
Black Hole Candidates					
Cyg X-1	6			1	
Low State		1.0	0.8		0.2
High State		0.3	0.2		< 0.1
LMC X-1				4	1.0
QPOs					
Cyg X-3	1	1.5	0.6	0.2	0.4
Sco X-1	1	0.7	0.1	0.01	0.2
4U1822–37				2	3.6
AGN's					
Cen A	1	7.6	1.9	1	1.0
Mkn 421	6	4.6	18.6	1	1.9
3C273	6	3.8	6.1	1	1.6
PKS2155–304				1	1.5
ESO 141-G55				1	2.6
NGC 7469				1	1.9
Mkn 509				1	1.7
Mkn 501				1	2.1
2A1218+304				1	1.8

The photoelectric polarimeter, as configured, did not worked for a experimental mistake but the expected sensitivity was great in the soft-X-rays albeit with low modulation factor.

So Enrico Costa and Paolo Soffitta had the idea to replace CsI photocatode and vacuum with a suitable gas mixture (with low atomic number!) to make the charge image of the track of the photoelectron! and went to visit Ronaldo Bellazzini.

Kaaret et al., OptEng 1990, SPIE 1994 Tomsick et al., SPIE 1997, Soffitta et al., NIM A, 1998

SECOND WE USE TO CORRECT FOR THE SECULAR GAIN INCREASE

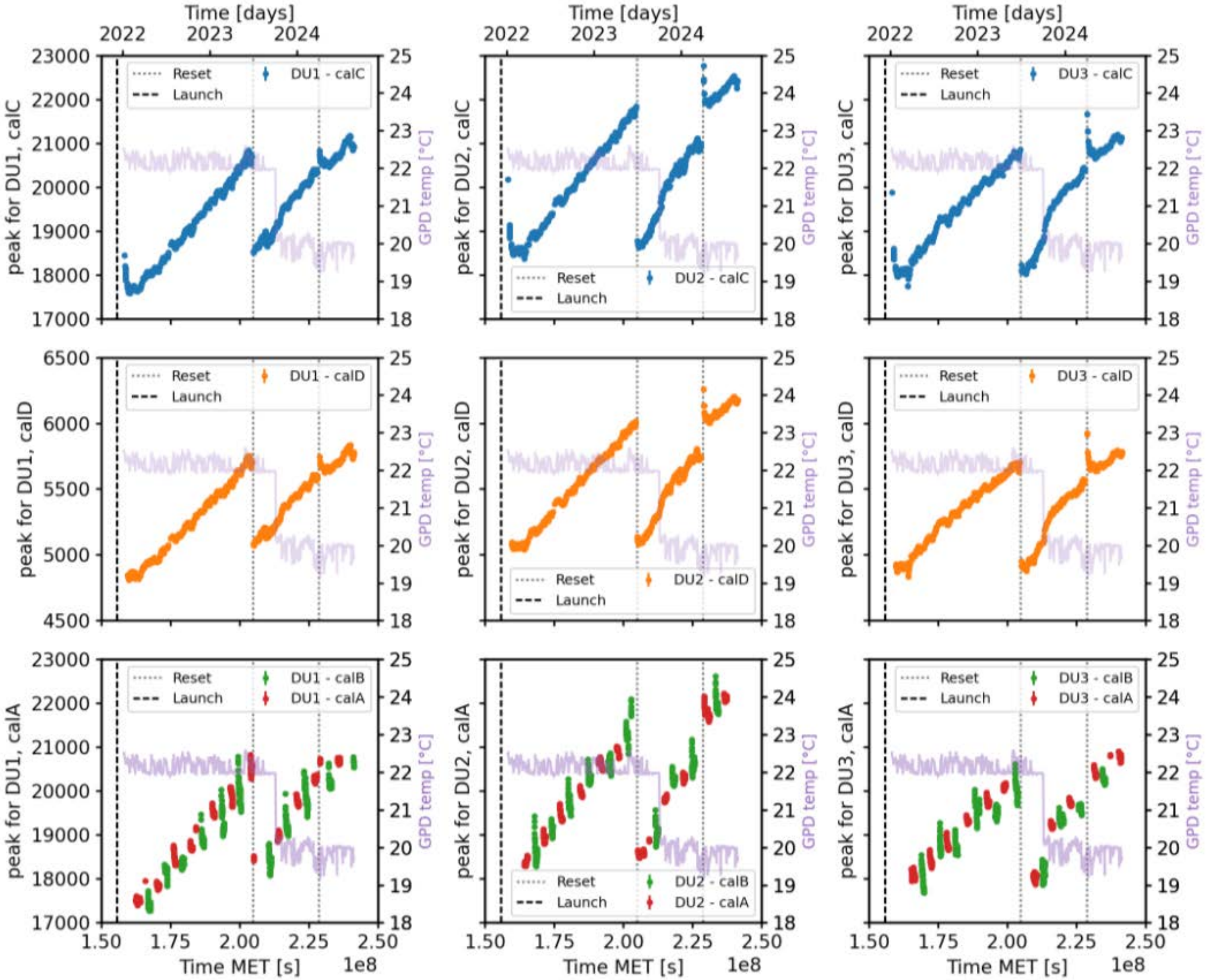

The gain increase is well understood in terms of absorption of the gas from the glue which is used to build the detector.

It is accompanied by a decrease of the pressure at level of 1.2 %/year

The modulation factor increases with time making the loss of sensitivity very small

It requires:

(1) Adjustment of the HV once/year

(2) New response matrices each 6 months

TimePIX3: from MEDIPIX CERN collaboration

Timepix3: a 65K channel hybrid pixel readout chip with simultaneous ToA/ToT and sparse readout

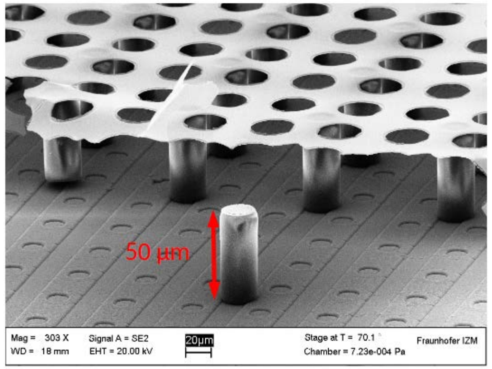

Kaminski, 2017, Lupberger 2015

Parameter	Value
Pixel matrix	256 x 256 = 65536 pixels (2x4 superpixels)
Pixel size	55 x 55 μm^2
Technology	CMOS 120 nm
Measurement type	1. Simultaneous 10 bit TOT, 14 + 4 bit ToA 2. 14 + 4 bit ToA only 3. 14 bit integral ToT
Readout type	1. Data Driven (zero-suppression) 2. Frame based (zero-suppression)
Dead time per pixel	ToT + 457 ns (pulse processing + data transfer)
Output bandwidth	Up to 5.12 Gbs (parallel 8 channels x 640 Mbps)
Maximum Counting rate	Data Driven up to 40Mhits/cm^2/s with duty cycle of 100 %
TOA precision (resolution)	1.56ns
Front End noise, minimum threshold	60 e_{rms} , 500 e^-

3-D imaging of the track is possible.

High rate for large optics is possible

Ongoing collaboration with University of Bonn

FROM A MISTAKE TO A TRUE PHOTOELECTRIC X-RAY POLARIMETRY

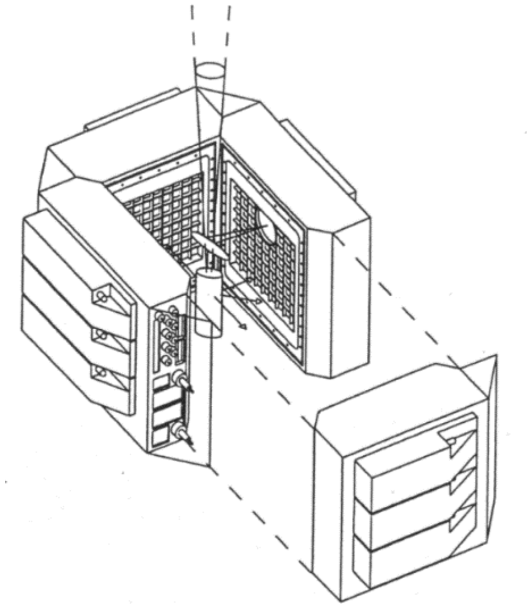

The Stellar X-ray Polarimeter on board Spectrum-X-Gamma SRG
(USA, Italy, Russia)

Kaaret et al., OptEng 1990, SPIE 1994 Tomsick et al., SPIE 1997, Soffitta et al., NIM A, 1998

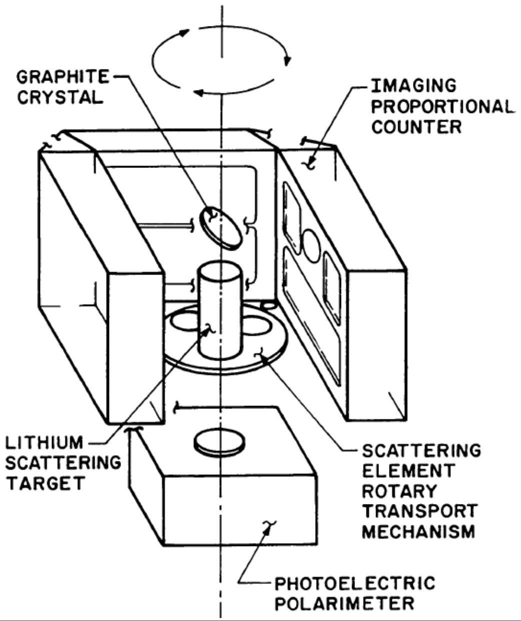

Hanany, S. et al., 1995

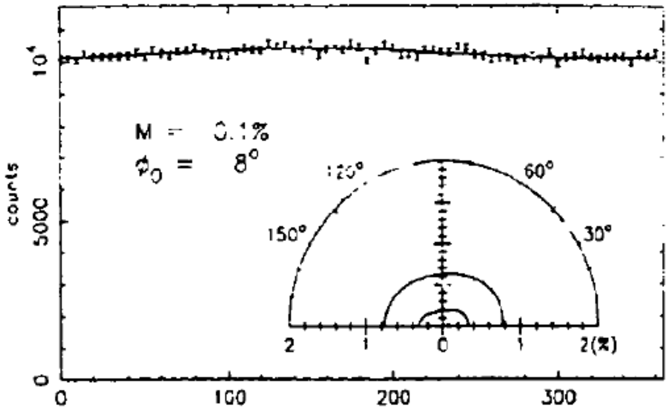

The photoelectric polarimeter, as configured, did not worked for a experimental mistake but the expected sensitivity was great in the soft-X-rays albeit with low modulation factor.

So Enrico Costa and Paolo Soffitta had the idea to replace CsI photocatode and vacuum with a suitable gas mixture (with low atomic number!) to make the charge image of the track of the photoelectron! and went to visit Ronaldo Bellazzini.

TABLE I. Sample observing plan for the SXRP mission.

Source	Observing Time (10^5sec)	Min. Det. Pol. (%) Graphite	Min. Det. Pol. (%) Lithium	Observing Time (10^5sec)	MDP (%) CsI
Energy (keV)		2.6	5 – 10		0.1 – 5
Radio Pulsars					
Crab Primary Pulse (Avg.)	2	6.0	6.2	1	0.8
Leading Edge	2	8.0	7.6	1	1.1
Trailing Edge	2	9.4	7.6	1	1.2
Supernova Remnants					
Crab Nebula	2	0.5	0.4	1	< 0.1
PSR 1055–52				2	10
Binary Pulsars*					
Her X-1**	7	2.8	1.6	1.5	0.8
4U0900-4	1	2.8	0.9	0.5	0.5
GX1+4	1	4.3	1.2	0.5	0.8
4U1223–62	2	3.8	0.9	1	0.7
4U1626–67	2	3.4	1.8	1	0.6
Cen X-3	1	1.8	0.6	0.2	0.5
Black Hole Candidates					
Cyg X-1	6			1	
Low State		1.0	0.8		0.2
High State		0.3	0.2		< 0.1
LMC X-1				4	1.0
QPOs					
Cyg X-3	1	1.5	0.6	0.2	0.4
Sco X-1	1	0.7	0.1	0.01	0.2
4U1822–37				2	3.6
AGN's					
Cen A	1	7.6	1.9	1	1.0
Mkn 421	6	4.6	18.6	1	1.9
3C273	6	3.8	6.1	1	1.6
PKS2155–304				1	1.5
ESO 141-G55				1	2.6
NGC 7469				1	1.9
Mkn 509				1	1.7
Mkn 501				1	2.1
2A1218+304				1	1.8

GRB 221009A

We did not plan to follow-up on GRBs, because of the relatively slow reaction time (2-3 days).

However, GRB 221009A (the 'BOAT' GRB) was so exceptional in terms of brightness, that we decided to observe it.

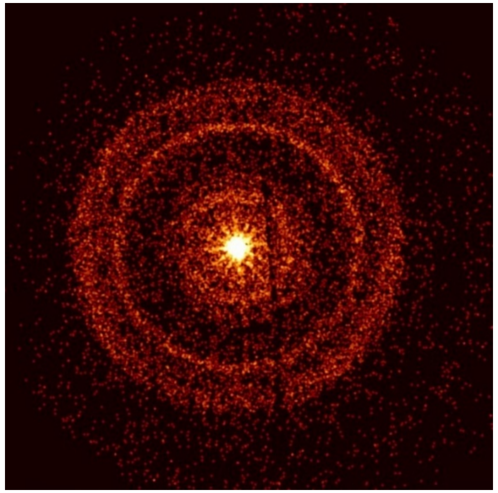

Swift/XRT image

P<13.8% (99% c.l.)

(Negro et al. 2023)

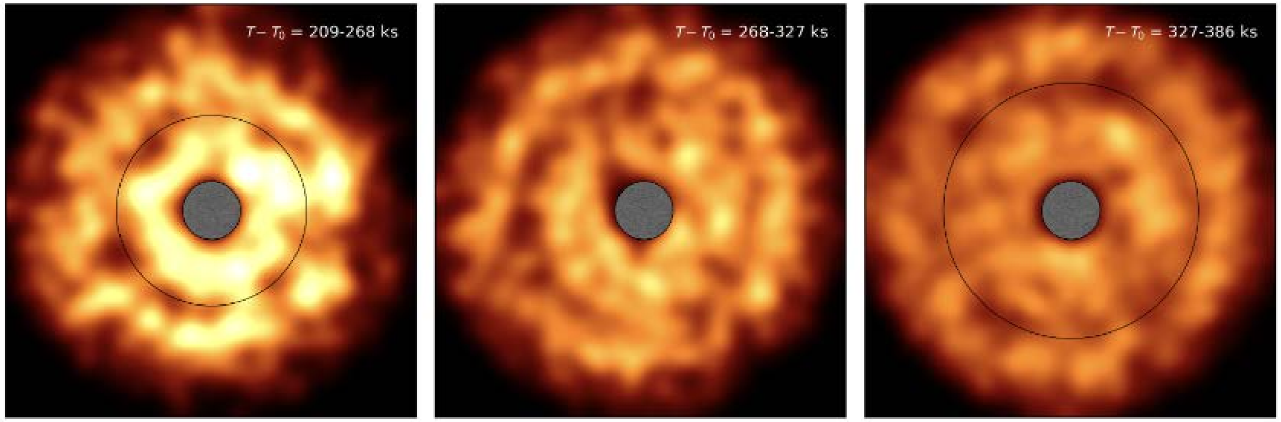

Time evolution of dust rings as seen by IXPE

Dust rings also observed → polarization of the prompt emission (<55%)

HSP blazars recap:

Marsher, A. et al., 2024

Table 1. Contemporaneous X-ray and optical polarization of HSP blazars.

Object (Date)	X-ray Π_X (%)	X-ray ψ_X (°)	Optical R-Band [a] Π_O (%)	Optical R-Band [a] ψ_O (°)	Jet PA (°) at 43 GHz [b]
1ES0229 + 200 [c] (23 January 2023)	18 ± 3	25 ± 5°	2.4 ± 0.7%	2 ± 8°	163 ± 8
Mrk421 (5 May 2022)	15 ± 2%	35 ± 4	2.9 ± 0.5	32 ± 5	−29 ± 18
Mrk421 (5 June 2022)	10 ± 1	Rotation	4.4 ± 0.4	−40 ± 6	−29 ± 18
Mrk421 (8 June 2022)	10 ± 1	Rotation	5.4 ± 0.4	−35 ± 1	−29 ± 18
Mrk421 (17 December 2022)	14 ± 1	−73 ± 3	4.6 ± 1.3	26 ± 9	−29 ± 18
PG1553 + 113 (2 February 2023)	10 ± 2	86 ± 8	4.2 ± 0.5	Rotation	50 ± 10
Mrk501 (7 March 2022)	9.8 ± 1.7	136 ± 5	6.6 ± 0.4	110 ± 5	120 ± 12
Mrk501 (27 March 2022)	10.3 ± 1.4	115 ± 4	4.7 ± 0.3	120 ± 3	120 ± 12
Mrk501 (9 July 2022)	6.9 ± 1.8	134 ± 8	2.7 ± 0.5	109 ± 5	120 ± 12
Mrk501 (12 February 2023)	9.0 ± 2.4	110 ± 8	6.6 ± 0.9	150 ± 4	120 ± 12
Mrk501 (19 March 2023)	6.0 ± 2.1	107 ± 11	6.1 ± 0.7	125 ± 3	120 ± 12
Mrk501 (16 April 2023)	18.5 ± 2.2	103 ± 3	5.9 ± 1.5	108 ± 6	120 ± 12
1ES1959 + 650 (3 May 2022)	8.0 ± 2.3	123 ± 8	4.5 ± 0.2	159 ± 1	120–150
1ES1959 + 650 (10 June 2022)	< 5.1 [d]	—	4.7 ± 0.6	151 ± 19	120–150
1ES2155−304 (30 October 2023)	31 ± 2	129 ± 2	4.3 ± 0.7	116 ± 8	135 ± 45
1ES2155−304 (4 November 2023)	15 ± 2	125 ± 4	3.8 ± 0.9	116 ± 8	135 ± 45

Dawoon Kim, 2024

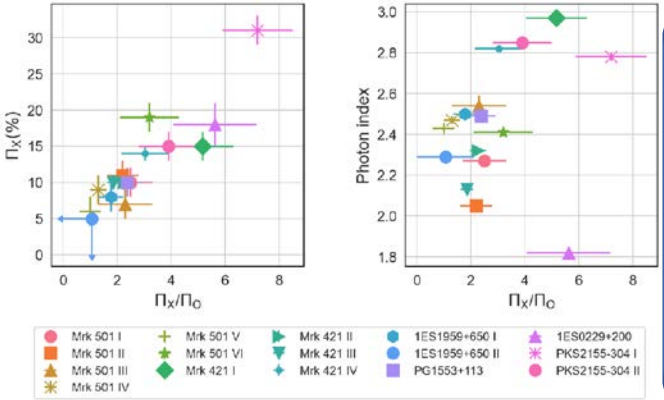

Energy stratified shock acceleration model: If the pre-shock medium is turbulent the PA can fluctuate around the jet direction.

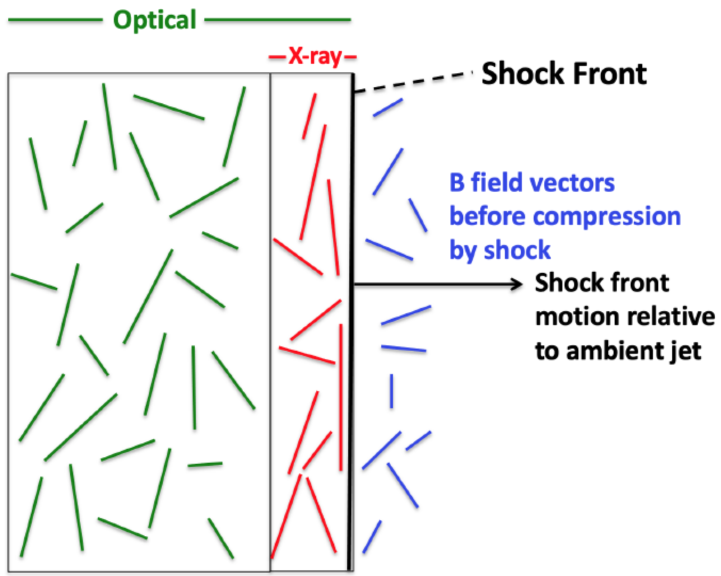

PD & PA shows variability for most of the IXPE observed HSP.

Magnetic reconnection can provide (1) stratification if acceleration start on a single small size (2) polarization angle parallel to the jet and (3) variability in turbulent region.

A very nice serendipitous discovery: Polarized emission from the X-ray bright filament G0.13-0.11

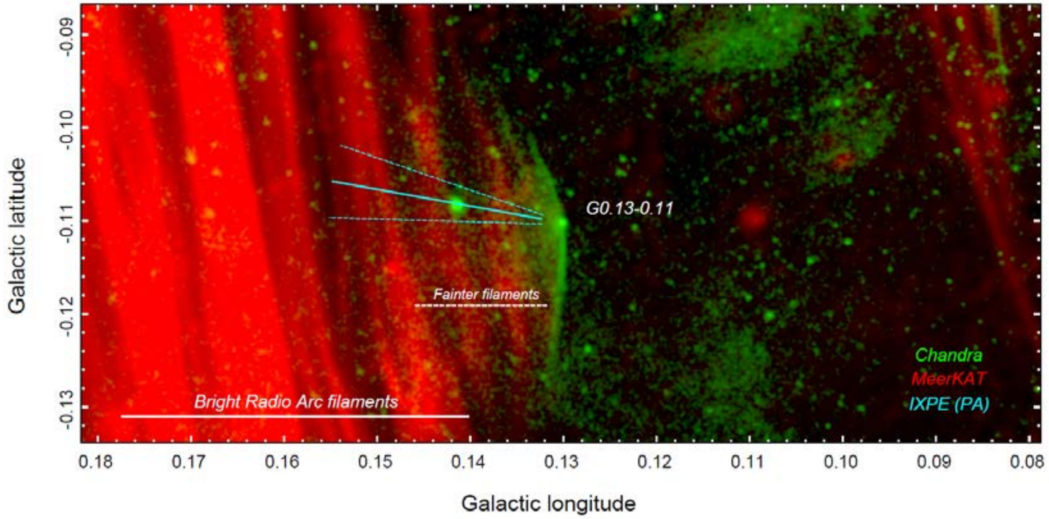

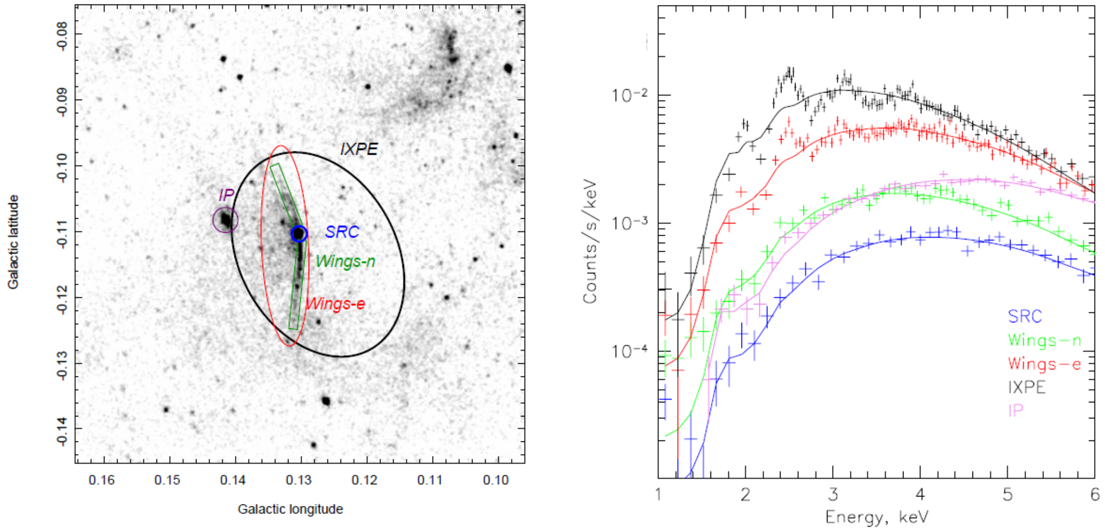

E. Churazov, A&A 2024 et al.

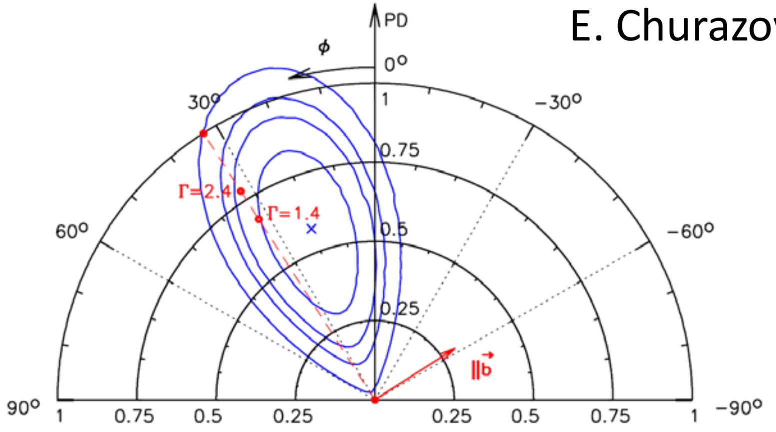

- A tight upper limit would neglect synchrotron emission or the magnetic field is very disordered at variance of other radio filament or G01.13-0.11 is not a PWN

- The polarization angle found is perpendicular to that of the molecular clouds. Tomography of the molecular clouds around the GC would be affected by smaller PD.

The high degree of polarization proves the synchrotron origin of X-rays. The polarization angle shows that the magnetic field (≈ 100 μGauss) is parallel to the radio filaments that may be part of the GC Radio Arc

X-RAY POLARIZATION OF THE EASTERN LOBE OF S433

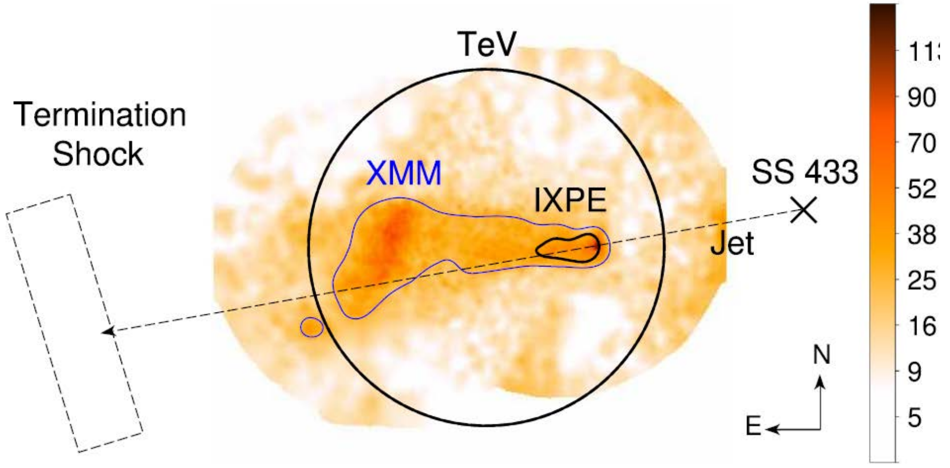

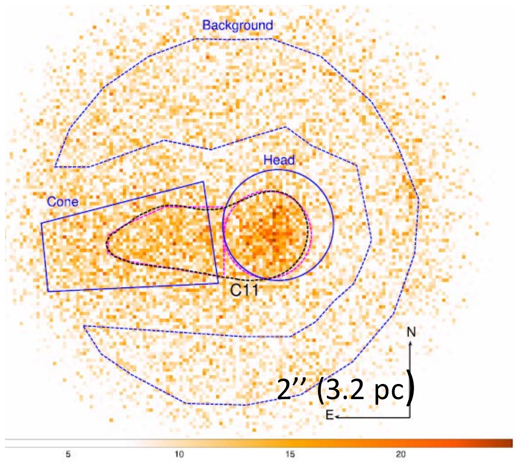

- The jet X-rays are thermal.
- East and West lobes (from 30 pc) are non-thermal (synchrotron).
- Termination shock is thermal.
- Lobes show TeV emission (HAWC, LHAASO. HESS)
- Head: non-thermal hard X-ray emission Γ≈1.6

  Head site of acceleration ?

The same electrons which produces X-rays produce TeV photons via Inverse Compton scattering on CMB. ùTherefore IXPE probes probes the magnetic field configuration in the same region producing VHE

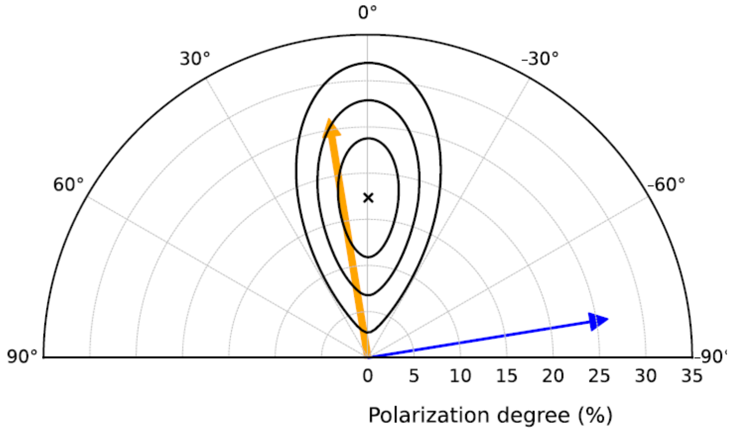

The key result of IXPE observations is that the magneti field near the acceleration region contains a significant component that is well ordered and parallel to the flow direction (shear ? Loclized ordered magnetic field ?.
Acceleration: Stochastic by shock, stochastic by turbulence, reconnection ?

Alternative scenario is scattering from SS433 being a ULX. But large optical depth requested

Peculiarity of the current GPD design

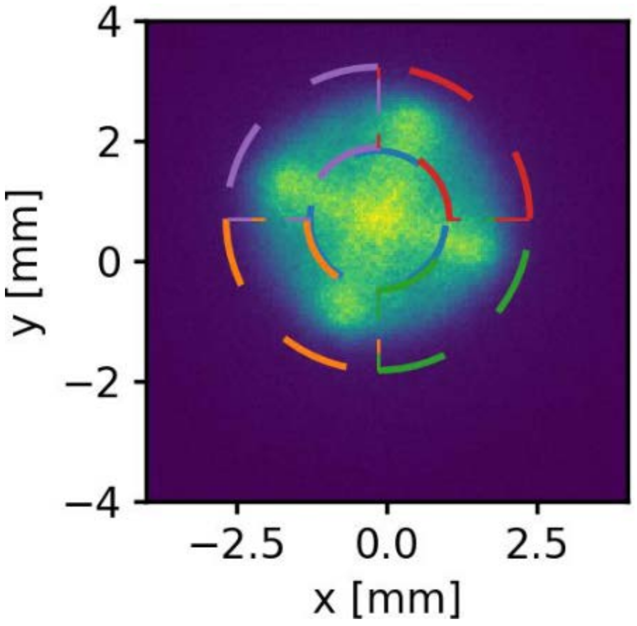

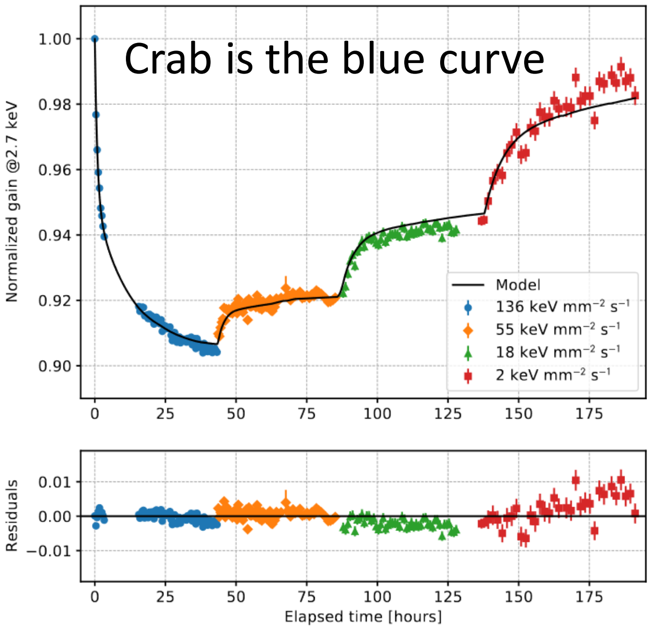

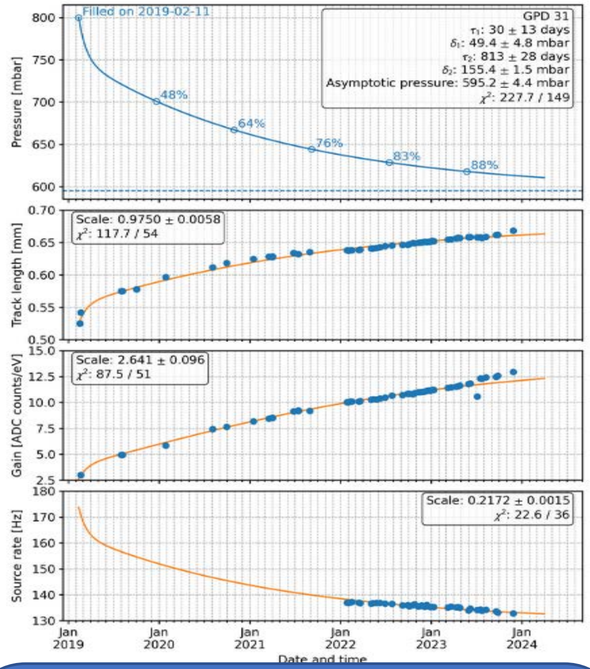

Being un-useful the rotation, a dithering is required to facilitate the ground calibration.

Gain shift due to charging is not yet totally corrected.
Charging is responsible for a residual mis-calibration of 10-20 eV

Pressure drop due to absorption of the DME by the glue.
650 mbar current pressure

THE FIRST LIMIT: IN POLARIMETRY THE SENSITIVITY IS A MATTER OF PHOTONS

$$MDP = \frac{4.29}{\mu R_S}\sqrt{\frac{R_S + R_B}{T}}$$

Minimum Detectable Polarization (MDP)

R_S is the Source rate, R_B is the Background rate, T is the observing time
μ is the modulation factor: the response of the polarimeter to a 100% polarized beam (spanning from 0 or no sensitivity, to 1 or maximum sensitivity)

If background is negligible: $$\mathrm{MDP} = \frac{4.29}{\mu\sqrt{N_{ph}}}$$

To reach MDP=1% with μ=0.5: $$N_{ph} = \left(\frac{4.29}{\mu\,\mathrm{MDP}}\right)^2$$ = 736 10^3 ph

Source detection > 10 counts
Source spectral slope > 100 counts
Source polarization > 100.000 counts

Caution: the MDP describes the capability of rejecting the null hypothesis (no polarization) at 99% confidence.

POLARIZATION ANALYSIS: MDP AND CONTOURS

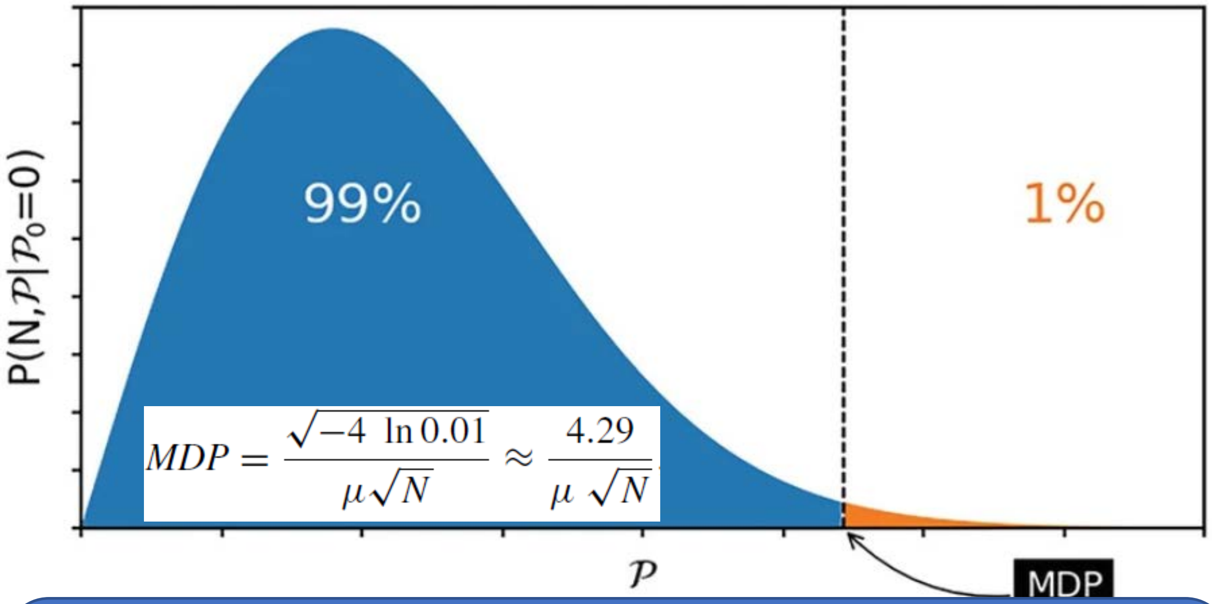

The probability to measure a polarization P from an un-polarized source. The value of P for which this probability is 1 % or smaller is the Minimum Detectable Polarization (MDP).

Muleri F., 2023

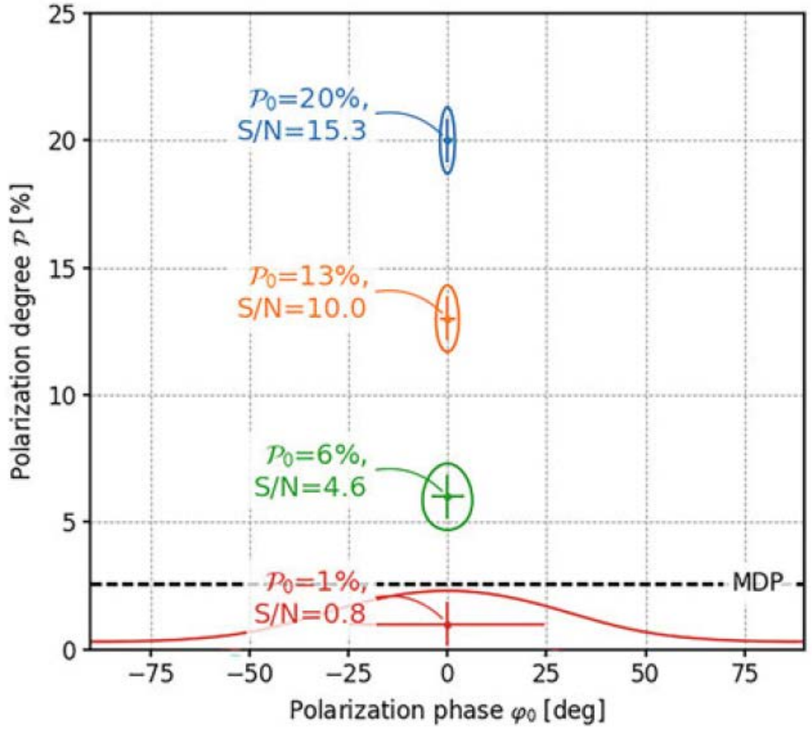

Contours representing the joint probability for P.D. and P.A. at 68 % confidence level. P.D. and P.A. are covariant.

For P < MDP the angle is unconstrained albeit not all the angle are equiprobable.

IXPE HELPS TO CONSTRAIN THE TORUS OPENING ANGLE

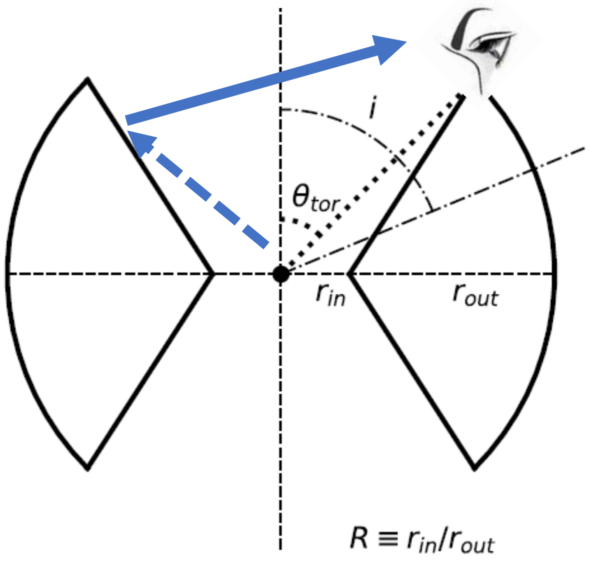

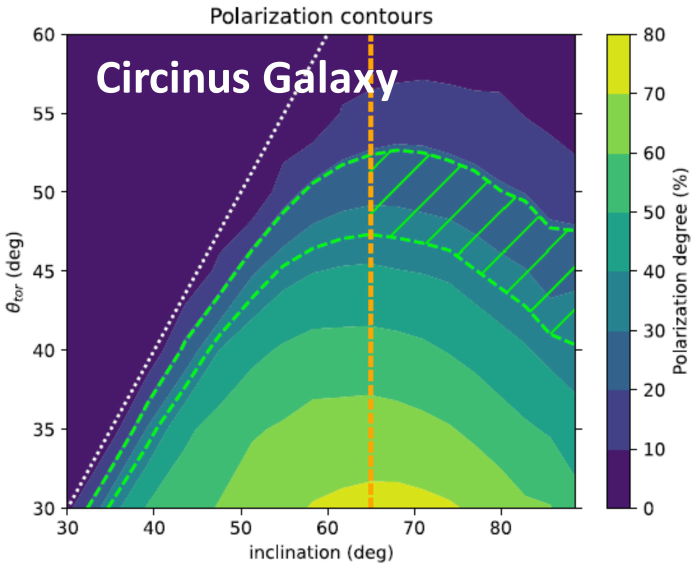

The orange vertical line set the lower limit to the inclination as provided by the inclination of the galaxy. The dashed lines mark the 68% confidence level region consistent with the measured polarization of the cold reflector. The hashed region mark the constraints on inclination and torus aperture.

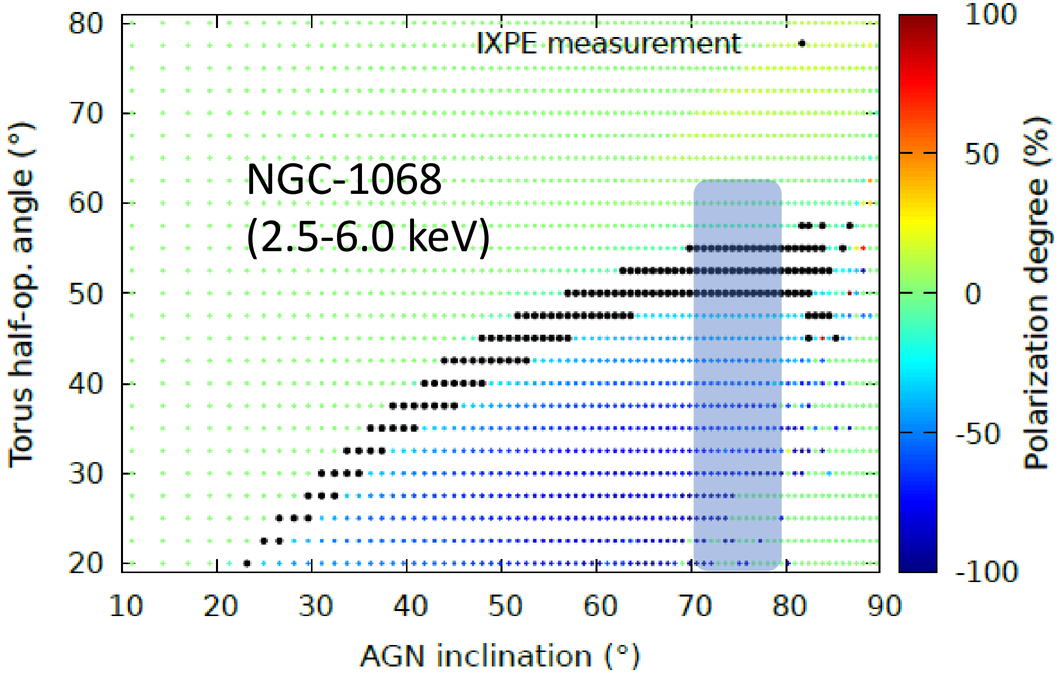

The positive polarization is parallel to the jet, the negative polarization is perpendicular to the jet. Each colored dot represent a simulation. Black dots are consistent with IXPE polarimetry. Shaded region is the constraint from the literature on the torus inclination.

For both Circinus galaxy and NGC-1068 X-ray polarimetry constraints on the torus aperture are similar 50º-55º

IXPE helps to constrain the geometry of the corona.

MCG 05-23-16 (Tagliacozzo et al. 2023)

Simulations with MONK

NCG 4151 (Gianolli et al 2023)

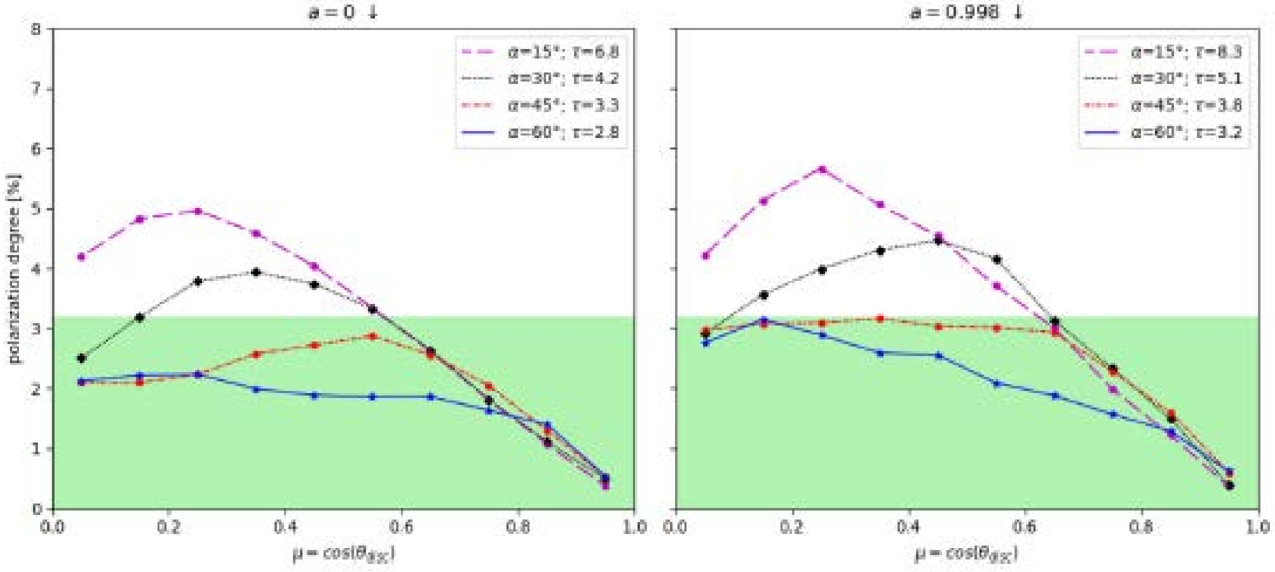

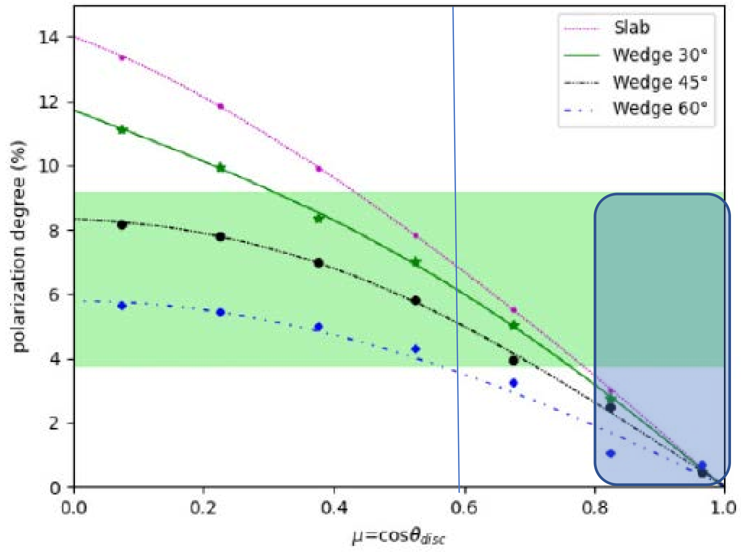

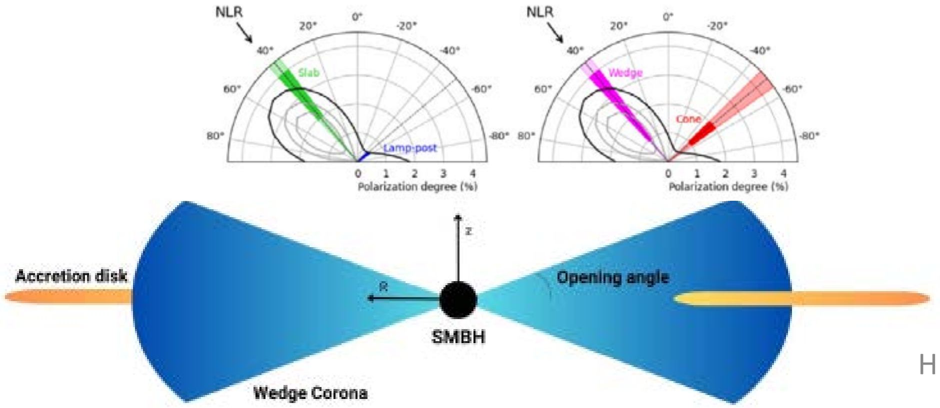

For both MCG 05-23-16 and NGC 4151 Slab o Wedge geometry of he corona are consistent with the IXPE data. NCG4151 favors disk inclinations obtained by reverberation and disfavor inclination obtained by spectra

New observations! Wong, J et al. 2024 submitted to ApJ.

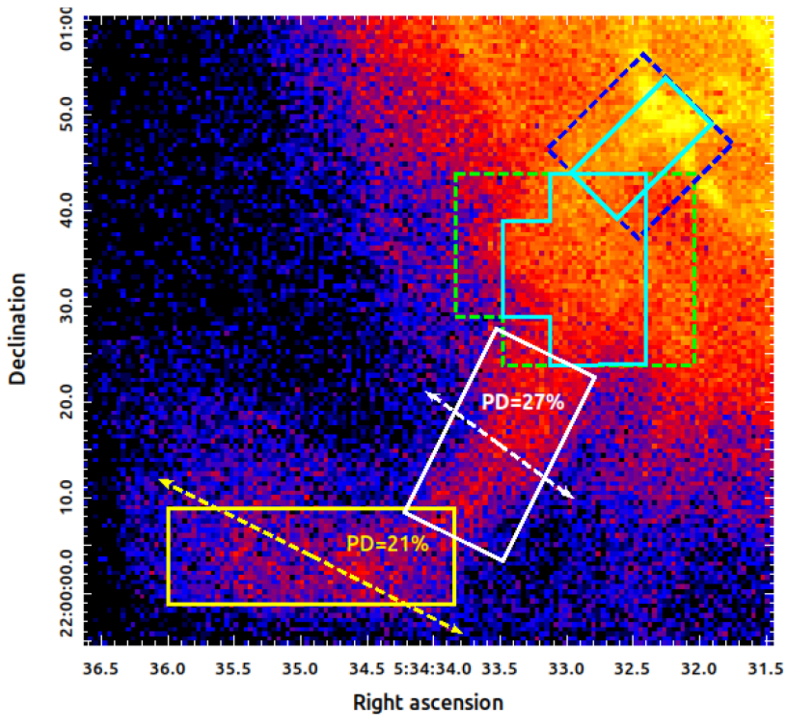

300 ks

>5σ;
>3 σ
>19 σ

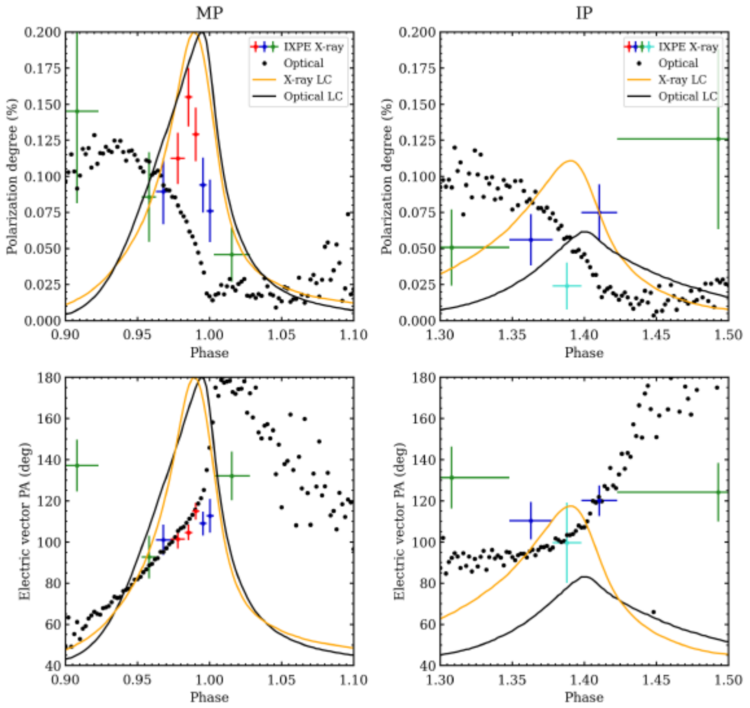

The new observation of Crab is confirming polarimetry of the nebula while providing additional points especially for the jet with perpendicular and parallel magnetic field (kink instabilities, or collision with a dense medium).

Additional points for the pulsar polarization especially for the main pulse are compared with the OPTIMA optical data Slowikowska (2009). Deviation in X-rays from the optical polarization is evident by the data in the main pulse.

IXPE TRACES A STATE TRANSITION WITH SWIFT J1727.8-1613

Discovered on 24th August 2023 (7 Crab in 2-20 keV band)

Most probably a BH-binary transient: (X-ray spectrum, QPO, flat-spectrum radio emission)

Ingram, A. et al., 202ApJ accepted, Podgorny', A&A submitted

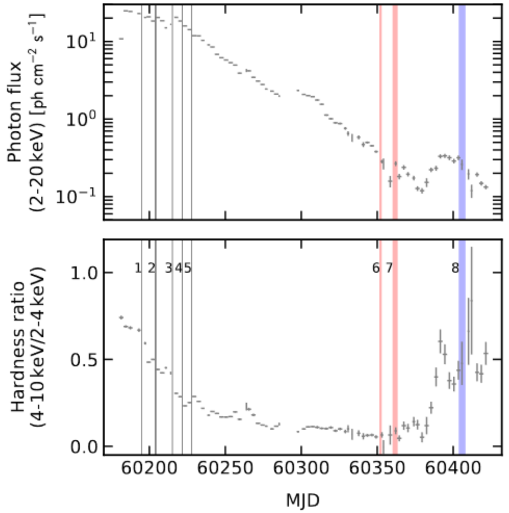

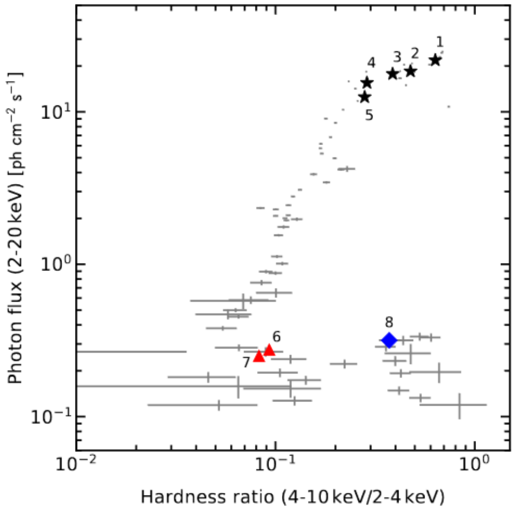

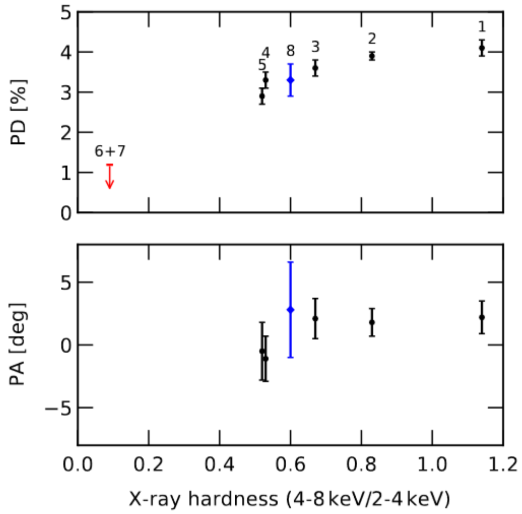

IXPE is covering the hard-to-soft-hard transition. X-ray PA is parallel to Radio-PA implying that corona is extended along the disk in all observations.
PD decreases with time implying that disk emission with orthogonal or null polarization is coming into play.
PD increases with energy as in others BH-Binaries
PD drops in the soft state while recovers in the hard dim state at level of outburst

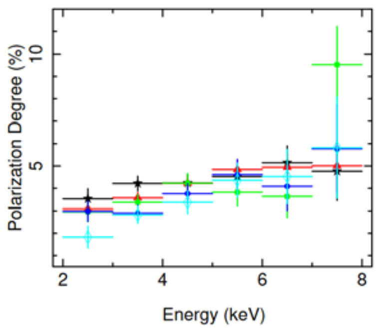

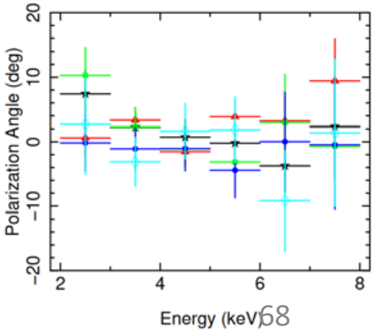

Low Magnetized Neutron Stars

IS = Iland State, LB= Lower Banana, UB = Upper Banana

HB = Horizontal Branch, NB = Normal Branch, FB = Flaring Branch

BL = Boundary Layer; SL = Spreading Layer

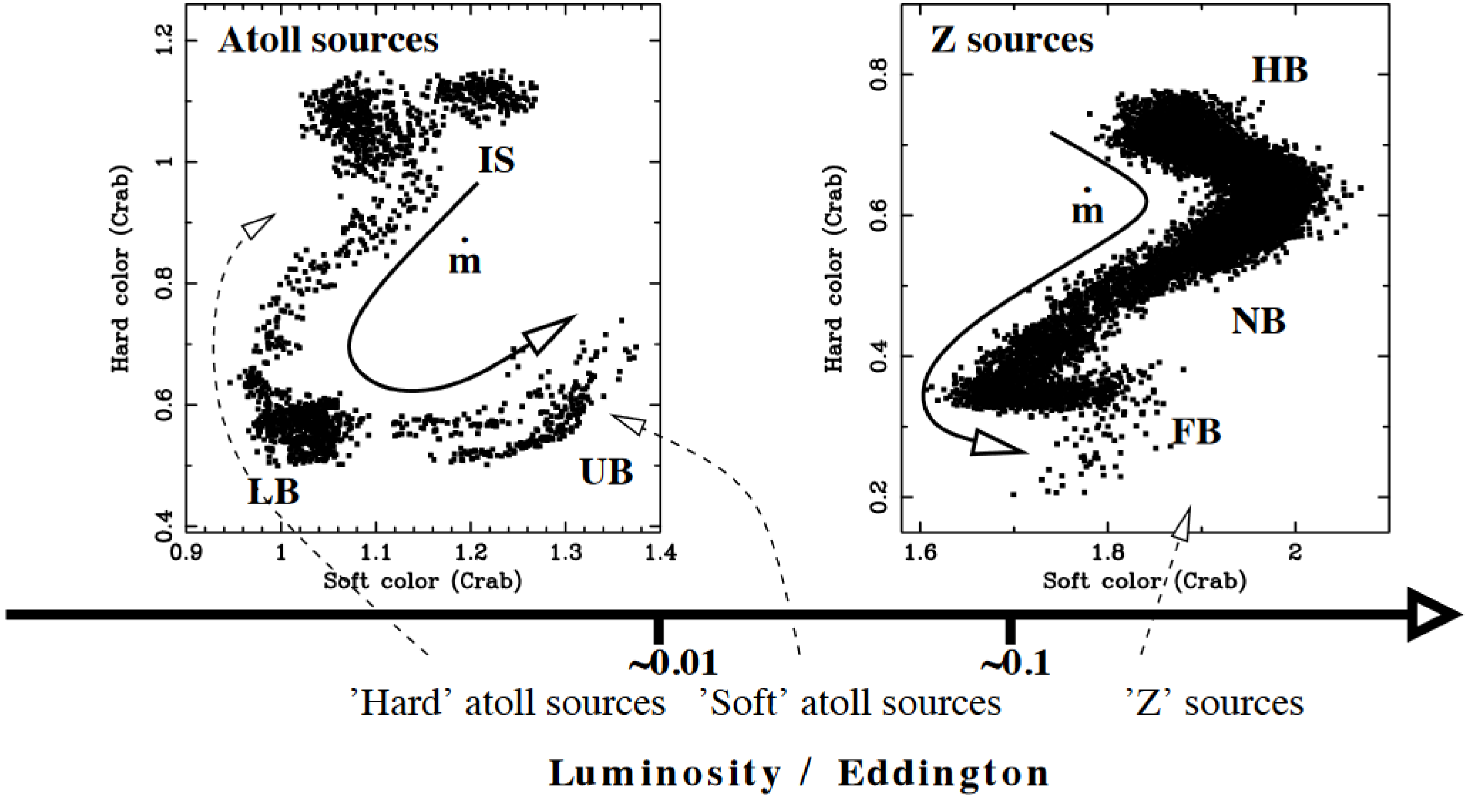

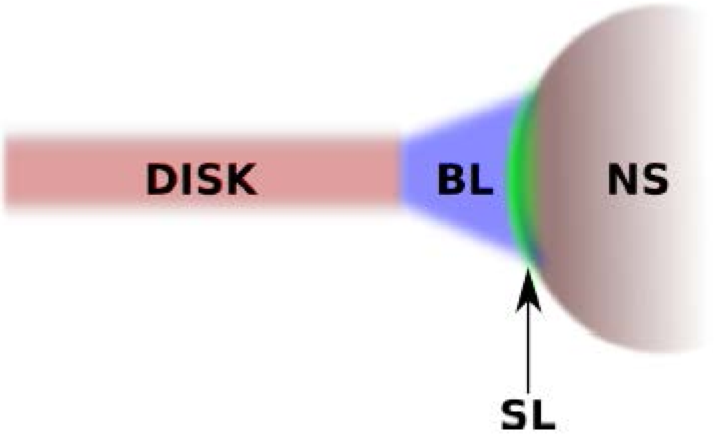

NS: B < 10^{10} G,
$M_{com} \approx M_{\odot}$
Accreting matter via Roche-lobe overflow

Di Salvo et al., 2023

ATOLL SOURCES, 4U 1820-303, GX9+9

Di Marco et al., 2023

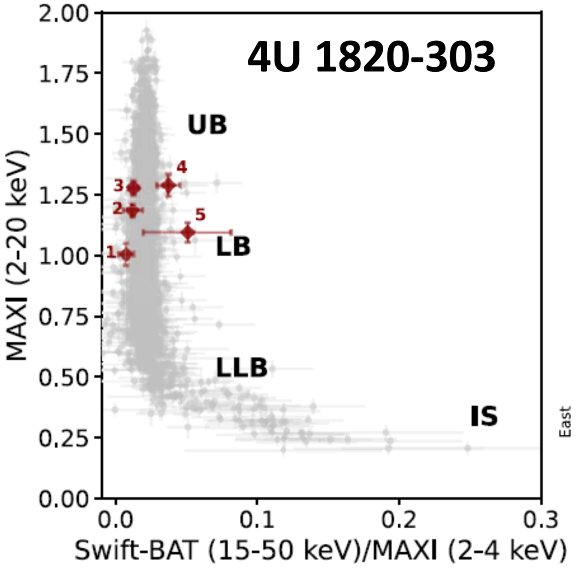

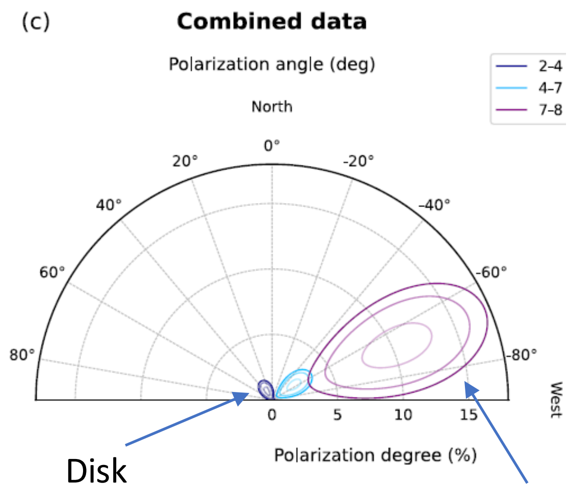

Ursini et al. 2023

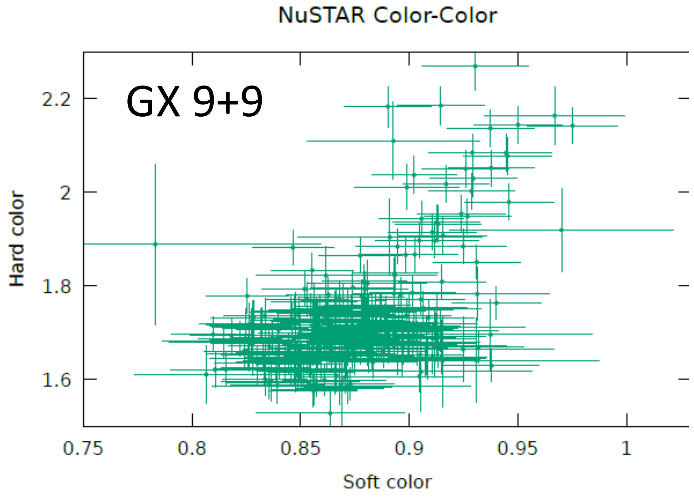

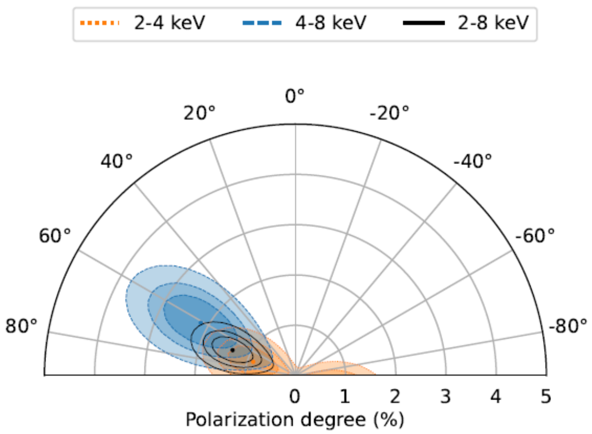

In 4U 1820 a rotation of the polarization angle of 90° with energy may indicate that the disk (low energy) is polarized orthogonal to the spreading/boundary layer. The reflection fraction is negligible < 5%.

In GX 9+9 the 4-8 keV polarization is significant and may be a combination of reflection from the disk and a of Comptonization (boundary/spreading layer) and reflection from the disk.

In GS1826-238 (Capitanio et al., 2023) only upper limit albeit significant were measured.

Z-source Sources: XTE J1701-462, Cyg X-2 and Sco X-1

Cocchi et al., 2023

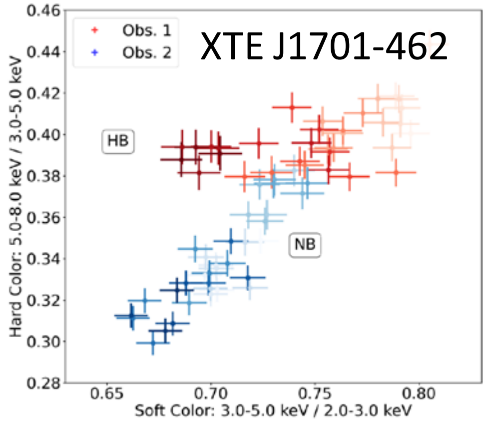

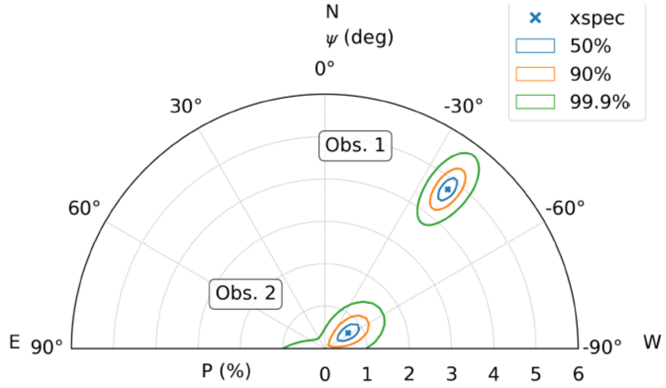

Farinelli et al. 2023

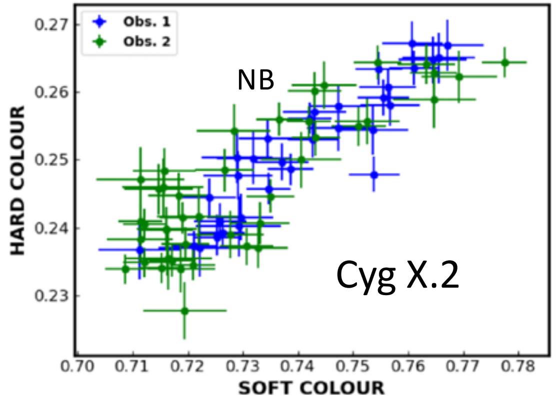

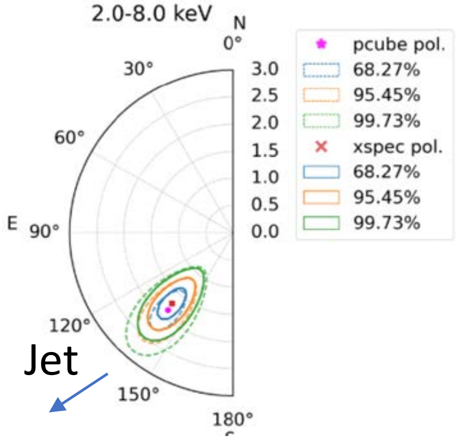

La Monaca et al 2024

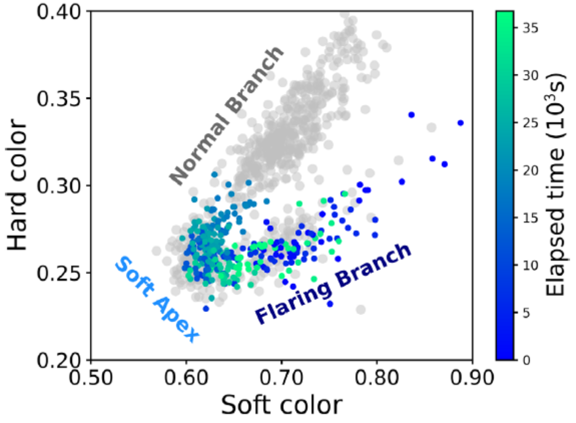

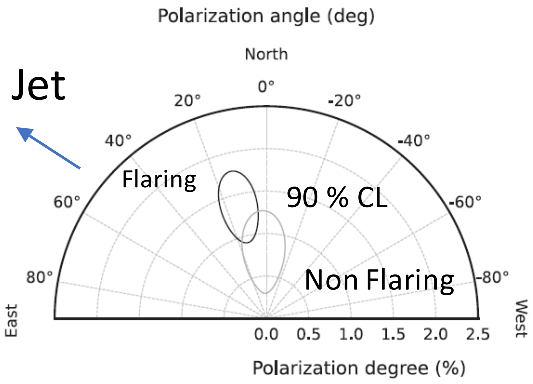

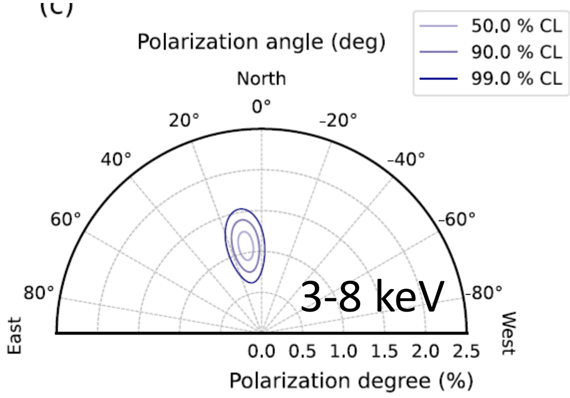

The polarization on the Horizontal Branch seems larger with respect to the polarization of the Normal Branch (See also GX 5.1, Fabiani et al., 2023). In Sco X-1 flaring and non Flaring seems to have comparable PD and PA not aligned with the jet. I Data shows a larger polarization with energy may be connected to a larger contribution of scattering.

BLACK HOLES X-RAY BINARIES:

- High Mass X-ray binaries:

Source (no. obs)	Goal of the study
Cyg X-1 Hard State (2)	Corona
Cyg X-1 Soft State (5)	Corona + Disk
Cyg X-3 hard & Intermediate (2)	Reflection from cone
LMC X-1 High Soft State (1)	Disk
LMC X-3 High Soft State (1)	Disk

- Low Mass X-ray binaries:

Source (no. obs)	Goal of the study
4U 1630-47 High-Soft State (1)	Disk
4U 1630-47 Steep PL/Interm (1)	Disk + Corona
SWIFT J1727 Low Hard/Inter (5)	Disk + Corona
SS 433 Eastern Lobe (1)	Synchrotron emission

GRB 221009A

We did not plan to follow-up on GRBs, because of the relatively slow reaction time (2-3 days).

However, GRB 221009A (the ‘BOAT’ GRB) was so exceptional in terms of brightness, that we decided to observe it.

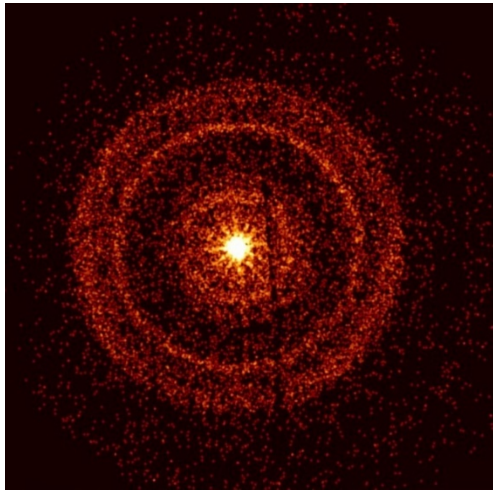

Swift/XRT image

P<13.8% (99% c.l.)

(Negro et al. 2023)

Dust rings also observed →

polarization of the prompt emission (<55%)

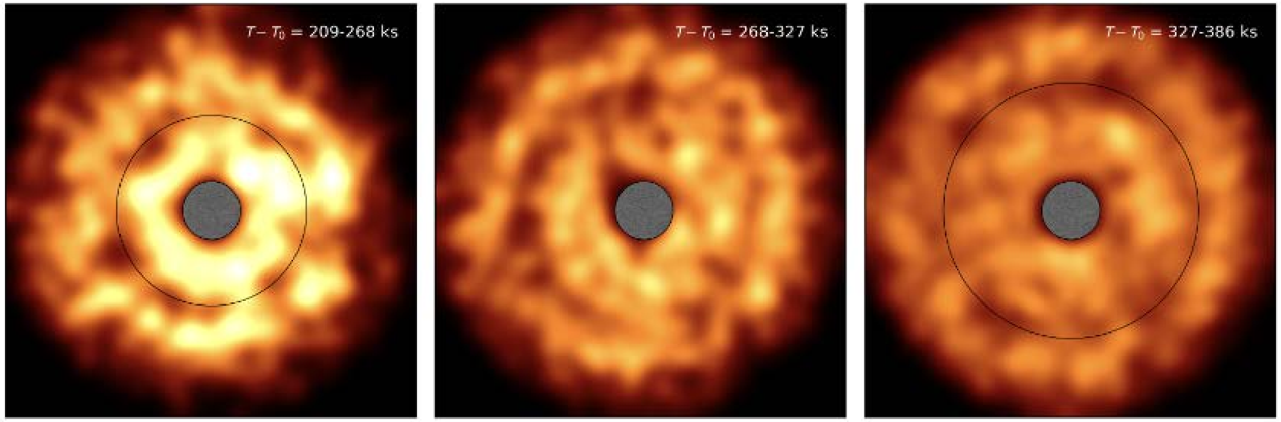

Time evolution of dust rings as seen by IXPE

THE STRANGE CASE OF SGR B2

SgrB2 is a giant molecular cloud at ~100pc projected distance from the Black Hole

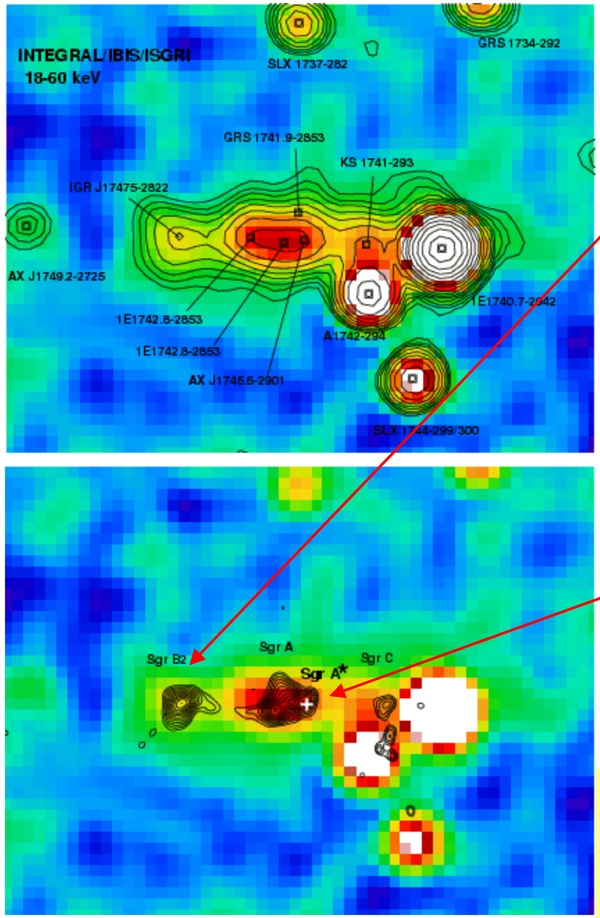

INTEGRAL Image of GC
(Revnivtsev 2004)

The spectrum of SgrB2 is a pure reflection spectrum (Sunyaev et al. 1993)

But no bright enough source is there !!!

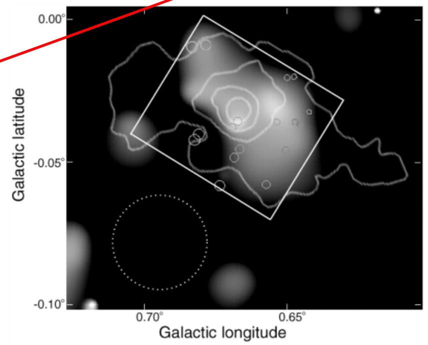

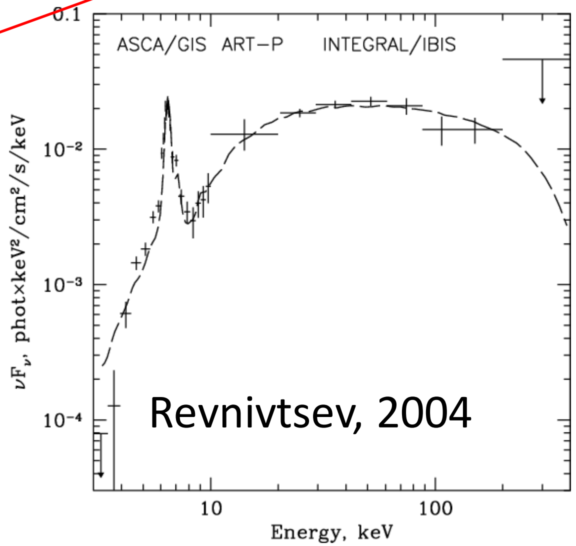

The emission from SgrB2 is extended and brighter in the direction of the BH (Murakami 2001). It is also varying in time (Inui et al. 2008).

Is SgrB2 echoing past emission from the BH, which was therefore one million time more active ~300 years ago ??? (e.g. Koyama et al. 1996)

SUMMARY OF HBL MULTI-WAVELENGTH POLARIMETRY

Table 1. Contemporaneous multiwavelength polarization properties of HSPs.

Source	X-ray		Optical & IR [a]		Radio [a]	
	$\Pi(\%)$	$\psi(^\circ)$	$\Pi(\%)$	$\psi(^\circ)$	$\Pi(\%)$	$\psi(^\circ)$
Mrk 501 I [1]	10 ± 2	134 ± 5	4 ± 1	119 ± 9	1.5 ± 0.5	152 ± 10
Mrk 501 II [1]	11 ± 2	115 ± 4	5 ± 1	117 ± 3	–	–
Mrk 421 I [2]	15 ± 2	35 ± 4	2.9 ± 0.5	32 ± 5	3.4 ± 0.4	55 ± 2
Mrk 421 II [3]	10 ± 1	Rotation	4.4 ± 0.4	140 ± 6	2.4 ± 0.1	139 ± 8
Mrk 421 III [3]	10 ± 1	Rotation	5.4 ± 0.4	145 ± 1	–	–
Mrk 421 IV [4]	14 ± 1	107 ± 3	4.6 ± 1.3	206 ± 9	1.8 ± 0.1	167 ± 4
1ES1959+650 I [5]	8 ± 2	123 ± 8	4.5 ± 0.2	159 ± 1	–	–
1ES1959+650 II [5]	<5	–	4.7 ± 0.6	151 ± 19	<1.6	–
PG1553+113 [6]	10 ± 2	86 ± 8	4.2 ± 0.5	Rotation	2.6 ± 0.7	133 ± 7
1ES0229+200 [7]	18 ± 3	25 ± 5	3.2 ± 0.7	-5 ± 9	<7	–

[1–8] Results compiled from the following references: [57–63]; [a] median polarization properties during the IXPE observation. Especially for optical and IR polarization, only corrected polarization values, accounting for the dilution of polarization by unpolarized starlight from the host galaxy, were considered for calculation; [b] at the lowest radio frequency (4.85 GHz).

Kim et al., 2024

X-ray polarization of HBL are comparable higher than at longer wavelength

Notably Mrk 421 was found rotating in X-rays and not in longer wavelength while PG1553 was rotating in longer wavelength but not in X-rays

The Formalism

Fit function: $\mathcal{M}(\phi) = A + B\cos^2(\phi - \phi_0)$

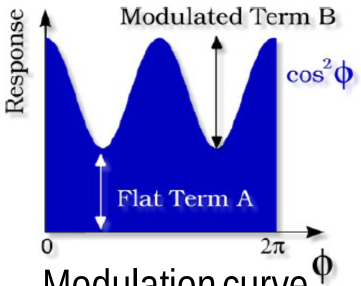

Modulation curve

Modulation: $\frac{\mathcal{M}_{\max} - \mathcal{M}_{\min}}{\mathcal{M}_{\max} + \mathcal{M}_{\min}} = \frac{B}{B+2A}$

Polarization: $\frac{1}{\mu}\frac{B}{B+2A}$

μ is the modulation factor, i.e. the modulation for 100% polarized radiation

Or by using Stokes Parameters

$$S(\varphi) = I + U\sin(2\varphi) + Q\cos(2\varphi)$$

$$I = (A + \frac{B}{2}) \qquad U = \left(\frac{B}{2}\right) * \sin(2\varphi_0) \qquad Q = \left(\frac{B}{2}\right) * \cos(2\varphi_0)$$

$$P = \frac{\sqrt{Q2+U2}}{I} \qquad \varphi = \frac{1}{2} atan \frac{U}{Q}$$

No V → no circular polarization with present techniques

Kislat et al. (2015) introduced the Stokes parameters from the direction of the single carrier of polarimetric observation

The first limit: In polarimetry the sensitivity is a matter of photons

$$MDP = \frac{4.29}{\mu R_S}\sqrt{\frac{R_S + R_B}{T}}$$

Minimum Detectable Polarization (MDP)

R_S is the Source rate, R_B is the Background rate, T is the observing time
μ is the modulation factor: the response of the polarimeter to a 100% polarized beam (spanning from 0 or no sensitivity, to 1 or maximum sensitivity)

If background is negligible: $$\mathrm{MDP} = \frac{4.29}{\mu\sqrt{N_{ph}}}$$

To reach MDP=1% with μ=0.5: $$N_{ph} = \left(\frac{4.29}{\mu\,\mathrm{MDP}}\right)^2$$ = 736 10^3 ph

Source detection > 10 counts
Source spectral slope > 100 counts
Source polarization > 100.000 counts

Caution: the MDP describes the capability of rejecting the null hypothesis (no polarization) at 99% confidence.

POLARIZATION ANALYSIS: MDP AND CONTOURS

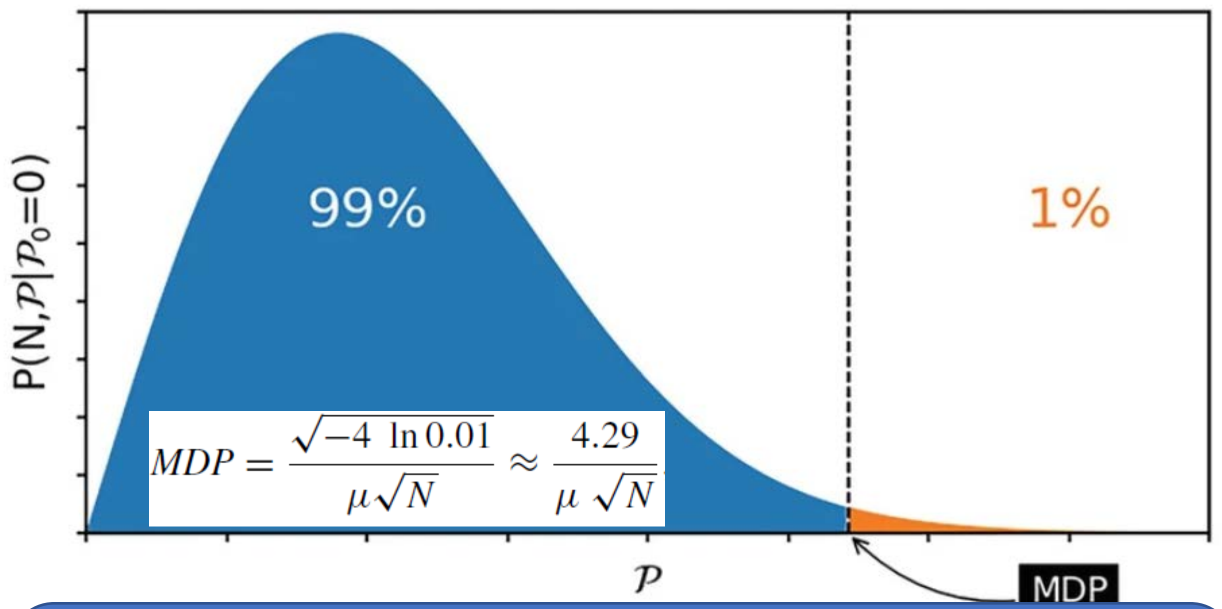

$$MDP = \frac{\sqrt{-4\ \ln 0.01}}{\mu\sqrt{N}} \approx \frac{4.29}{\mu\ \sqrt{N}}$$

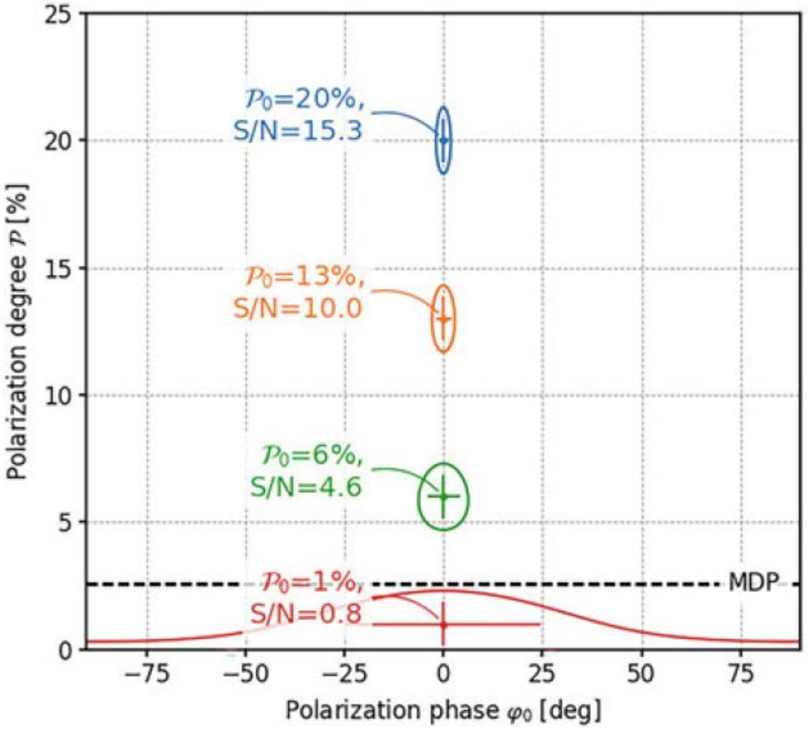

The probability to measure a polarization P from an un-polarized source. The value of P for which this probability is 1 % or smaller is the Minimum Detectable Polarization (MDP).

Contours representing the joint probability for P.D. and P.A. at 68 % confidence level. P.D. and P.A. are covariant.

For P < MDP the angle is unconstrained albeit not all the angle are equiprobable.

Muleri F., 2023

IXPE Imaging X-Ray Polarimetry Explorer

TOP SCIENTIFIC REQUIREMENTS OF IXPE (ENERGY-TIME-ANGLE RESOLVED POLARIMETRY)

Physical Parameter	Observable	Property	Value	
Linear Polarization	Degree Π, angle ψ	Sensitivity $MDP_{99}(F_{2-8} = 10^{-11}$ cgs, $\Delta t = 10$ d)	$\leq 5.5\%$	Ok
		Systematic error in polarization degree Π (5.9 keV)	$\leq 0.3\%$	Ok
		Systematic error in position angle ψ (6.4 keV)	$\leq 1^\circ$	Ok
Energy dependence	$F(E)$, $\Pi(E)$, $\psi(E)$	Energy band E_{min}–E_{max}	2–8 keV	Ok
		Energy resolution ΔE ($E = 5.9$ keV), $\propto \sqrt{E}$	≤ 1.5 keV	1 keV
Spatial dependence	$F(k)$, $\Pi(k)$, $\psi(k)$	Angular resolution HPD (system-level)	$\leq 30''$	30”
		Field of view FOV >> HPD	$\geq 9'.0$	Ok
Time dependence	$F(t)$, $\Pi(t)$, $\psi(t)$	Time accuracy << source pulse periods	≤ 0.25 ms	1-2 µs (GPS)
Areal background rate	R_B/A_{det}	$R_B/A_{det} << R_S/A_S$ for faint source (2-8 keV, per DU)	$< 0.004\ s^{-1}cm^{-2}$	0.04

See Xie, F. et al., 2021

The requirement on the background was set at the time of phase A as a fraction of the expected counting rate of the most dim (and extended) IXPE source: a molecular clouds in the galactic center region.
Such requirement was corroborated by the internal background expectation of Ne-based OSO-8 proportional counter (Bunner, 1978). Subsequent GEANT four simulation showed that the expected background was indeed larger (Xie et al., 2021).

IMAGES AND MODULATION FACTORS OF THE CALIBRATION SOURCES

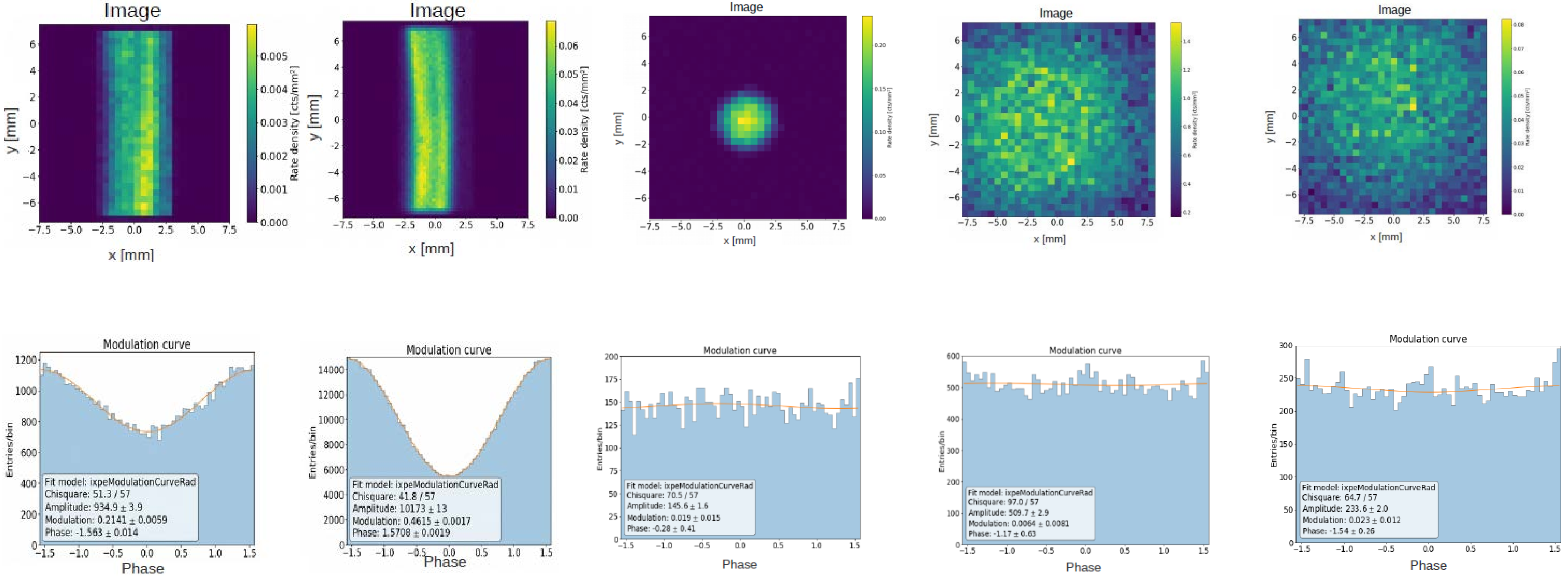

3.0 keV Cal A Pols | 5.9 keV Cal A Pol | 5.9 keV Cal B | 5.9 keV Cal C | 1.7 keV Cal D

MODULATION FACTOR AND SPURIOUS MODULATION CHECK

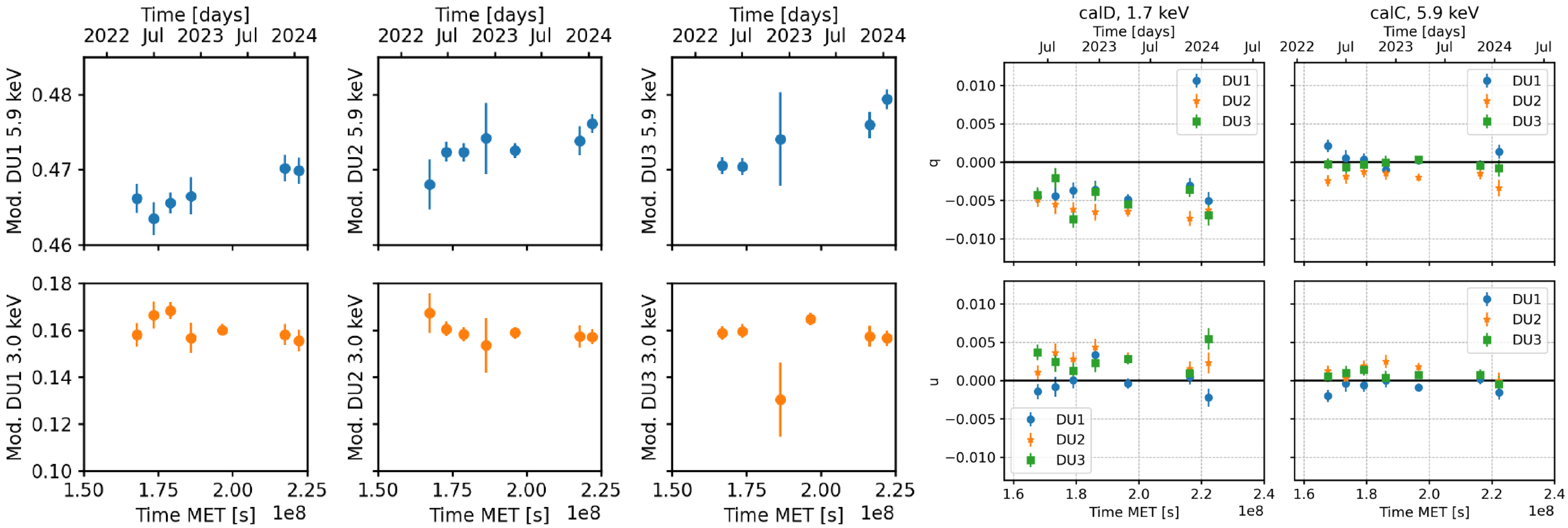

Modulation factor as expected slightly rises (0.25-0.5%/yr)
Spurious modulation (before the event-by-event-correction) stay constant&small

Some IXPE results

TWG 1: (Pulsar Wind Nebulae): The magnetic field is very ordered even at a large distance from the pulsar.

TWG 2: (Supernova Remnants): The magnetic field can be radially directed even in vicinity of the shock.

TWG 3: (Accreting Black Holes): The corona in hard X-ray is along the disk plane the accretion disk and the lamp-post is excluded.

TWG 4: (Accreting Neutron Stars): The rotating vector model works in X-rays. The degree of polarization is 5-6 times smaller with respect to models predictions.

TWG 5: (Magnetars): Different magnetars showed unexpectedly very different behavior on the polarization degree and angle.

TWG 6: (Radio-Quiet AGN & SgrA clouds): Corona is sandwiching the disk. Lamp-post is excluded. Reflection confirms obscuring torus in Compton-thick AGNs. Molecular clouds points to Sgr A* as origin of their reflected emission.

TWG 7: (Blazars and Radio Galaxies): Energy stratified shock acceleration is confirmed. In X-ray fast rotation of the polarization vector with time is present in Synchrotron dominated blazars. Inverse Compton dominated blazars

TimePIX3: from MEDIPIX CERN collaboration

Timepix3: a 65K channel hybrid pixel readout chip with simultaneous ToA/ToT and sparse readout

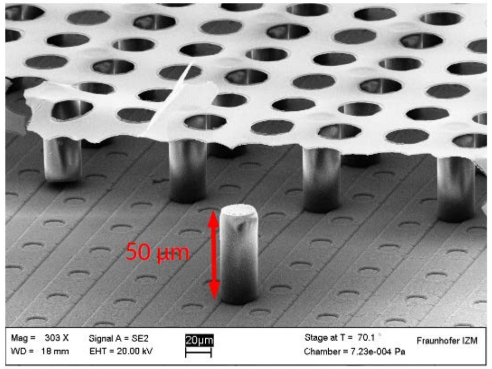

Kaminski, 2017, Lupberger 2015

Parameter	Value
Pixel matrix	256 x 256 = 65536 pixels (2x4 superpixels)
Pixel size	55 x 55 μm^2
Technology	CMOS 120 nm
Measurement type	1. Simultaneous 10 bit TOT, 14 + 4 bit ToA 2. 14 + 4 bit ToA only 3. 14 bit integral ToT
Readout type	1. Data Driven (zero-suppression) 2. Frame based (zero-suppression)
Dead time per pixel	ToT + 457 ns (pulse processing + data transfer)
Output bandwidth	Up to 5.12 Gbs (parallel 8 channels x 640 Mbps)
Maximum Counting rate	Data Driven up to 40Mhits/cm^2/s with duty cycle of 100 %
TOA precision (resolution)	1.56ns
Front End noise, minimum threshold	60 e_{rms} , 500 e^-

3-D imaging of the track is possible.

High rate for large optics is possible

Ongoing collaboration with University of Bonn

A collimated experiment of X-ray polarimetry requires a large area

Li, 2021

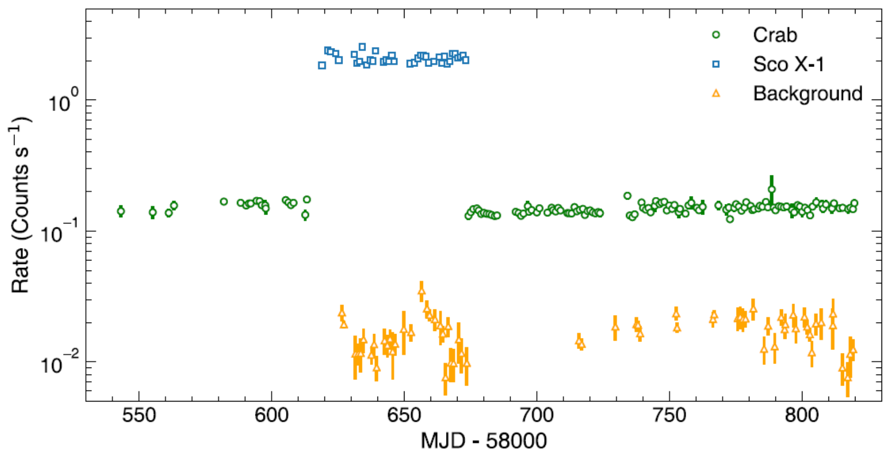

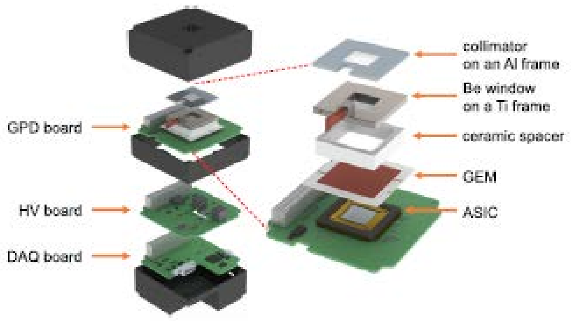

Feng et al.,, 2019

No optics!
Small Mission!
Bright Galactic Sources!

An alternative approach

- Background Polar Light : about 80 mCrab after discrimination, (Jiahuan Zhu 2021)
- Collimator open fraction 71 %
- Area 1000 cm^2
- Crab rate = 65 c/s (2-8 keV)
- Background = 5 c/s
- MDP (1 Crab 100 000 s) = 0.5 %

512x448 pixels (55x55 μm^2)
Area 1 ASIC 7 cm^2
Tiling on 4 Sides
200 ps time resolution
140 ASICs to cover 1000 cm^2

Large power required

Llopart et al., 2022, TimePIX 4

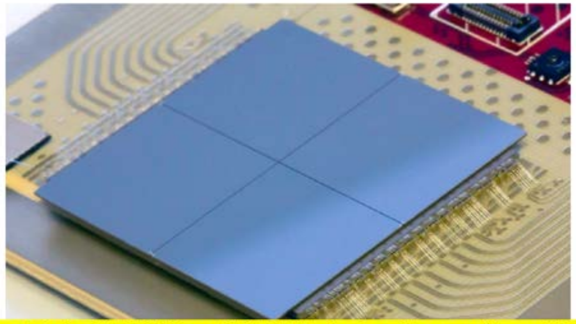

Timepix4v0 with 4x300 µm (256x256) edgeless Si sensor (August 2020)

Baracchini et al., 2020, Amaro et al., 2022

Optical photoelectron track imaging

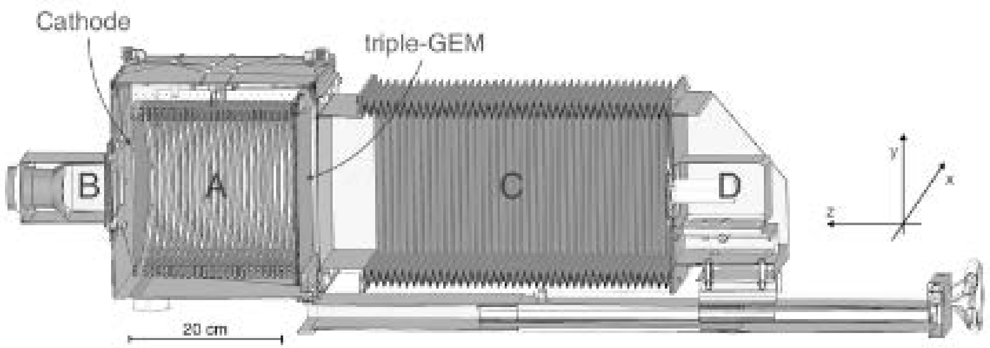

Nicely solve the problem of large collecting area !

ORTHOGONAL ROTATORS

GRO J1008-57 Tsygankov et al., 2023

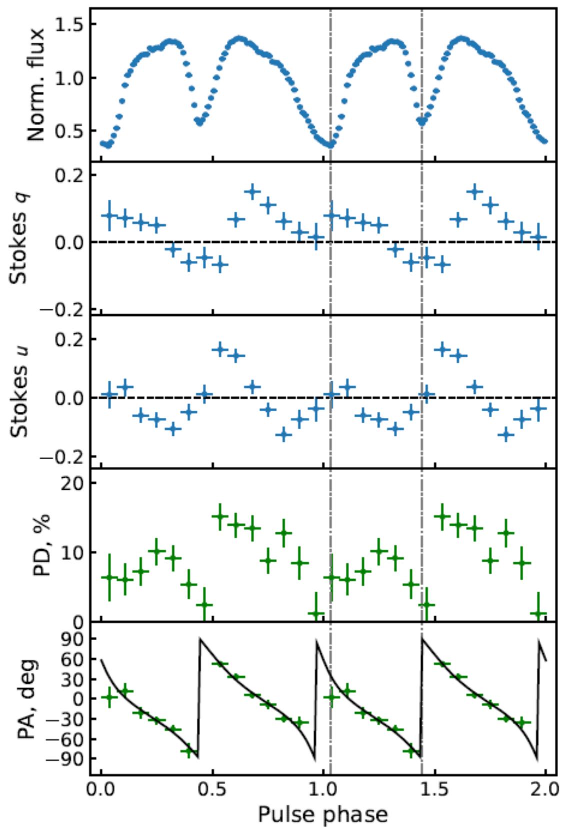

$$\tan(\mathrm{PA} - \chi_{\mathrm{p}}) = \frac{-\sin\theta\ \sin(\phi - \phi_0)}{\sin i_{\mathrm{p}} \cos\theta - \cos i_{\mathrm{p}} \sin\theta \cos(\phi - \phi_0)},$$

i_p is the angle between the pulsar spin and the line-of-sight, θ is the angle between the magnetic dipole and the spin axes, X_p, is the position angle of the spin axis

	GRO J1008-57	X Persei
i_p	130°.2+/-3°.3	162°+/-12°
θ	73°.5+/-1°.9	≈ 90° (>75° 68%)
$X_{p,O}$	74°.8+/-4°.2	70°+/-30°

$X_{p,X} = X_{p,O}$ +/- 90°

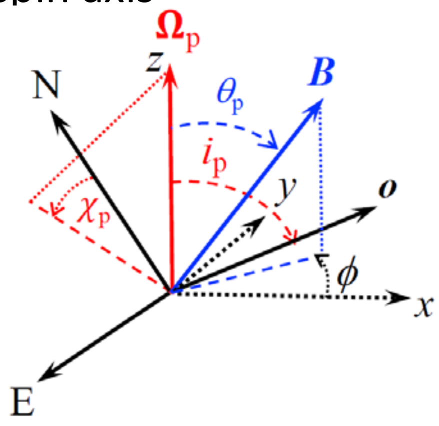

X Persei Mushtukov et al., 2023

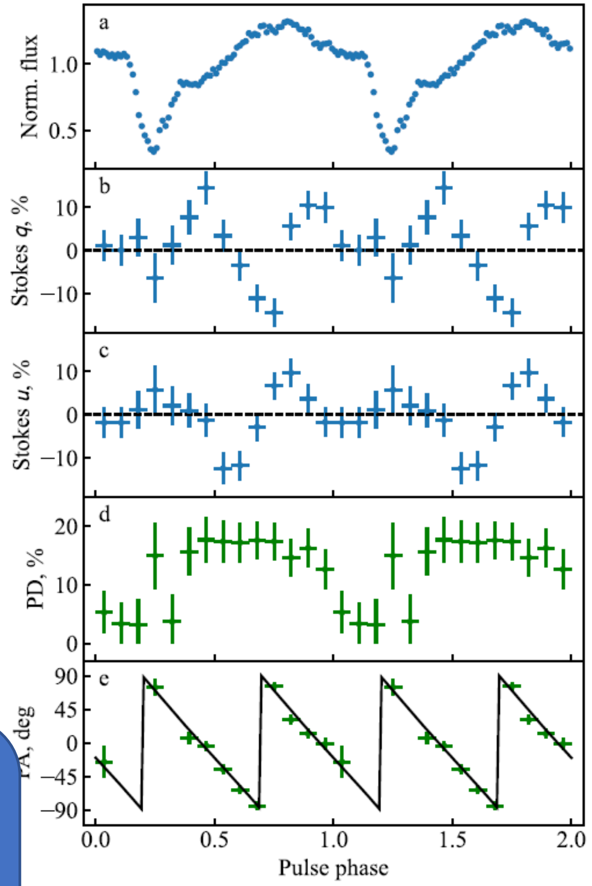

The rotating vector model showed two oblique rotator.
They were in sub-critcle regime
GRO J1008-57: L ≈ 10^{36} erg/s << few10^{37} erg/s = L_{crit}
X Persei: L ≈ 5x10^{34} erg/s << L_{crit} 3 10^{37}
In Subcritical regime the phase resolved PD and flux correlate

IXPE Pipeline, Analysis Software &web pages

- *Model independent analysis tool and IXPE observation simulator IXPE.* Baldini L. et al. SoftwareX 2021
- *Spectro-polarimetric forwarding folding fit based on XSPEC that includes polarization phenomenological models.* (Arnaud, K. , Ast.Src.Code, 1999)

Algorithms and response matrices designed by the instrument team we engineered for the flight pipeline by the SSDC .

Two completing different software approaches provided when eventually compared consistent results.

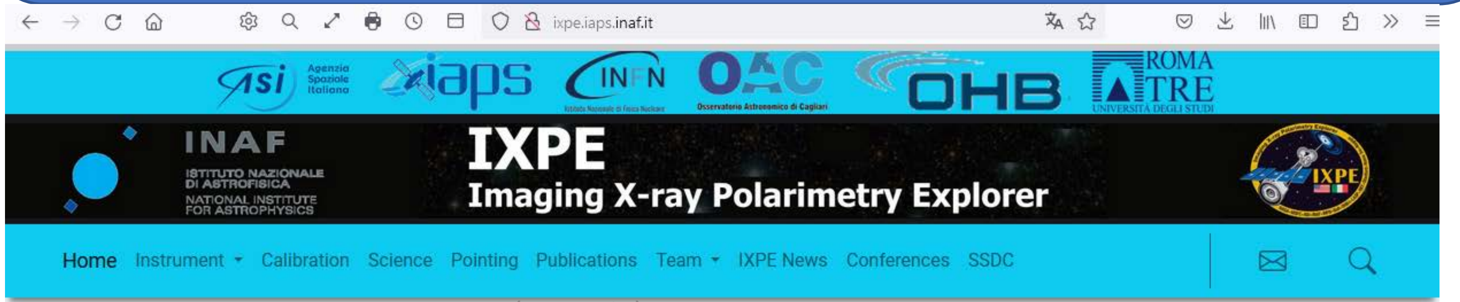

BLACK HOLES X-RAY BINARIES SOME PUBLICATIONS:

- High Mass X-ray binaries:

Source	Main result	Reference
LMC X-1 High Soft State	MDP_{99}=1.1% Standard thin disk compatible	Podgorny et al., MNRAS, 2023
LMC X-3 High Soft State	PD=(3.2+/-0.6)% PA=-42°+/-6° Low-spin (a= 0.2, a<0.7 from pol. analysis only)	Svoboda et al., ApJ, 2024

- Low Mass X-ray binaries:

Source	Goal of the study	
4U 1630-47 Steep PL/Interm.	PD = (6.8+/-0.2)% PA = 21°.3+/-0°.9 PL emitting region like the disk ?	Rodriguez Cavero, N., ApJ, 2023
4U 1957+11 High Soft State	PD: (1.9+/-0.4)%; PA:-41° +/-5°.7 High spin (a> 0.96)	Marra et al., Sub A&A, 2023
SWIFT J1727 Low Hard/Inter	Disk + Corona (confirming sandwich corona)	Veledina, A. et al ApJ, 2023 Ingram, A. et al. ApJ 2024
SS 433 Eastern Lobe (1)	Synchrotron emission	Kaaret, P. et al, ApJ, 2023

MODULATION FACTOR (FROM CALIBRATION)

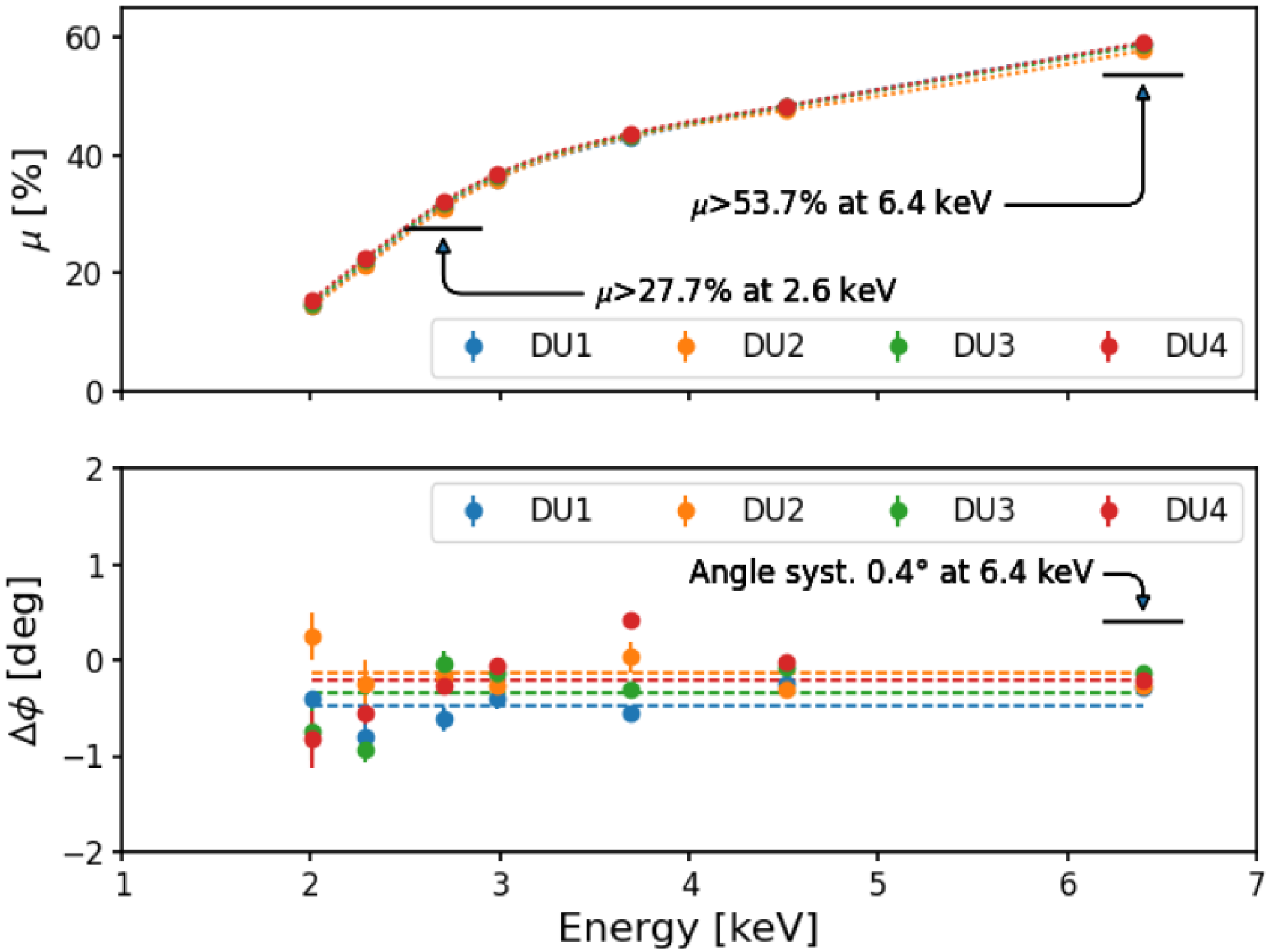

ENERGY RESOLUTION

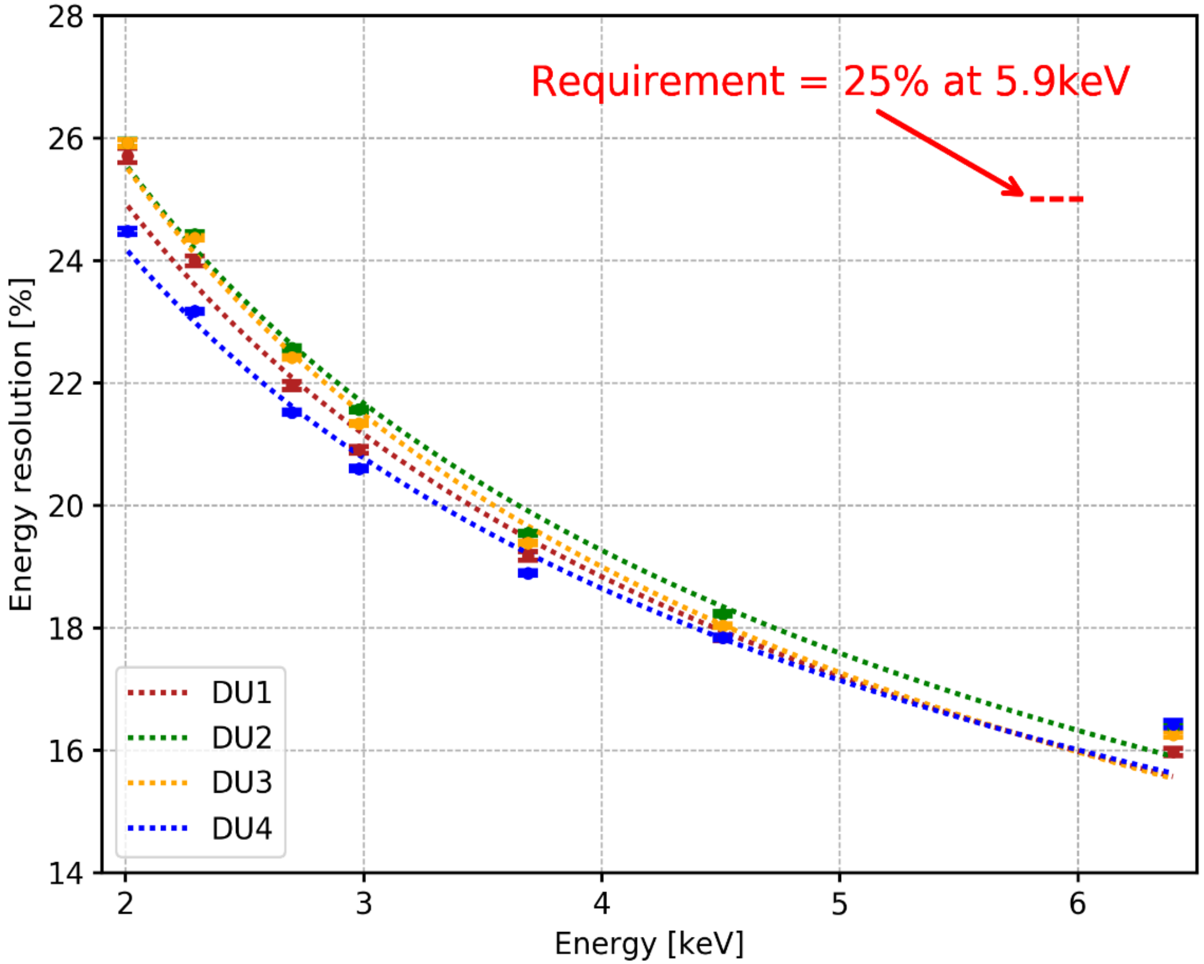

Energy calibration is much better of a typical proportional counter after gain equalization.

The gain equalization (Rankin J., et al. AJ 2023) is performed by comparing the average charge in one pixel with the one of the other pixel in the ROI.

Gain spatial maps are applied to the event energy reconstruction by the flight pipeline

Position resolution of the detector (From calibration)

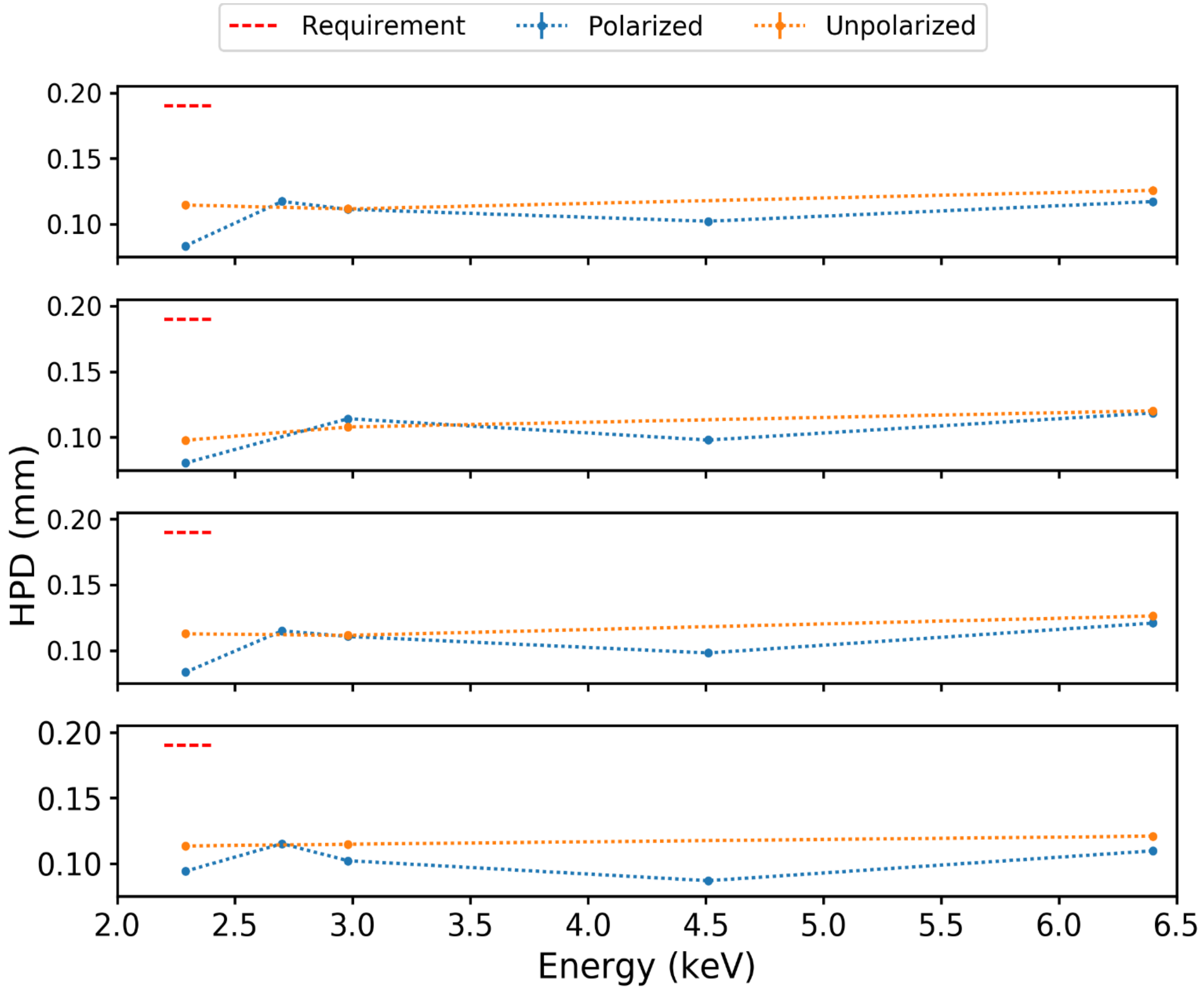

SXRP (Stellar X-ray Polarimeter)

- A step forward in the sensitivity was done devising and building a polarimeter based on Bragg diffraction and Thomson scattering in the focus of a large X-ray telescope.
- Photons coming from the SODART telescope are diffracted by a thin mosaic graphite crystal at 2.6 keV and 5.2 keV creating a secondary focus. The photons at E > 5 keV that do not satisfy the Bragg condition pass through and are diffused around by a lithium scatterer. 4 position sensitive proportional counters detect simultaneously the radiation. SXRP is in rotation around the telescope axis.
- Bragg diffraction saves the images and is more sensitive at low flux, Thomson scattering provides better sensitivity at large fluxes but the image is lost.

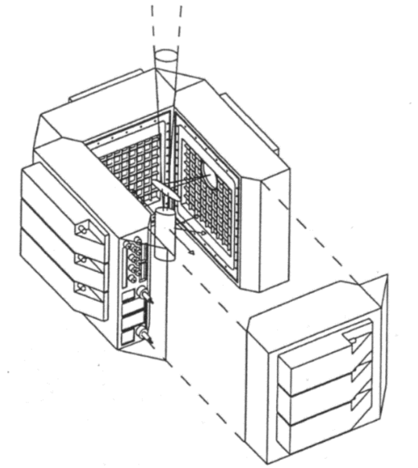

- 4 x 100 cm^2 imaging proportional counter
- Composite window thickness :
  - 150 μm for Thomson scattered photons
  - 50 μm for Bragg diffracted photons, ø = 3.3 cm)
- Graphite mosaic cristal (50 μm thick)
- Lithium scatterer 7 cm long and Ø = 3 cm encapsulated in 150 μm thick beryllium case
- Rotary motor for the ensamble detector/analyser at 1 rpm

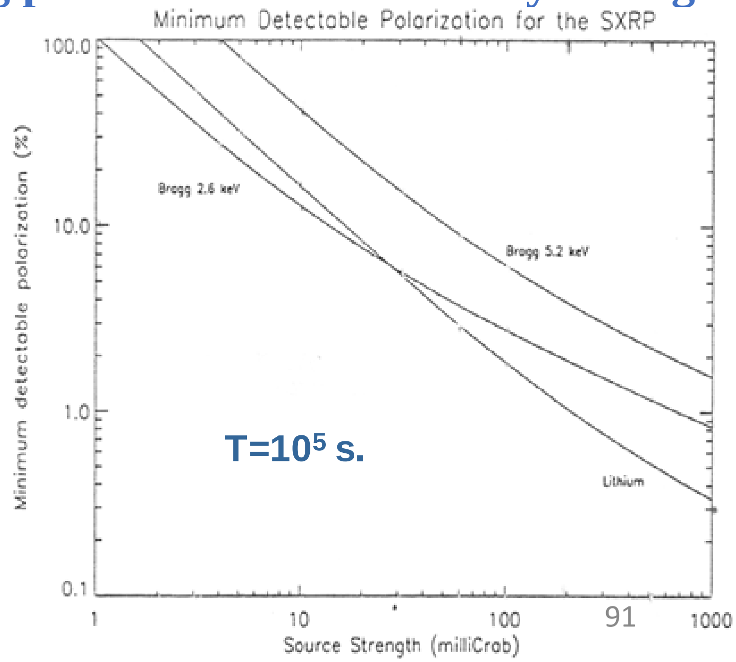

Kaaret et al., OptEng 1989, SPIE 1994 Tomsick et al., SPIE 1997, Soffitta et al., NIM A, 1998

TELESCOPE CALIBRATION (DURING PANDEMIC!)

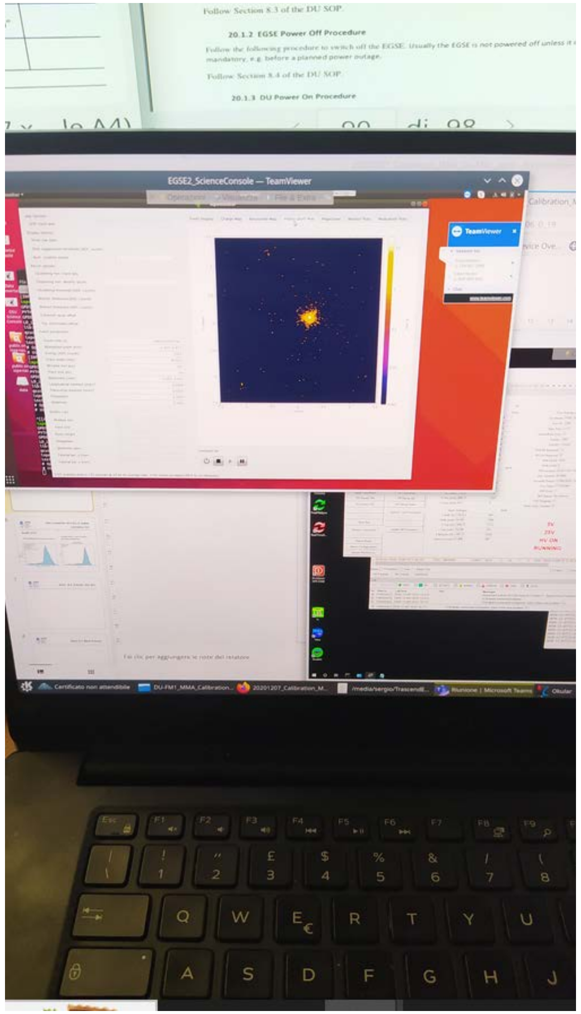

First light 9 December 2020
@IAPS computer 8000km away

Telescope calibration were performed with a Mirror unit spare and a Detector Unit Spare to validate the separate calibration

A link for active monitoring the command was set-up for remote check and commanding.

INAF-IAPS team worked following the working hours of NASA-MSFC so up to very late at night.

Calibrations lasted about two weeks (working days).

The Stray Light facility at MSFC was adapted for the telescope calibration following the experience of the two calibration equipment built at INAF-IAPS for Calibration of prototypes and Calibration of 4 flight detector Units.

MODULATION FACTOR AND SYSTEMATICS COMPARISON

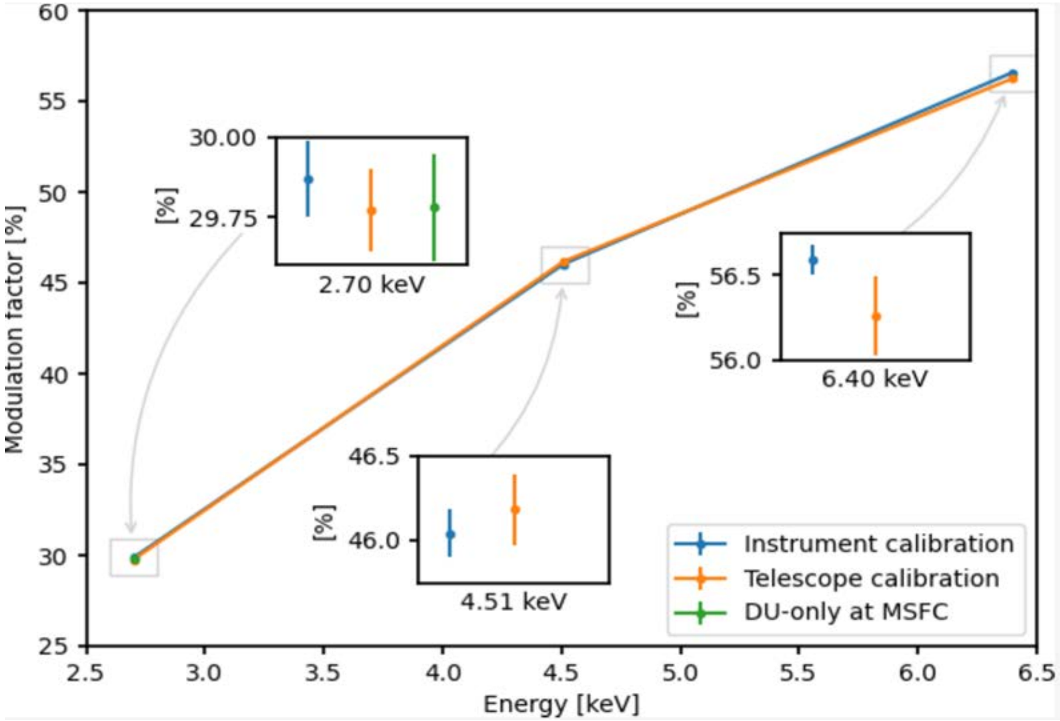

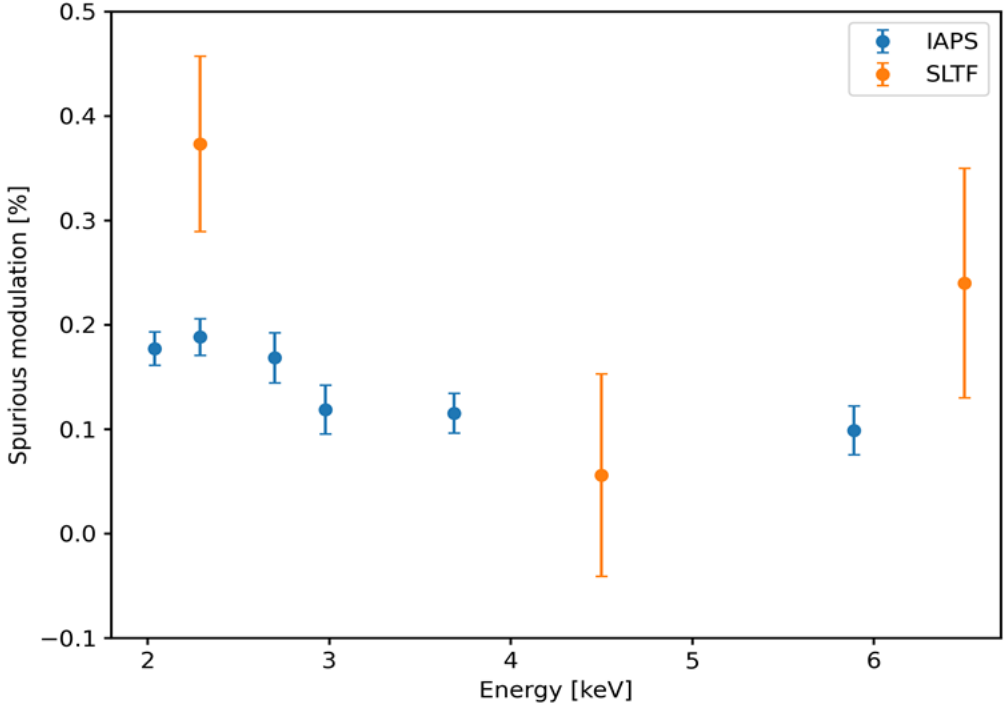

Adapted by Fabiani, S. presentation at ASI

As expected by first principles the presence of the optics does not alter the polarization: modulation factor @MSFC were the same as @ IAPS. The same for the spurious modulation

1-D PHOTOELECTRIC POLARIMETER

- CCD (Tsunemi et al., 1992, Holland 1995, Kotthaus, 1998) Edge effect polarimeter (Range is .short in Silicon)
- Gas Imager (Austin et al. 1990, La Monaca et al., 1998, Sakurai 2004) High energy/Cumberson device

Sanford , Cruise & Culhane 1970

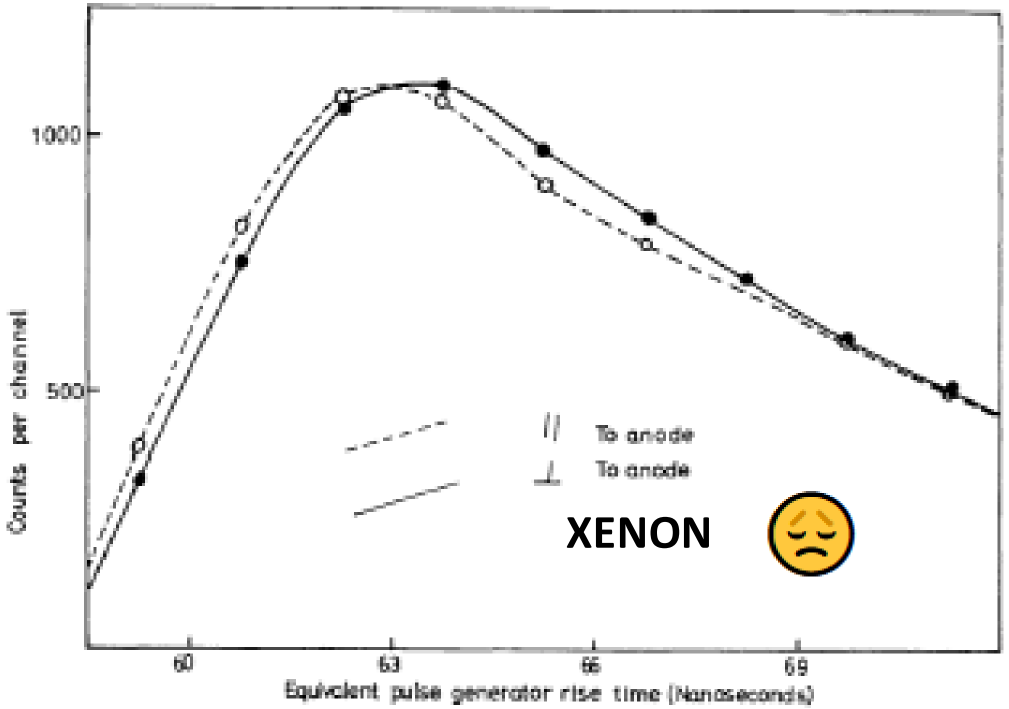

Soffitta P. et al., 1995, 2001

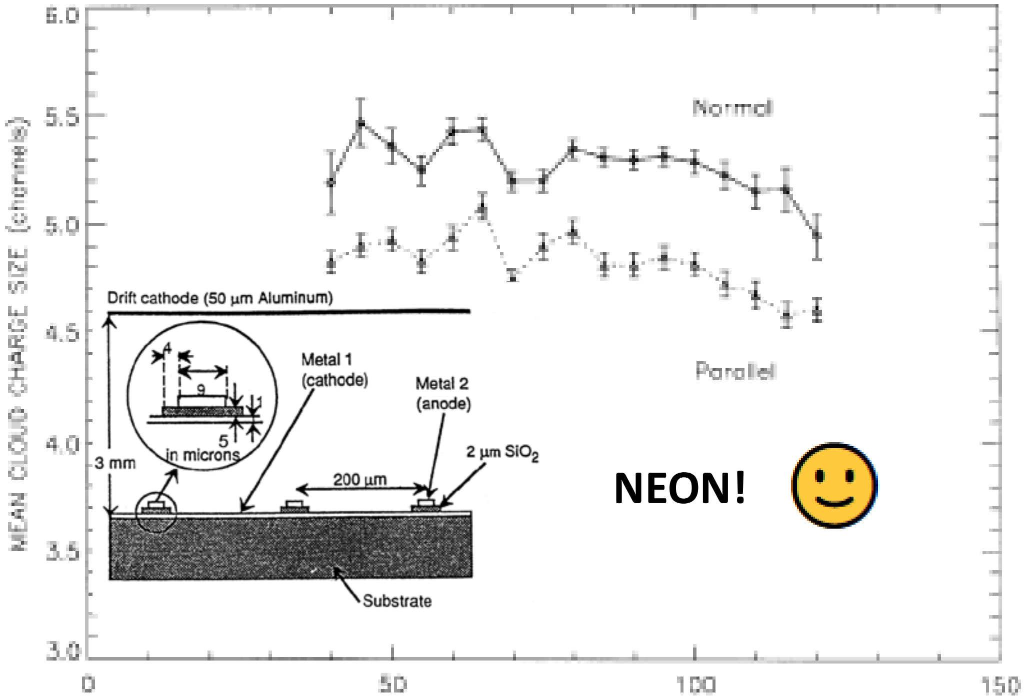

We soon pointed into a low-Z gas mixture (neon) and to a highly segmented gas detector having as a goal an imaging focal plane experiment.

By the way IXPE won the 2024 Bruno Rossi Prize of HEAD:

High Energy Astrophysics Division

The 2024 Prize Winner: Martin Weisskopf, Paolo Soffitta, and the IXPE team

The 2024 Bruno Rossi Prize has been awarded to Dr. Martin Weisskopf, Dr. Paolo Soffitta, and the IXPE team for their development of the Imaging X-ray Polarimetry Explorer whose novel measurements advance our understanding of particle acceleration and emission from astrophysical shocks, black holes and neutron stars. Please see the press release for more information.

Winter Meetings

- 245th AAS Meeting: 12–16 January 2025, Gaylord National Resort & Convention Center, National Harbor, MD

SITE-VISIT TEAM (END OF PHASE A)

At the end of Phase A in November 2016 IXPE team met the evaluation board in MSFC to review the outcome of phase A + DEMONTRATION OF A WORKING DETECTOR + POLARIZED X-ray SOURCE.

Martin Weisskopf on the 3rd January 2017 sent an e mail saying that IXPE was selected but no-proprietary data was awarded to the team.

FROM A MISTAKE TO A TRUE PHOTOELECTRIC X-RAY POLARIMETRY

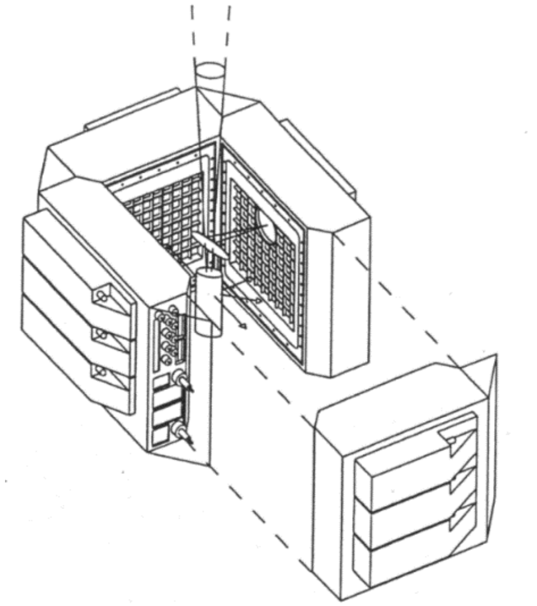

The Stellar X-ray Polarimeter (USA, Italy, Russia)

Kaaret et al., OptEng 1989, SPIE 1994 Tomsick et al., SPIE 1997, Soffitta et al., NIM A, 1998

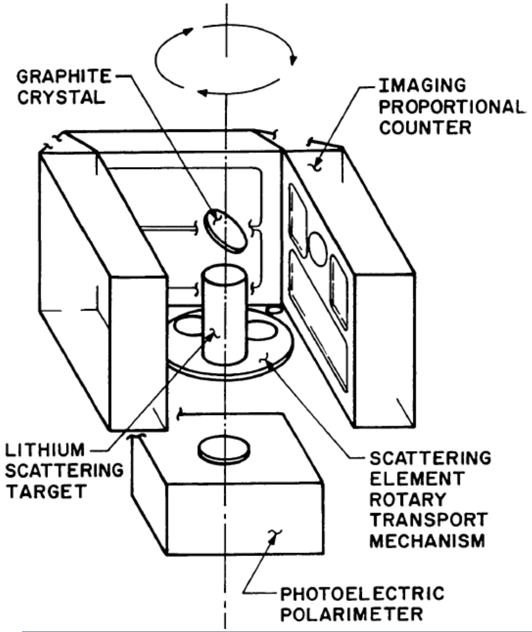

Hanany, S. et al., 1995

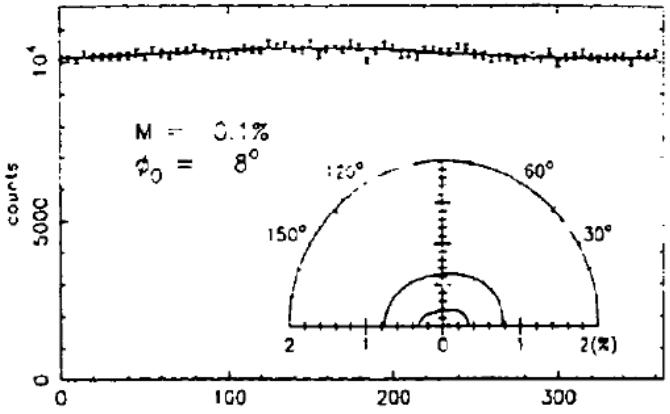

TABLE I. Sample observing plan for the SXRP mission.

Source	Observing Time (10^5sec)	Min. Det. Pol. (%) Graphite	Min. Det. Pol. (%) Lithium	Observing Time (10^5sec)	MDP (%) CsI
Energy (keV)		2.6	5 – 10		0.1 – 5
Radio Pulsars					
Crab Primary Pulse (Avg.)	2	6.0	6.2	1	0.8
Leading Edge	2	8.0	7.6	1	1.1
Trailing Edge	2	9.4	7.6	1	1.2
Supernova Remnants					
Crab Nebula	2	0.5	0.4	1	< 0.1
PSR 1055–52				2	10
Binary Pulsars*					
Her X-1**	7	2.8	1.6	1.5	0.8
4U0900-4	1	2.8	0.9	0.5	0.5
GX1+4	1	4.3	1.2	0.5	0.8
4U1223–62	2	3.8	0.9	1	0.7
4U1626–67	2	3.4	1.8	1	0.6
Cen X-3	1	1.8	0.6	0.2	0.5
Black Hole Candidates					
Cyg X-1	6			1	
Low State		1.0	0.8		0.2
High State		0.3	0.2		< 0.1
LMC X-1				4	1.0
QPOs					
Cyg X-3	1	1.5	0.6	0.2	0.4
Sco X-1	1	0.7	0.1	0.01	0.2
4U1822–37				2	3.6
AGN's					
Cen A	1	7.6	1.9	1	1.0
Mkn 421	6	4.6	18.6	1	1.9
3C273	6	3.8	6.1	1	1.6
PKS2155–304				1	1.5
ESO 141-G55				1	2.6
NGC 7469				1	1.9
Mkn 509				1	1.7
Mkn 501				1	2.1
2A1218+304				1	1.8

The photoelectric polarimeter, as configured, did not worked for a experimental mistake but the expected sensitivity was great in the soft-X-rays .

So we had the idea to replace CsI photocatode and vacuum with a suitable gas mixture (with low atomic number!) to make the charge image of the track of the photoelectron!.

End of successful Mission Critical Design Review

June 24 (2019), the IXPE passed the Mission Critical Design Review (M-CDR)

I-CDR Final report 01-08-2018: The Instrument (I) CDR end was anticipated with respect to the Mission CDR by almost 1 year (20 months after IXPE approval by NASA) !

OPTICS MADE, INTEGRATED AND CALIBRATED BY MSFC

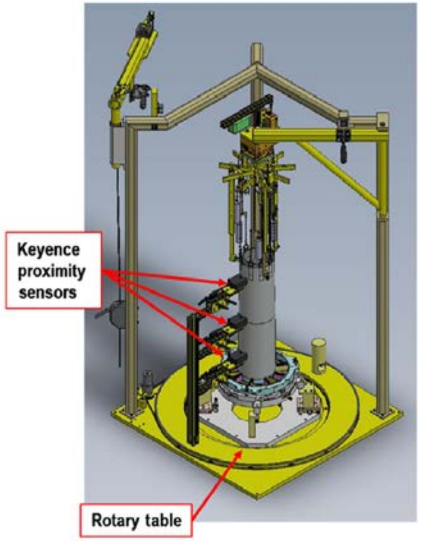

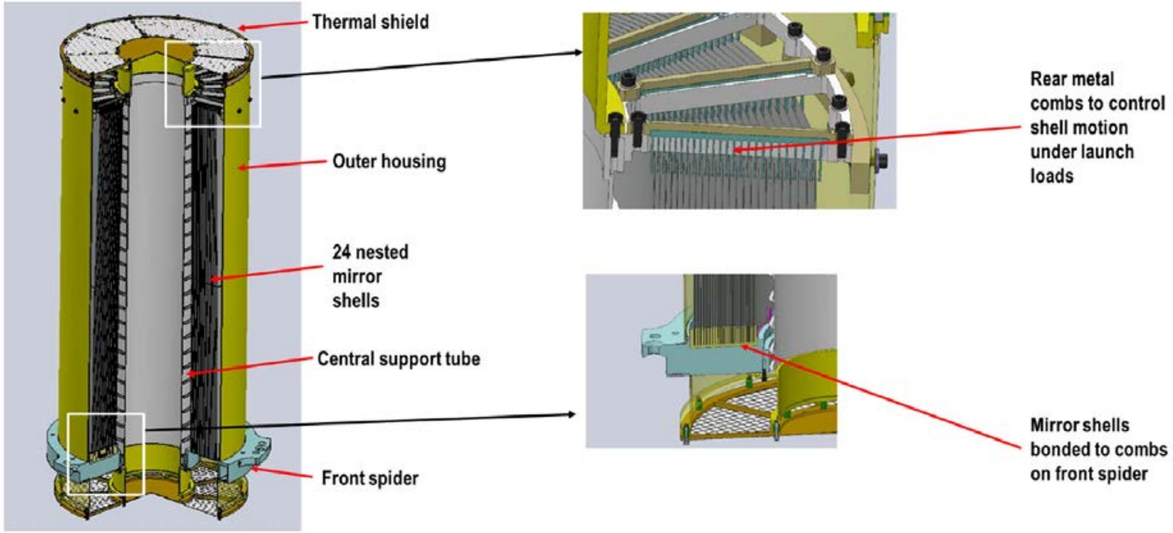

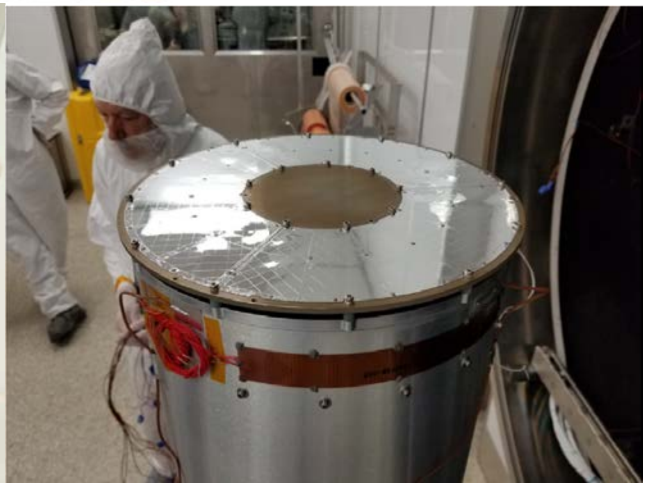

Rear Spider of the MMA

Thermal Shield

Ramsey, B. et al, JATIS, 2022
Bongiorno, S. et al., SPIE, 2021

HPD MEASURED IN-FLIGHT

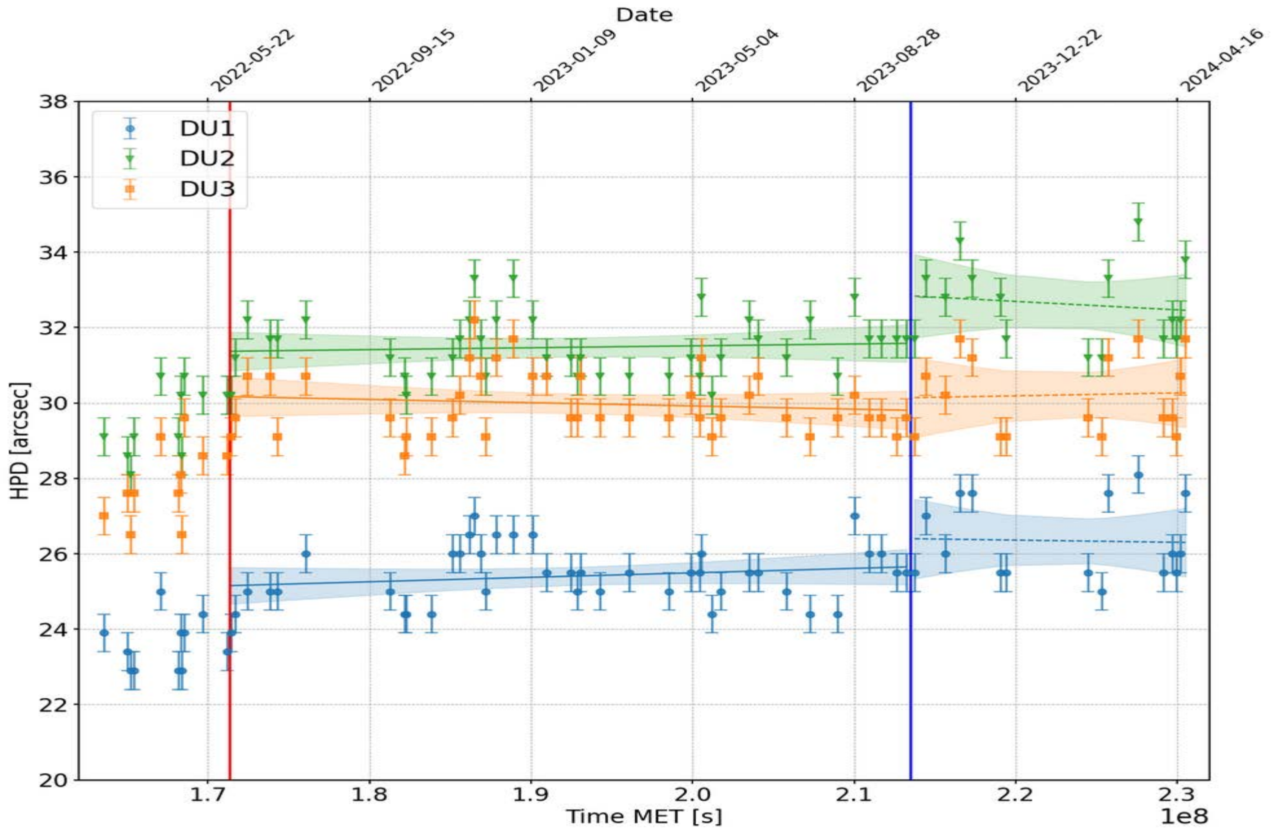

John Rankin et al., 2024 in preparation

The in-flight performance of the detector + mirror systems are in line with the expectation. The HEW is indeed dominated first by the quality of the optics, then by the inclined penetration effects finally much less by the position resolution of the detector.

THE IXPE COMMISSIONING

The Instrument commissioning team
Two week of instrument commissioning ending
9 January 2022

The Mission Operation Center was held at Laboratory for Atmospheric and Space Science of University of Colorado (Boulder, Co).

The use of a University facility with operators as trained student allowed for keeping the cost low keeping safety. But only working hours.

A large contribution from INAF and INFN was required with direct participation in the in the decision flow in the Decision Room together with the flight director.

PECULIARITY OF THE CURRENT GPD DESIGN

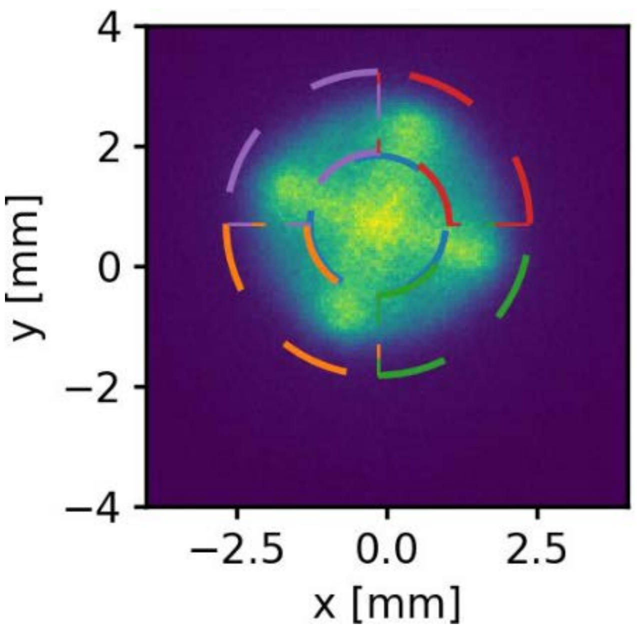

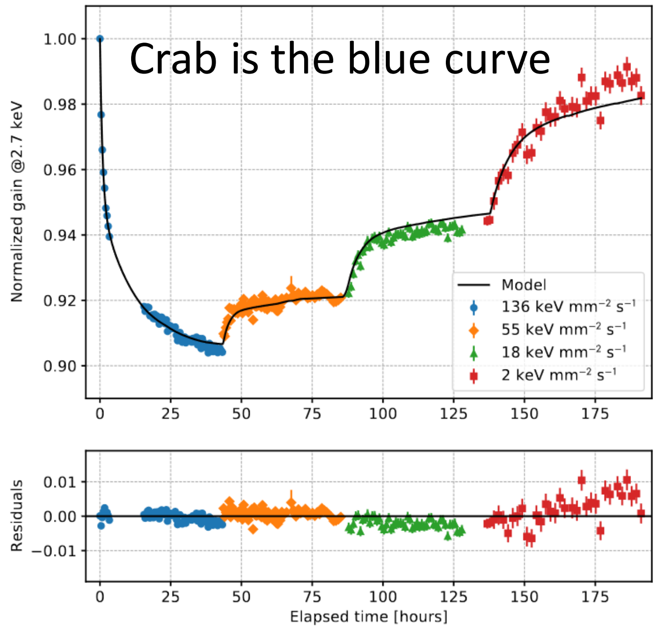

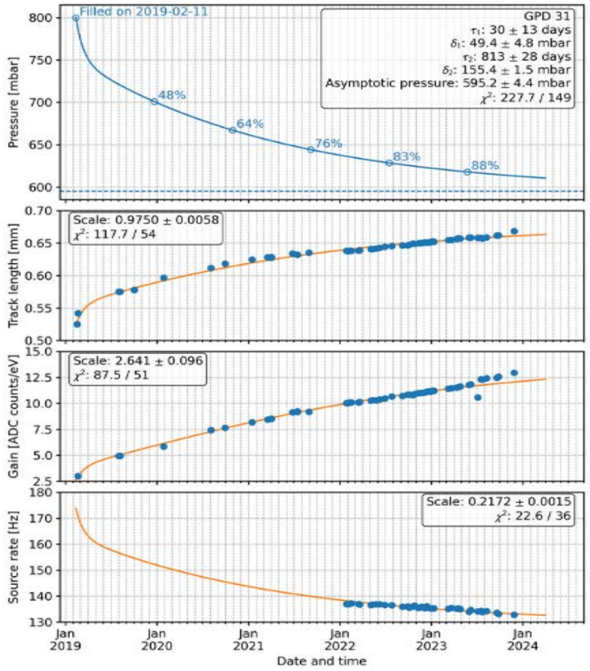

Being un-useful the rotation, a dithering is required to facilitate the ground calibration.

Gain shift due to charging is not yet totally corrected. Charging is responsible for a residual miscalibration of 10-20 eV

Pressure drop due to absorption of the DME by the glue (model in Baldini L. et al 2021).
c.a. 650 mbar current pressure (much more precise value in the CalDB)

CHECK ON THE EFFECTIVENESS OF GAIN CALIBRATION IN ORBIT

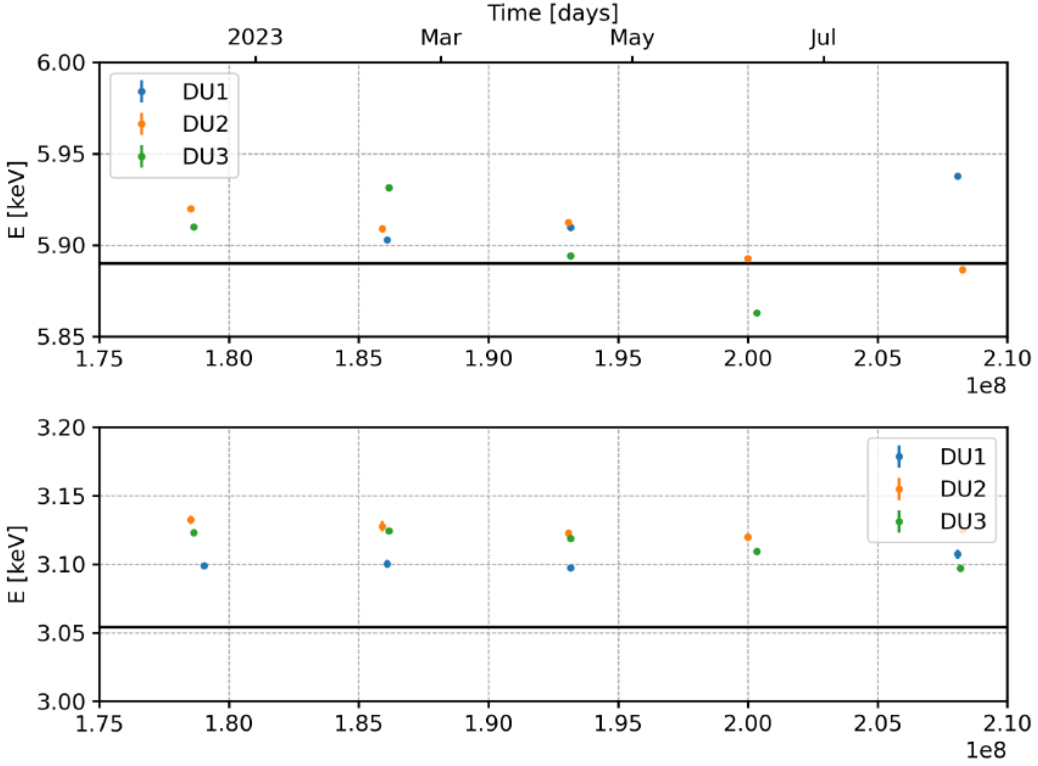

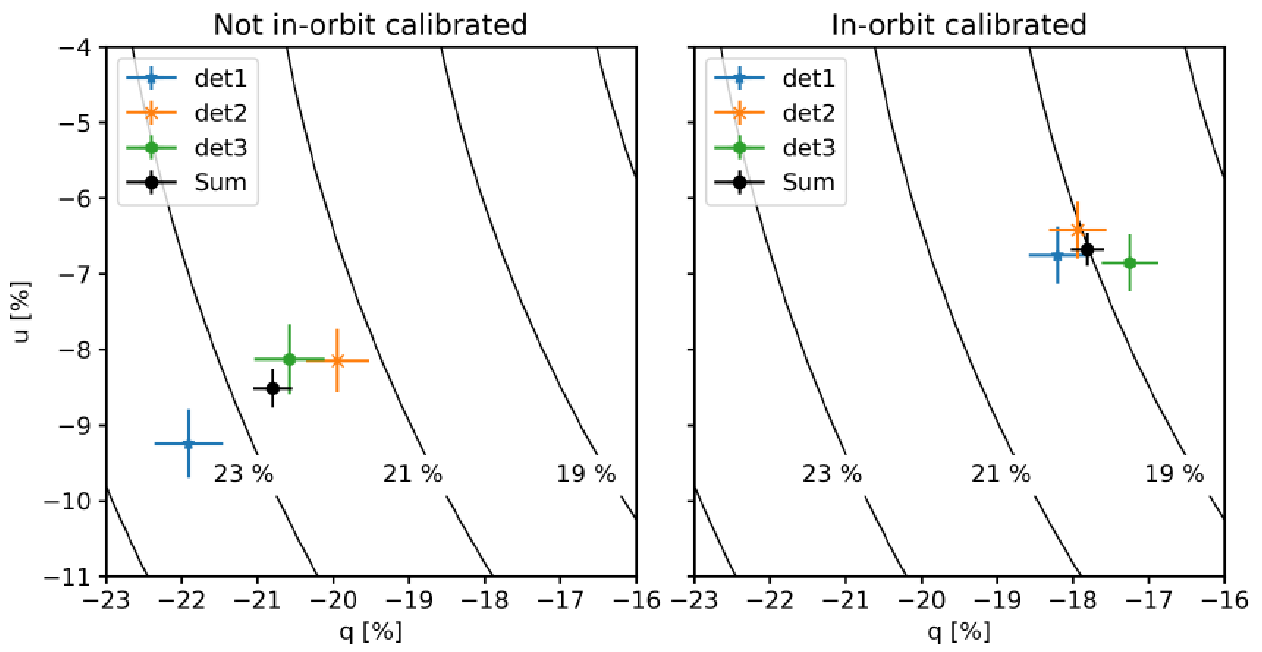

John Rankin et al., 2024 in preparation

The charging effect is mitigated by the use of the calibration sources.

A mis-calibration of 5-10 eV on the energy determination of the two Cal-A lines is detected

Crab Polarization is correctly determined

IN-ORBIT DETERMINATION OF THE ENERGY RESOLUTION

(John Rankin 2024 in preparation)

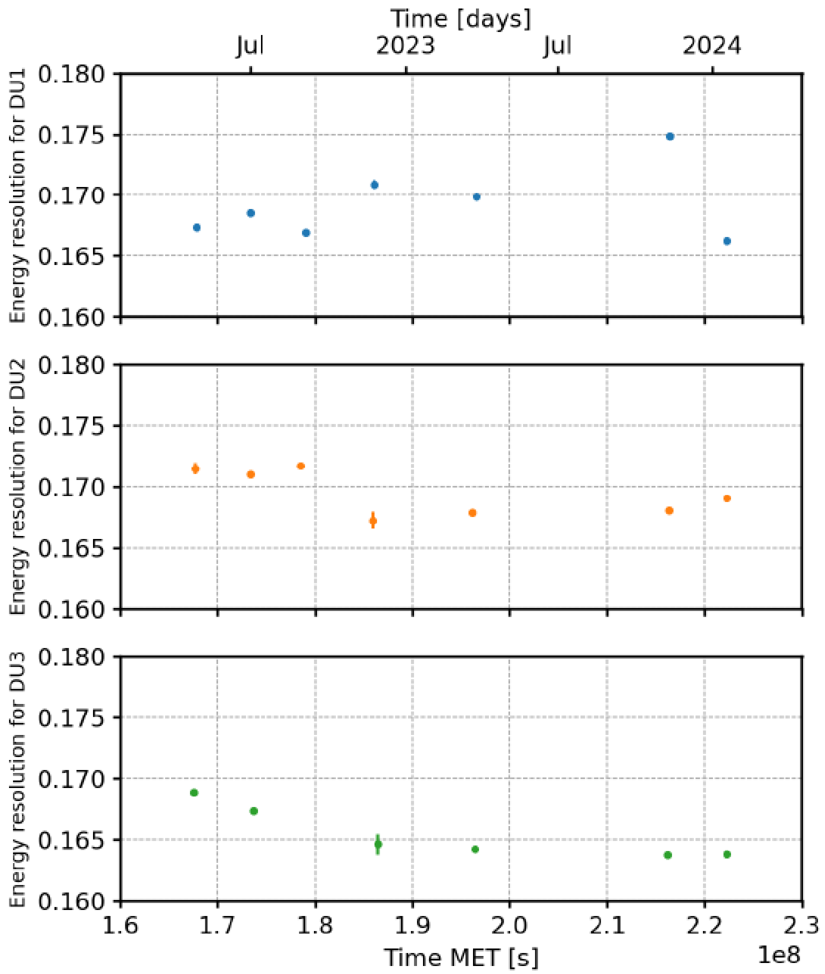

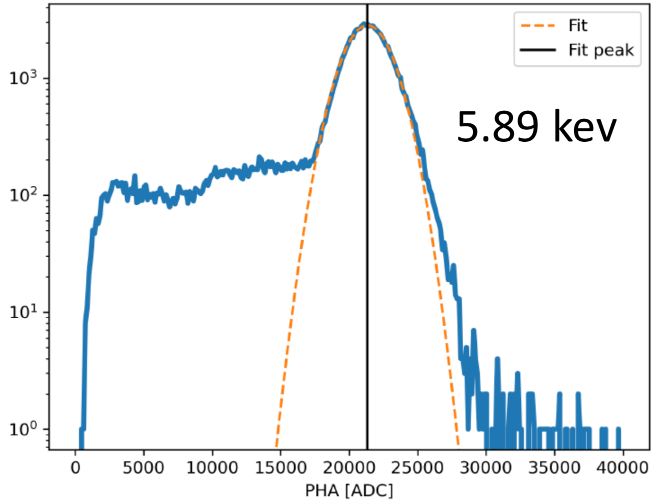

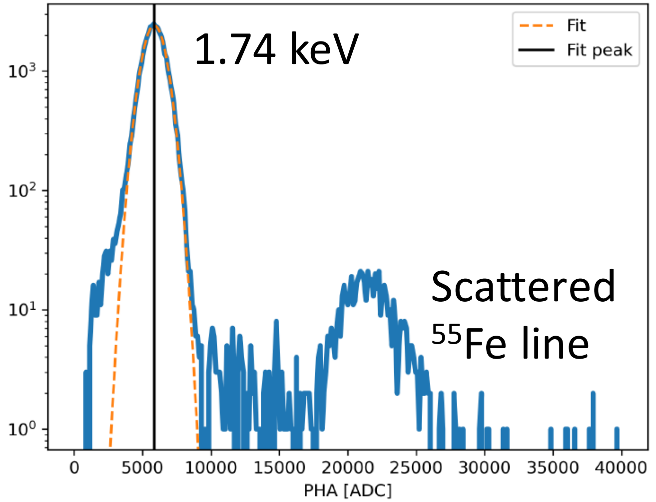

The energy resolution does not degrade with time.
No gas pollution.

GAIN, TRACK-LENGTH, PRESSURE

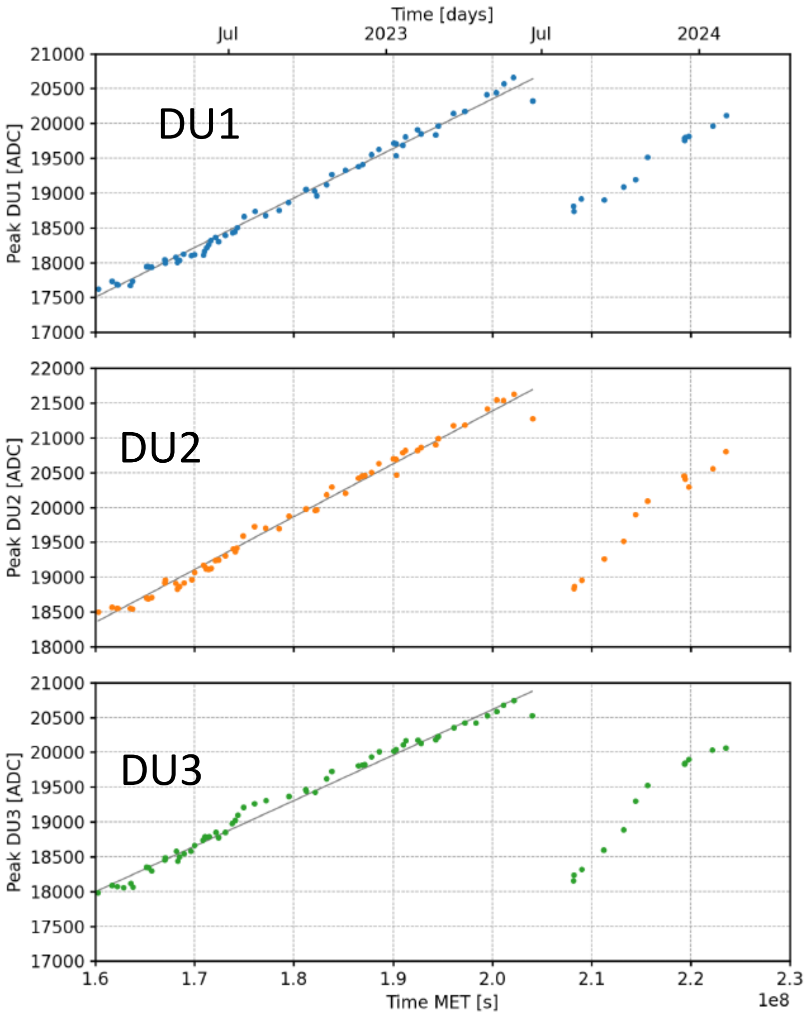

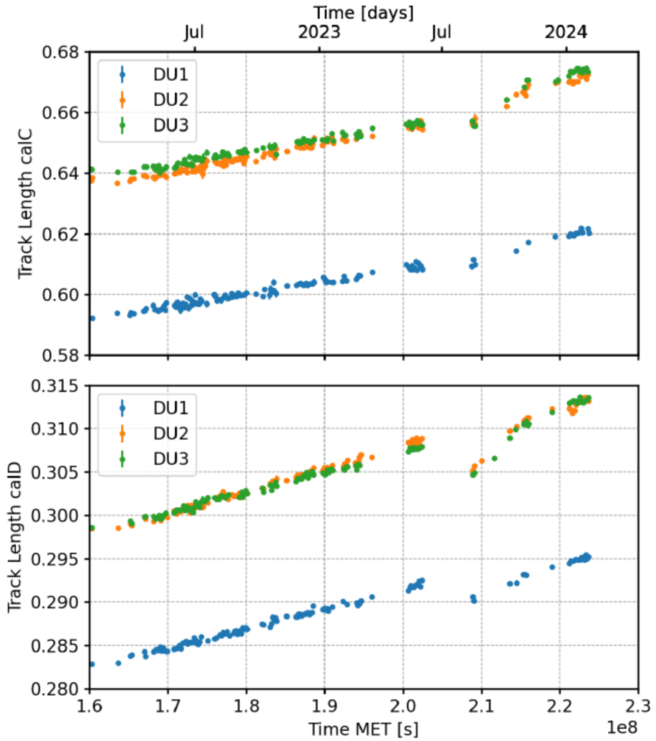

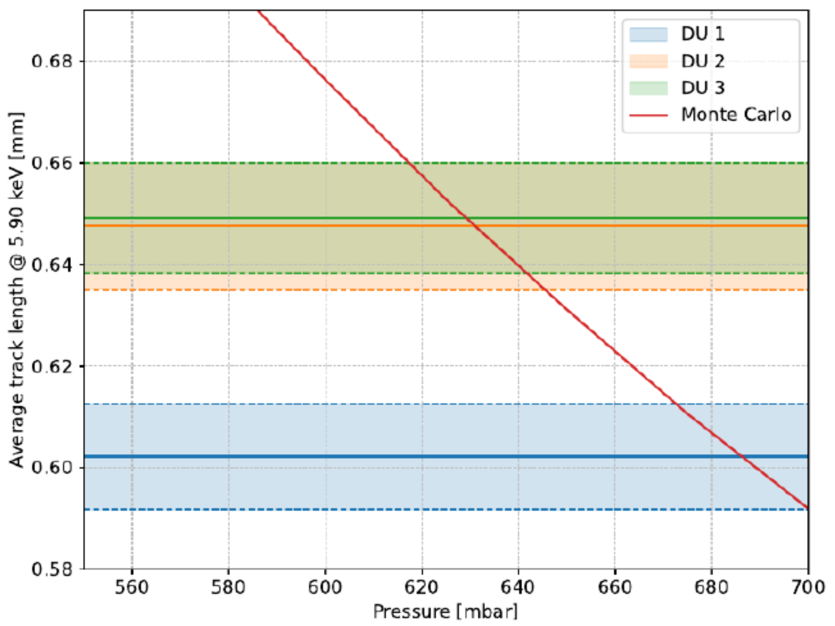

By comparing the track length measured in orbit with the expected pressure using Geant-4 Monte Carlo simulation. It is possible to derive the efficiency of the detector and create the correct response matrice
The decrement is about 10 mbar/yr

Low Magnetized Neutron Stars

IS = Iland State, LB= Lower Banana, UB = Upper Banana

HB = Horizontal Branch, NB = Normal Branch, FB = Flaring Branch

BL = Broad Line Region; SL = Spreading Layer

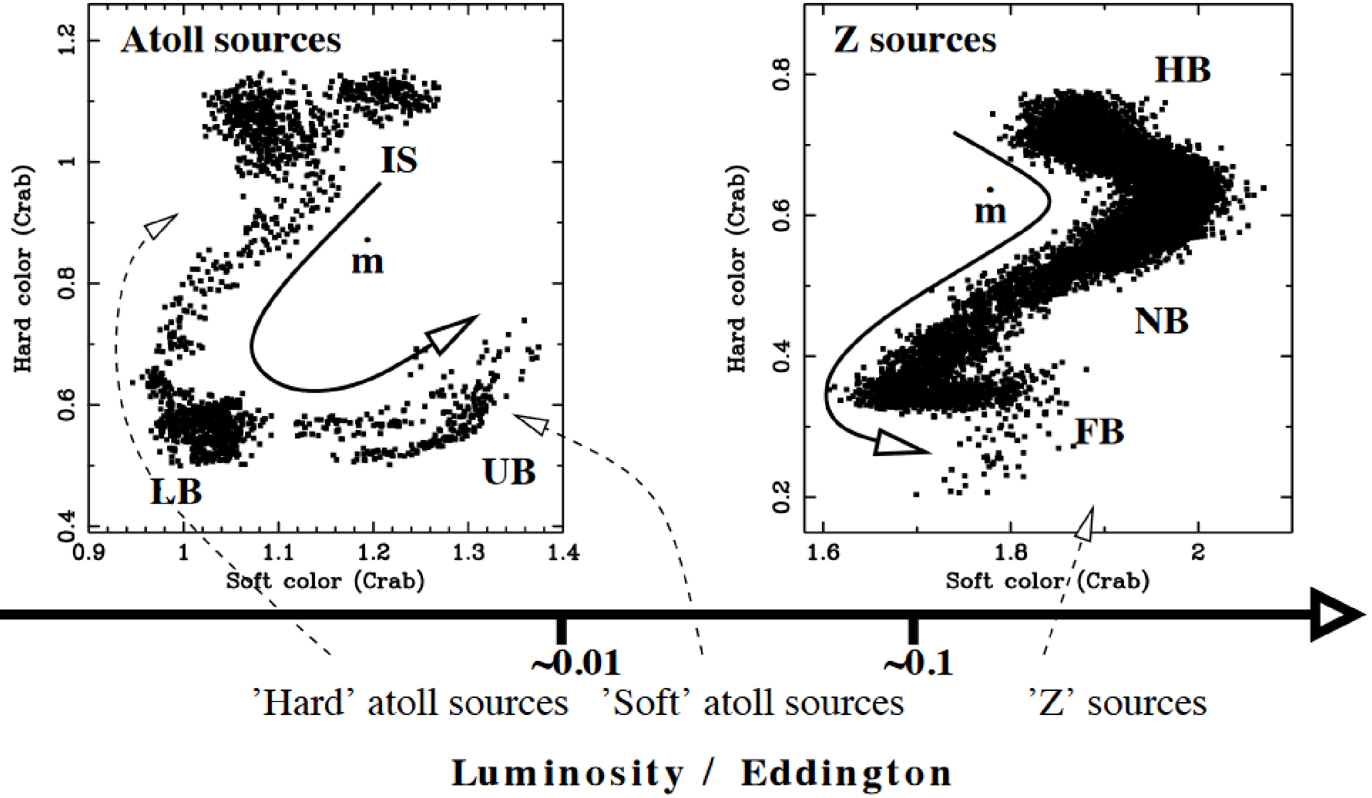

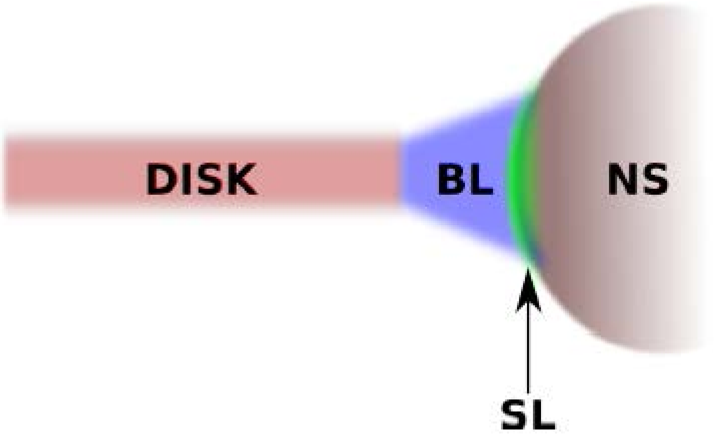

NS: B < 10^{10} G,
$M_{com} \approx M_{\odot}$
Accreting matter via Roche-lobe overflow

Di Salvo et al., 2023

ATOLL SOURCES, 4U 1820-303, GX9+9

Di Marco et al., 2023

Ursini et al. 2023

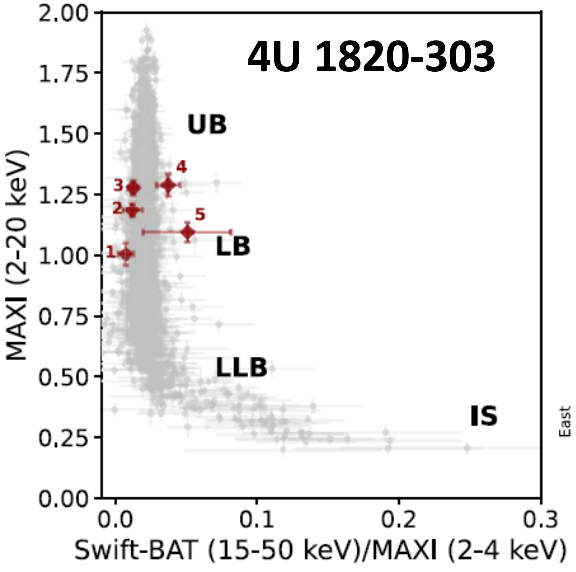

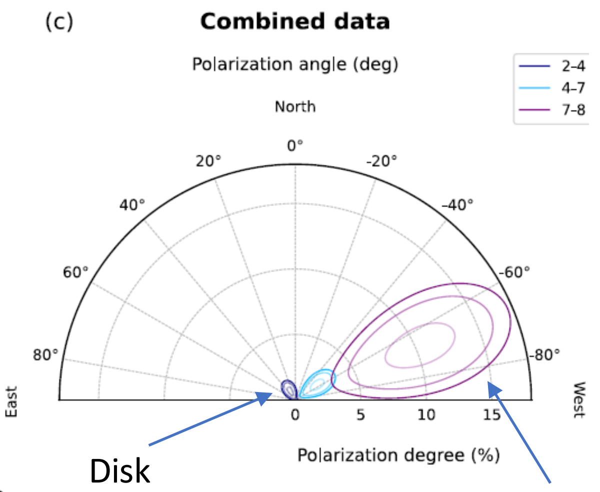

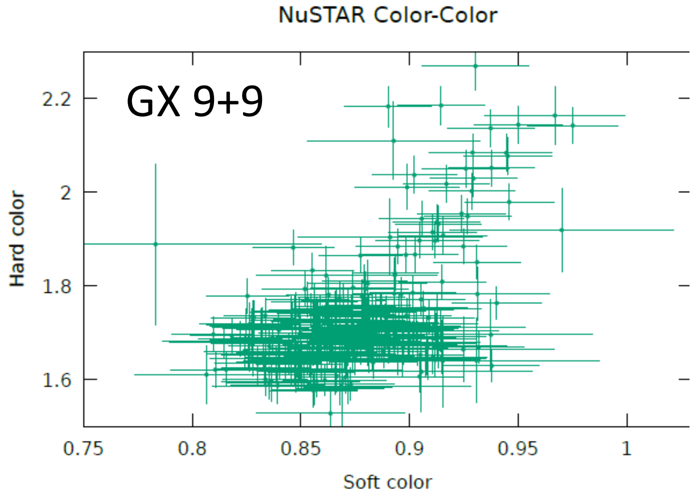

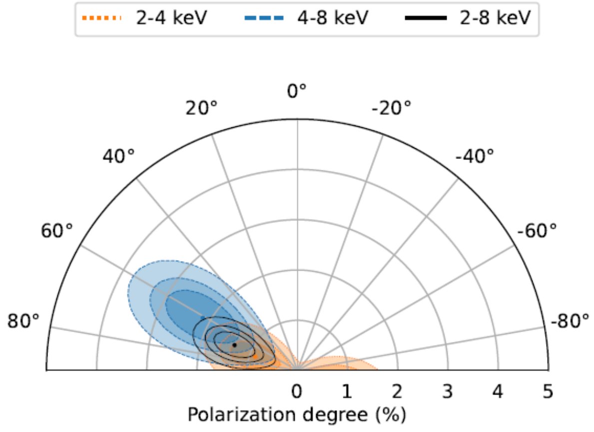

In 4U 1820 a rotation of the polarization angle of 90° with energy may indicate that the disk (low energy) is polarized orthogonal to the spreading/boundary layer. The reflection fraction is negligible < 5%.

In GX 9+9 the 4-8 keV polarization is significant and may be a combination of reflection from the disk and a of Comptonization (boundary/spreading layer) and reflection from the disk.

In GS1826-238 (Capitanio et al., 2023) only upper limit albeit significant were measured.

Z-SOURCE SOURCES: XTE J1701-462, CYG X-2 AND SCO X-1

Cocchi et al., 2023

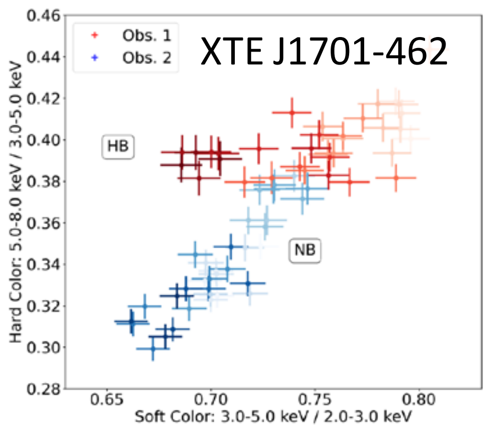

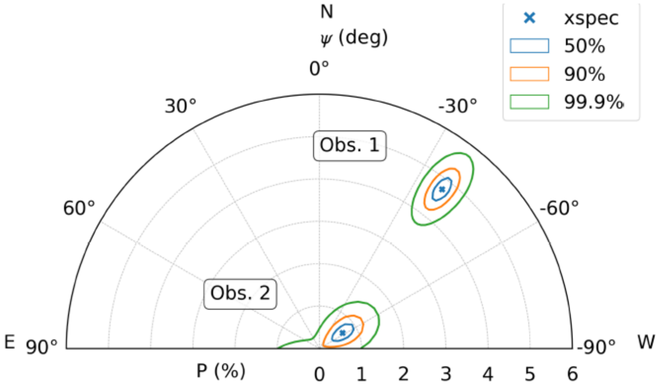

Farinelli et al. 2023

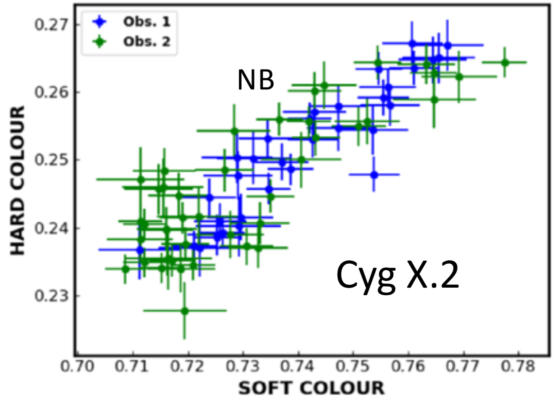

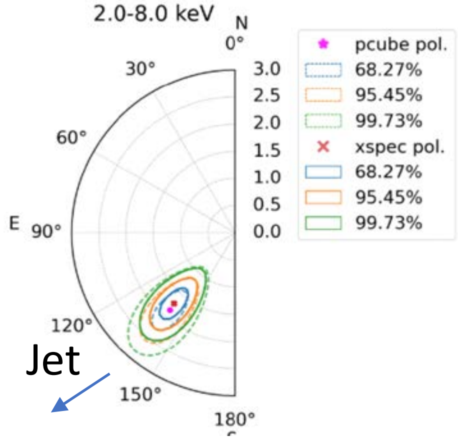

La Monaca et al 2024

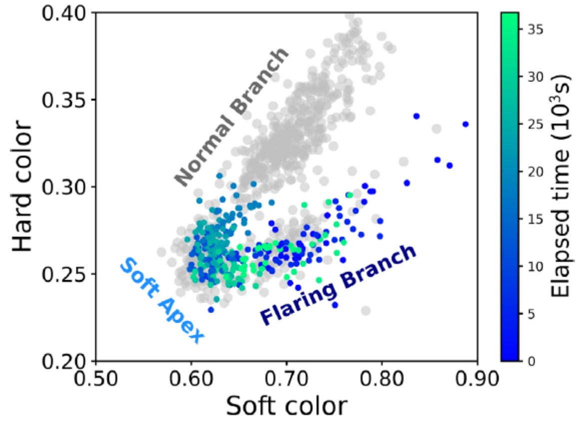

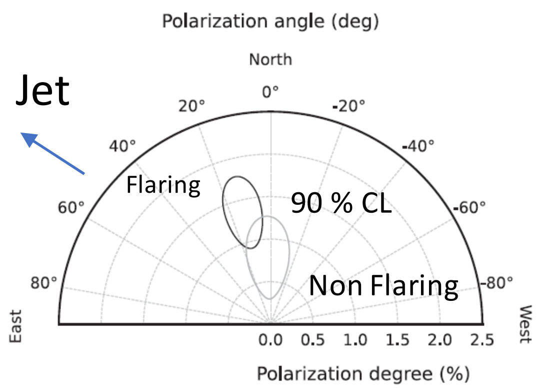

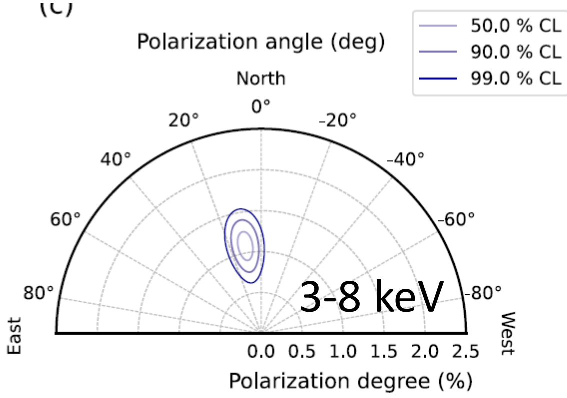

The polarization on the Horizontal Branch seems larger with respect to the polarization of the Normal Branch (See also GX 5.1, Fabiani et al., 2023). In Sco X-1 flaring and non Flaring seems to have comparable PD and PA not aligned with the jet. I Data shows a larger polarization with energy may be connected to a larger contribution of scattering.

IXPE
Imaging X-Ray Polarimetry Explorer

ASIC FEATURES 105600 PIXELS 50 MM PITCH

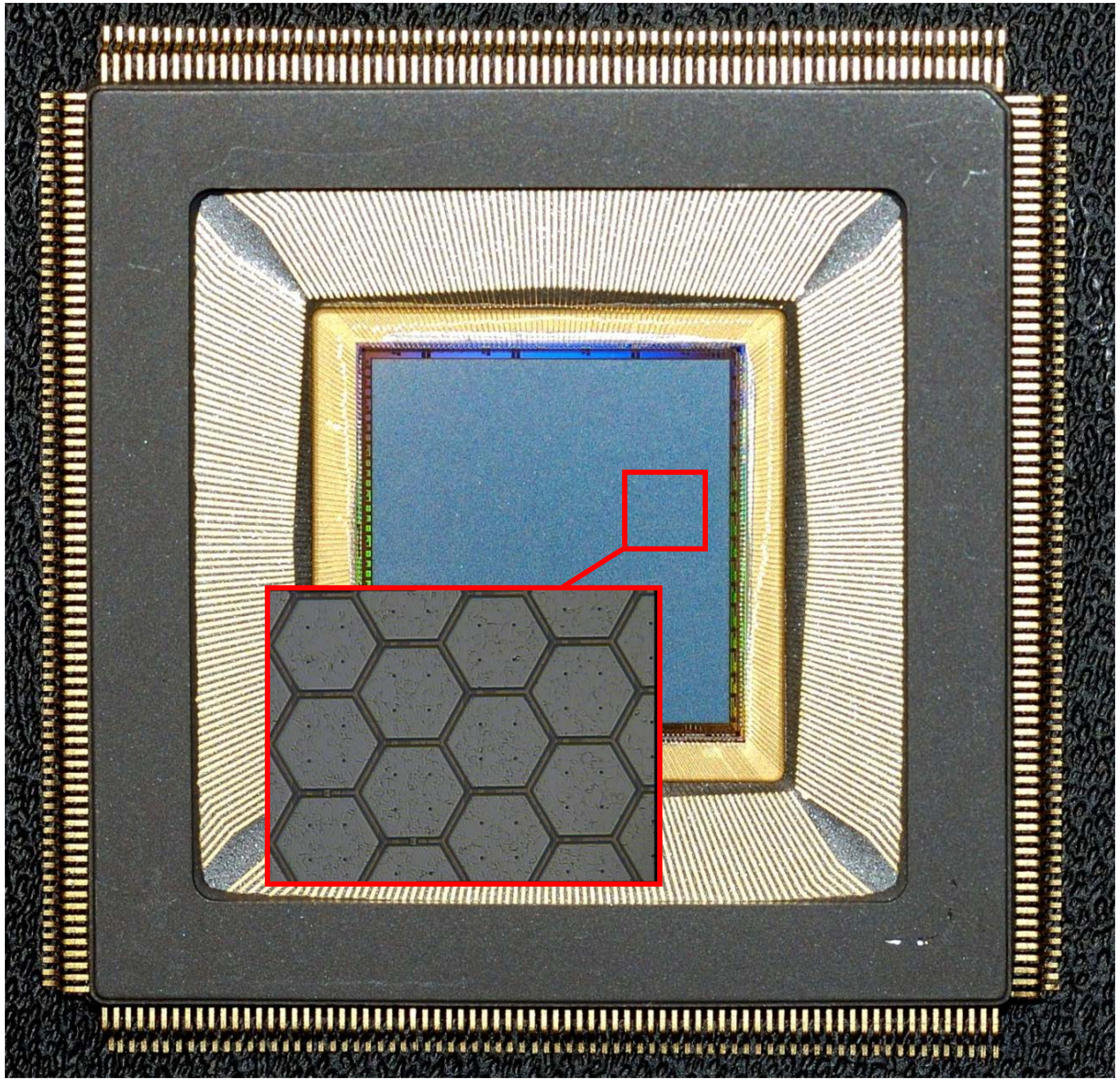

- Peaking time: 3-10 μs, externally adjustable;
- Full-scale linear range: 30000 electrons;
- Pixel noise: 50 electrons ENC;
- Read-out mode: asynchronous or synchronous;
- Trigger mode: internal, external or self-trigger;
- Read-out clock: up to 10MHz;
- Self-trigger threshold: 2200 electrons (10% FS);
- Frame rate: up to 10 kHz in self-trigger mode (event window);
- Parallel analog output buffers: 1, 8 or 16;
- Access to pixel content: direct (single pixel) or serial (8-16 clusters, full matrix, region of interest);
- Fill fraction (ratio of metal area to active area): 92%)

The chip is self-triggered and low noise. The top layer is the collection plane. The bottom 4 layers are a complete analogue chain for each pixel with preamplifier/shaper/sample and hold and serial readout.

It defines the sub-frame that surrounds the track. The dead time, downloading an average of 1000 pixels is 100 time lower, than for 1E5 pixels.

Bellazzini et al., NIM, 2006

$$MDP = \frac{4.29}{\mu R_S}\sqrt{\frac{R_S + R_B}{T}}$$

Minimum Detectable Polarization (MDP)

R_S is the Source rate, R_B is the Background rate, T is the observing time
μ is the modulation factor: the response of the polarimeter to a 100% polarized beam (spanning from 0 or no sensitivity, to 1 or maximum sensitivity)

If background is negligible: $$\mathrm{MDP} = \frac{4.29}{\mu\sqrt{N_{ph}}}$$

To reach MDP=1% with μ=0.5: $$N_{ph} = \left(\frac{4.29}{\mu\,\mathrm{MDP}}\right)^2$$ = 736 10^3 ph

Source detection > 10 counts
Source spectral slope > 100 counts
Source polarization > 100.000 counts

Caution: the MDP describes the capability of rejecting the null hypothesis (no polarization) at 99% confidence.

THE FORMALISM

Fit function: $\mathcal{M}(\phi) = A + B\cos^2(\phi - \phi_0)$

Modulation: $\frac{\mathcal{M}_{\max} - \mathcal{M}_{\min}}{\mathcal{M}_{\max} + \mathcal{M}_{\min}} = \frac{B}{B+2A}$

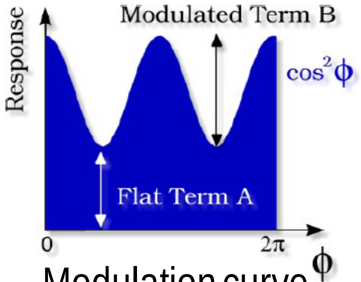

Modulation curve

Polarization: $\frac{1}{\mu}\frac{B}{B+2A}$

μ is the modulation factor, i.e. the modulation for 100% polarized radiation

Or by using Stokes Parameters

$$S(\varphi) = I + U\sin(2\varphi) + Q\cos(2\varphi)$$

$$I = (A + \frac{B}{2}) \qquad U = \left(\frac{B}{2}\right) * \sin(2\varphi_0) \qquad Q = \left(\frac{B}{2}\right) * \cos(2\varphi_0)$$

$$P = \frac{\sqrt{Q2+U2}}{I} \qquad \varphi = \frac{1}{2} atan\frac{U}{Q}$$

No V → no circular polarization with present techniques

Kislat et al. (2015) introduced the Stokes parameters from the direction of the single carrier of polarimetric observation